TECHNISCHE UNIVERSITÄT WIEN

VIENNA UNIVERSITY OF TECHNOLOGY

DIPLOMARBEIT

Long Wave Instabilities in Periodic Structures

ausgeführt zum Zwecke der Erlangung
des akademischen Grades einer Diplom-Ingenieurin
unter der Leitung von

Univ.Ass. Dipl.-Ing. Dr. habil. Thomas Daxner

Institut für Leichtbau und Struktur-Biomechanik (E317)

eingereicht an der Technischen Universität Wien
Fakultät für Maschinenwesen und Betriebswissenschaften

von

Melanie Todt
E700/e0225058
Canongasse 16/3
1180 Wien.

Wien, im August 2008

Für meine Großmutter
Margarete Krivec

Ein Freund ist, wer dich für gutes Schwimmen lobt,
nachdem du beim Segeln gekentert bist.
(Werner Schneider)

Die Menschen stolpern nicht über Berge, sondern über Maulwurfshügel.
(Konfuzius)

Danksagung

Mein herzlichster Dank geht an meinen Betreuer Herrn Univ. Ass. Dipl.-Ing. Dr. habil. Thomas Daxner, der immer die Zeit gefunden hat meine (häufig) gestellten Fragen zu beantworten. Seine wertvollen Anregungen und seine Bereitschaft zu Diskussionen haben entscheidend zum Gelingen dieser Diplomarbeit beigetragen. Zusätzlich möchte ich mich für die Durchführung der mühevollen Korrekturarbeiten bedanken, die die Qualität der Arbeit äußerst positiv beeinflusst haben.

Ich möchte mich außerdem beim ILSB bedanken, dass die benötigte Hard- und Software zur Verfügung gestellt hat. Mein spezieller Dank gilt Herrn Dr. Thomas Daxner und Herrn Dr. Dieter Pahr, deren Programm zur Generierung der periodischen Randbedingungen die Arbeit wesentlich erleichtert hat.

Weiters möchte ich mich bei Herr Dipl.-Ing. Robert Bitsche bedanken, der mir die Geometriedaten der Weaire-Phelan Zelle und die Bilder aus seiner Diplomarbeit zur Verfügung gestellt hat und mit seinen Anregungen zum Gelingen des letzten Kapitels dieser Arbeit eine wichtigen Beitrag geleistet hat.

Außerdem möchte ich mich bei Herrn Ing. Gerhard Schneider bedanken, der für jedes EDV-Problem eine rasche Lösung gefunden hat. In diesem Zusammenhang gilt mein Dank auch Herrn Dipl.-Ing. Robert Bitsche und Herrn Dipl.-Ing. Sergio Nogales.

Mein Besonderer Dank gilt meiner Familie, die mir dieses Studium ermöglicht hat und ohne deren Liebe, Fürsorge und Geduld diese Arbeit nicht zustande gekommen wäre. Ganz speziell möchte ich mich bei meiner Mutter Hedwig Todt bedanken, die mir in der letzten Phase meines Studiums den Rücken frei gehalten hat, sodass ich mich ganz auf mein Studium konzentrieren konnte.

Kurzfassung

Ziel der vorliegenden Arbeit ist die Implementierung einer Methode, die den numerischen Aufwand für die Suche nach Gleichgewichtsverzweigungspunkten für unter Druck belastete periodische Strukturen stark reduziert. Die durchgeführten Berechnungen basieren auf der sogenannten Bloch-Wellen-Methode. Diese Methode nutzt die Periodizität der Struktur und erlaubt die Bestimmung des Verzweigungspunktes und der dazugehörigen Versagensform für eine Struktur bestehend aus zahlreichen Zellen anhand einer einzigen Einheitszelle. Im Rahmen dieser Arbeit wird die Methode für die Analyse eines periodischen offenporigen Schaumes, eines periodischen zweidimensionalen Gitters und eines periodischen geschlossenporigen Schaumes verwendet.

Zur Beschreibung der Skelettlinien des offenporigen Schaumes wird eine Kelvin Zellgeometrie herangezogen. Die geometrischen Eigenschaften werden aus der Literatur übernommen. Die Suche nach dem kritischen Zustand erfolgt für ein- und mehrachsige Spannungszustände. Die Wellenlänge des kritischen Beulmodes ist abhängig vom Belastungszustand und von der Anzahl der Zellen der periodischen Struktur. Die Ergebnisse sind vergleichbar mit den Ergebnissen aus der Referenzliteratur und werden zusätzlich durch begleitende Eigenwertanalysen an Strukturen, bestehend aus mehreren Einheitszellen, bestätigt.

Für die Modellierung eines zweidimensionalen periodischen Gitters werden vier verschiedene Einheitszellen verwendet um sicherzustellen, dass die Implementierung unsensibel bezüglich Phasenverschiebungen der periodischen Geometriefunktion reagiert. Die Ermittlung des kritische Zustandes efolgt für einachsigen Druck und für ebene Spannungszustände. Der kritische Beulmode eines Gitters mit (theoretisch) unendlicher Ausdehnung entspricht, unabhängig vom Belastungszustand, einem Beulmode mit unendlicher Wellenlänge. Alle vier Einheitszellen liefern vergleichbare Ergebnisse, die auch durch Ergebnisse aus der Literatur bestätigt werden.

Das Modell des geschlossenporigen Schaumes basiert auf einer Weaire-Phelan Zellgeometrie. Unter Druckbelastung zeigt die Weaire-Phelan Zelle eine hohe Empfindlichkeit gegenüber kleinen geometrischen Imperfektionen. Die Bestimmung des kritischen Zustandes erfolgt für einachsigen Druck und hydrostatischen Druck. In beiden Fällen ist der kritische Spannungszustand und die Wellenlänge des zugehörige Beulmodes unabhängig von der Größe der periodischen Struktur. Der kritische Beulmode ist ein lokaler und weißt die gleiche Periodizität wie die Einheitszelle auf.

Abstract

The aim of the present thesis is the implementation of an efficient method for detecting the onset of buckling in spatially periodic structures loaded under compression. The calculations made are based on the Bloch Wave method. This method searches for the critical state of a (theoretically) infinite periodic structure using a single unit cell which can be as small as the smallest periodic building block of the structure, and therefore, reduces the required numerical effort for predicting buckling modes that involve multiple cells significantly. In the present thesis the Bloch Wave Analysis (BWA) is applied to three different periodic structures, namely: an open cell foam, a periodic two-dimensional lattice, and a closed cell foam.

The open cell foam is modeled on the basis of a space-filling Kelvin Cell. The struts of the Kelvin Cell are assigned several geometric properties reported in the literature. The results received for the Kelvin Cell are verified against published results. The Kelvin Cell is subjected to uniaxial loading and a set of triaxial loading cases. The wave length of the critical buckling modes depends on the triaxiality of the loading case. The results agree with those reported in the literature and with the results delivered by an accompanying eigenvalue analysis of Finite Element models containing multiple base cells.

The periodic 2D lattice is modeled using four different unit cells in order to investigate the influence of different realizations of periodic boundary conditions on the predicted behavior. These four cells are subjected to uniaxial and bi-axial compressive loads. The results received with all four cells are in good agreement. The wavelength of the critical buckling mode is independent of the multiaxiality of the loading case and corresponds to a mode with infinite wavelength. The results of the BWA are confirmed by an accompanying eigenvalue analysis and verified against results reported in the literature.

The closed cell foam model is based on the space-filling Weaire-Phelan Cell. The cell is subjected to uniaxial compressive loading and to pure hydrostatic pressure. For both cases the critical buckling mode is local to a single unit cell, even if the number of base cells that build up the investigated sturcture is far larger than one.

Contents

1 Introduction

1.1 Motivation

Ductile solids having a periodic microstructure, like composite materials or cellular solids, are widely used in engineering tasks. Loaded under compression the ultimate failure of these solids can be related to a buckling type instability. The onset of instability can correspond to the bifurcation point of the fundamental solution. For large structures the evaluation of the critical load and the prediction of the corresponding buckling mode can be a numerically expensive task. Exploiting the periodicity of the microstructure can reduce the numerical effort significantly.

1.2 Problem Statement

The calculations made in the present thesis are based on the so-called Bloch Wave method. Instead of dealing with the whole periodic structure this method uses a single unit cell for detecting the critical state and for predicting buckling modes that involve multiple cells. The detected buckling modes using the Bloch Wave method involve a finite number of cells. For detecting buckling modes with wavelengths that are much larger than the unit cell dimensions, a macroscopic onset-of-failure concept is used. To facilitate the search for the critical state a program using both, the Bloch Wave method and the macroscopic onset-of-failure concept, is implemented using PYTHON. The program is applied to different solids with a periodic microstructure, namely: an open cell foam, a periodic two-dimensional lattice and a closed cell foam. The results received with the implemented method are verified against the results reported in the literature and against the results obtained by an accompanying eigenvalue analysis of Finite Element models containing multiple cells.

1.3 Literature Overview

The stability criteria for rate-independent elasto-plastic solids was first formulated by [18]. The basic mathematical theory of the Bloch Wave method (microscopic onset-of-failure) and the macroscopic onset-of-failure concept is presented in [27]. In the same paper a Finite Element representation is given and both methods are applied to periodic two-phase solids (composites) subjected to general in-plane loading. The completeness of the Bloch Wave representation of the buckling eigenmode is proven in [13] and a nonlinear

homogenization method for nonlinear elastic composites is developed in the same work. It is shown that the macroscopic onset of failure is related to the loss of rank-one convexity of the homogenized moduli tensor of the periodic microstructure.

In [17] both the macroscopic and the microscopic onset-of-failure concept are applied to open-cell foams idealized using a space filling Kelvin Cell. The Finite Element formulation of the onset-of-failure concept is presented and a condensation algorithm is used to reduce the size of the stiffness matrix (see also [27]). The Kelvin Cell used in [17] is assigned the geometric properties of open cell foams tested in [16] and [14]. In [14] and [16] open cell polyurethane foams with different cell sizes are tested to characterize the properties of the base material and the geometric properties of the microstructure. Different models for predicting the elastic constants and the compressive response are developed and the results are verified against the experiments. [16] deals with the prediction of the elastic properties of the open-cell foams, and [14] deals with the compressive response and the crushing behavior of such foams.

In [20] long wave length buckling of elastic square honeycombs under in-plane bi-axial compression is investigated. The bifurcation behavior and the post-bifurcation behavior of the square honeycombs is analyzed and the dependence of the critical stress and the corresponding buckling mode of the periodic length is discussed. Based on the two-scale analysis (see [21]) a simple formula for estimating the critical stress corresponding to a long-wave-length mode is developed.

Bitsche [6] deals with the simulation of the mechanical behavior of closed cell dry foam structures. The foams are idealized using space-filling Kelvin Cells and space-filling Weaire-Phelan Cells. The dependence of the elastic properties on the density is discussed.

1.4 Chapter Overview

The structures investigated in the present work have periodic microgeometries. These periodic microgeometries can be described with unit cells subjected to periodic boundary conditions. Chapter 2 gives a short introduction to the unit cell method. The coupling equations for maintaining geometric periodicity of the displacement field of arbitrary periodic unit cells are presented and the forces acting on a unit cell subjected to a periodic displacement field are discussed.

The microscopic and macroscopic onset-of-failure concept are presented in Chapter 4 and Chapter 5, respectively. Chapter 4 gives a brief introduction to the general mathematical

theory of the microscopic onset of failure concept, and the Finite element representation of this method is presented. In Chapter 5 the general theory of the macroscopic onset-of failure concept is presented and the Finite element representation of this method given in [17] is extended to more general unit cell topologies.

Both the microscopic and macroscopic onset-of-failure concept are subsequently applied to different periodic structures see Chapter 6 to Chapter 8. In Chapter 6 an open cell foam is modeled using space filling Kelvin Cells. The Kelvin unit cell model is subjected to uniaxial compressive loading and a set of triaxial loading cases. In Chapter 7 the influence of different realizations of the periodic structure on the results obtained by the microscopic and macroscopic onset of failure concept are investigated for the case of a 2D periodic lattice. A closed cell foam modeled with the space filling Weaire-Phelan Cell and subjected to uniaxial loading and pure hydrostatic pressure is investigated in Chapter 8. To verify the results obtained with the microscopic and macroscopic onset-of-failure concept an accompanying linear eigenvalue analysis based on the eigenvalue buckling prediction of ABAQUS is used (see Chapter 3) in each case. The findings obtained for the respective topologies are summarized and discussed in Chapter 9.

Remark: If not otherwise stated positive values of stress correspond to compressive stresses in this thesis.

2 Finite Element Unit Cell Models

2.1 Boundary Conditions

This section gives a short overview about the periodic micro field approach also referred to as the unit cell method. A more detailed description of the finite element unit cell method can be found, e.g. in [10] in the context of modeling metallic foams.

Three possible types of boundary conditions (BC) used in the periodic micro field approach are: periodicity, symmetric and antisymmetric boundary conditions. Symmetry and antisymmetry BC can only handle deformation states that do not break symmetry (see [8]) whereas periodic BC can handle any spatially periodic deformation state. Therefore, the latter are the most general of these three types of boundary conditions.

For generating the stiffness matrices used in the Bloch Wave algorithm without being restricted to load cases that do not break symmetries, periodic boundary conditions are applied to all unit cells used in the present work. Examples for load cases that may break symmetry are shear load cases. Note, that this statement refers primarily to the prebuckling deformations applied in the Finite Element analysis. The spatially periodic buckling modes are implicitly contained in the Bloch Wave formulation (see Section 4). In the following the formulation of periodic displacement boundary conditions is demonstrated for the 2D case.

Figure 2.1 shows the periodicity boundary conditions applied to a 2D unit cell with the four edges being denoted as N (North), S (South), W (West), E (East) and the four corners being denoted as SW (South West), SE (South East), NE (North East), NW (North West). To restrict rigid body movements some of the displacement degrees of freedom of the corner nodes SW and SE are constrained ($\underset{\sim}{\boldsymbol{u}}_{\mathrm{SW}} = \{0, 0\}$, $\underset{\sim}{\boldsymbol{u}}_{\mathrm{SE}} = \{u_{\mathrm{SE}}, 0\}$). Geometric periodicity of the displacement field is maintained by coupling the degrees of freedom of opposite sides of the unit cell. The degrees of freedom of one side of such a pair remain unconstrained . This side is referred to as "master" side. The displacements of the opposite "slave" side are constrained to be identical to those on the master side except for an additional constant offset vector. Choosing W and S as unconstrained master sides and the unconstrained degrees of freedom (DOFs) of the corner nodes SW, SE and NW as macroscopic master DOFs the additional offset vectors (see Figure 2.1) can be written as $\underset{\sim}{\boldsymbol{u}}_{\mathrm{SE}} = \{u_{\mathrm{SE}}, 0\}$ and $\underset{\sim}{\boldsymbol{u}}_{\mathrm{NW}} = \{u_{\mathrm{NW}}, v_{\mathrm{NW}}\}$. For the displacements on the slave sides E

and N one receives:

$$\underset{\sim}{\boldsymbol{u}}_{\mathrm{E}} = \underset{\sim}{\boldsymbol{u}}_{\mathrm{W}} + \underset{\sim}{\boldsymbol{u}}_{\mathrm{SE}} \tag{2.1}$$

$$\underset{\sim}{\boldsymbol{u}}_{\mathrm{N}} = \underset{\sim}{\boldsymbol{u}}_{\mathrm{S}} + \underset{\sim}{\boldsymbol{u}}_{\mathrm{NW}} \tag{2.2}$$

The displacement of the slave corner node NE is a linear combination of the displacement vectors of the two master nodes NW and SE:

$$\underset{\sim}{\boldsymbol{u}}_{\mathrm{NE}} = \underset{\sim}{\boldsymbol{u}}_{\mathrm{NW}} + \underset{\sim}{\boldsymbol{u}}_{\mathrm{SE}} \tag{2.3}$$

For small strains and displacements the macroscopic strain state $\underset{\sim}{\boldsymbol{\epsilon}} = \{\varepsilon_{xx}, \varepsilon_{yy}, \gamma_{xy}\}$ is related to the components of the additional offset vectors $\underset{\sim}{\boldsymbol{u}}_{\mathrm{SE}}$ and $\underset{\sim}{\boldsymbol{u}}_{\mathrm{NW}}$ by:

$$\varepsilon_{xx} = \frac{u_{\mathrm{SE}}}{l_x}, \qquad \varepsilon_{yy} = \frac{v_{\mathrm{NW}}}{l_y}, \qquad \gamma_{xy} = \frac{u_{\mathrm{NW}}}{l_y} \tag{2.4}$$

If rotational DOFs θ are active in the Finite Element model, additional coupling equations have to be provided. In the case of a rectangular unit cell the rotations of all corner nodes have to be identical:

$$\theta_{\mathrm{SW}} = \theta_{\mathrm{SE}} = \theta_{\mathrm{NE}} = \theta_{\mathrm{NW}} \tag{2.5}$$

The rotational degrees of freedom on opposite sides must be coupled accordingly:

$$\theta_{\mathrm{E}}(y) = \theta_{\mathrm{W}}(y), \qquad \theta_{\mathrm{N}}(x) = \theta_{\mathrm{S}}(x) \tag{2.6}$$

It was shown by [24] that unit cell models react to concentrated loads on master nodes like the infinite structure would react to homogenized applied stresses. For this reason all loads are applied on the master nodes. Using horizontal and vertical forces H and V the homogenized stress state $\underset{\sim}{\boldsymbol{\sigma}} = \{\sigma_{xx}, \sigma_{yy}, \sigma_{xy}\}$ can, similar to Equation (2.4), be written as:

$$\sigma_{xx} = \frac{H_{\mathrm{SE}}}{l_y}, \qquad \sigma_{yy} = \frac{V_{\mathrm{NW}}}{l_x}, \qquad \sigma_{xy} = \frac{H_{\mathrm{NW}}}{l_x} \tag{2.7}$$

The scheme presented for the rectangular 2D unit cell can be adopted for cuboid-shaped

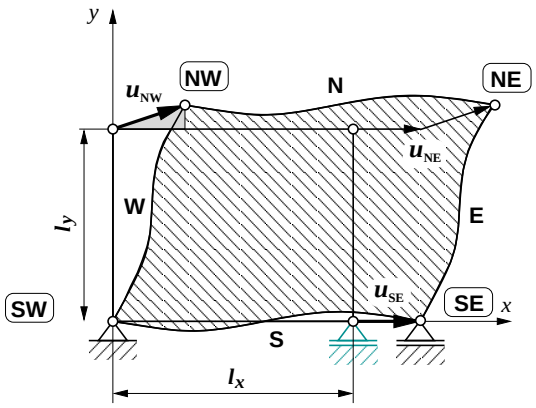

Figure 2.1: Idealized 2D unit cell in the undeformed and the deformed configuration. From [10].

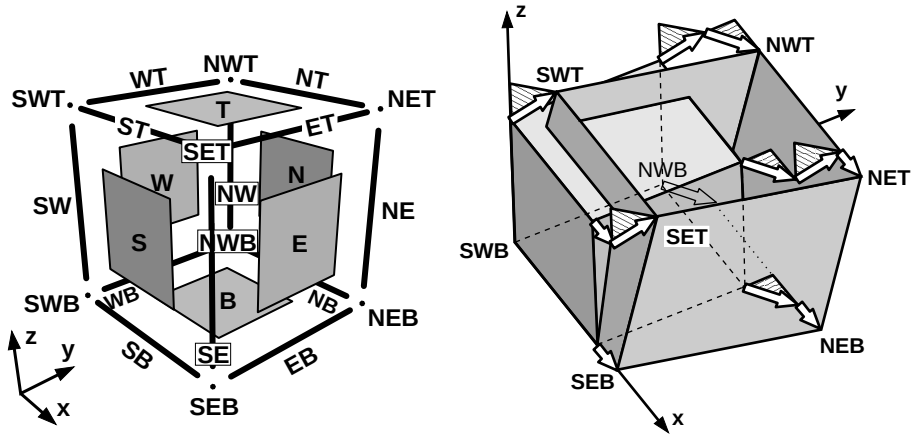

Figure 2.2: Default identifiers for the node sets on the unit cell cube (left) and general deformation state of the 3D unit cube (right). From [10].

3D unit cells. Figure 2.2 (left) shows the naming convention for face, edge and corner node sets of such a cell. To restrict the unit cell against rigid body movements some of the displacement degrees of freedom of the corner nodes SWB, SEB and NWB are constrained. The remaining six degrees of freedom of these master nodes correspond to the six macroscopic deformation modes of the cell (three normal and three shear modes). A general macroscopic deformation state with three normal and three shear deformation degrees of freedom being active is shown in Figure 2.2 (right). In this figure the local periodic deformations are omitted. Table 2.2 in [10] gives a complete description of the necessary boundary conditions and coupling equations for 3D unit cells.

2.2 Forces on the Unit Cell

The aim of this section is to find a relation for the reaction forces, due to a periodic deformation field, on opposite sides of a unit cell. This relation is used for deriving Equation (5.28) in Section 5 from which the strain functions, needed for calculating the homogenized tangent moduli tensor, are estimated.

Figure 2.3 shows an array of unit cells in the undeformed (dashed lines) and the deformed state (solid lines). To maintain periodicity of the deformed structure, the following condition for forces acting on opposite sides of the unit cell must be fullfilled:

$$\begin{aligned} \underset{\sim}{\boldsymbol{F}}_{\mathrm{N}} &= -\underset{\sim}{\boldsymbol{F}}_{\mathrm{S}} \\ \underset{\sim}{\boldsymbol{F}}_{\mathrm{E}} &= -\underset{\sim}{\boldsymbol{F}}_{\mathrm{W}} \end{aligned} \tag{2.8}$$

For the forces acting in the corner nodes, which are artefacts from the FE discretization, one finds:

$$\underset{\sim}{\boldsymbol{F}}_{\mathrm{SW}} + \underset{\sim}{\boldsymbol{F}}_{\mathrm{SE}} + \underset{\sim}{\boldsymbol{F}}_{\mathrm{NE}} + \underset{\sim}{\boldsymbol{F}}_{\mathrm{NW}} \approx \underset{\sim}{\mathbf{0}}. \tag{2.9}$$

To verify the statements given in Equations (2.8) and (2.9) a rectangular unit cell, meshed with 4-noded bi-linear stress elements, is subjected to different periodic displacement fields. In Figure 2.4 the meshed unit cell is depicted. The displacement fields are described using

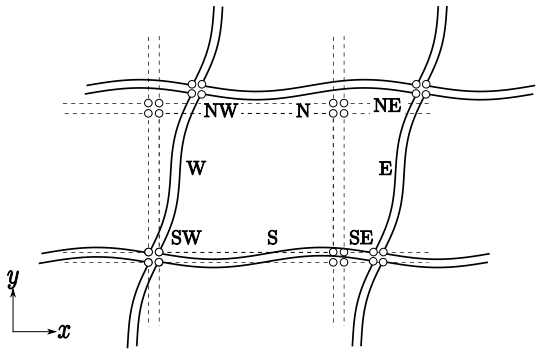

Figure 2.3: 2D unit cells in deformed and undeformed state.

the following equations:

$$\begin{aligned} u_{ij} &= A_{ux}\sin(0.2 + 2\pi x_{ij,\mathrm{rel}}) + A_{uy}\sin(0.2 + 2\pi y_{ij,\mathrm{rel}}) + \varepsilon_{xx}x_{ij} + \frac{\varepsilon_{xy}}{2}y_{ij} \\ v_{ij} &= A_{vx}\sin(0.1 + 2\pi x_{ij,\mathrm{rel}}) + A_{vy}\sin(0.9 + 2\pi y_{ij,\mathrm{rel}}) + \varepsilon_{yy}y_{ij} + \frac{\varepsilon_{xy}}{2}x_{ij} \end{aligned} \tag{2.10}$$

All nodes in the rectangular unit cell depicted in Figure 2.4 are treated like elements in a matrix, therefore, the position of each node can be defined using its row number i and its column number j. For the relative coordinates $x_{ij,\mathrm{rel}}$ and $y_{ij,\mathrm{rel}}$ of a node with index ij one finds:

$$\begin{aligned} x_{ij,\mathrm{rel}} &= \frac{j}{N_x - 1}, \qquad j = 0, 1, 2, \ldots N_x - 1 \\ y_{ij,\mathrm{rel}} &= \frac{i}{N_y - 1}, \qquad i = 0, 1, 2, \ldots N_y - 1 \end{aligned} \tag{2.11}$$

where N_x is the number of nodes in x direction and N_y is the number of nodes in the y direction. The SE master node, therefore, has the relative coordinates (1,0). For the absolute coordinates of the node ij one receives:

$$\begin{aligned} x_{ij} &= x_{ij,\mathrm{rel}} l_x \\ y_{ij} &= y_{ij,\mathrm{rel}} l_y \end{aligned} \tag{2.12}$$

The unit cell depicted in Figure 2.4 with l_x being 20 mm and l_y being 10 mm is subjected

Table 2.1: Deformation fields applied to a 2D unit cell.

	ε_{xx}	ε_{yy}	ε_{xy}	A_{ux}	A_{uy}	A_{vx}	A_{vy}
DF1	1.00	0.00	0.00	0.00	0.00	0.00	0.00
DF2	0.00	1.00	0.00	0.00	0.00	0.00	0.00
DF3	0.00	0.00	1.00	0.00	0.00	0.00	0.00
DF4	0.50	0.00	0.20	0.00	0.00	0.00	0.00
DF5	0.00	0.00	0.00	0.20	0.20	0.20	0.20
DF6	0.00	0.00	0.30	0.20	0.20	0.20	0.20

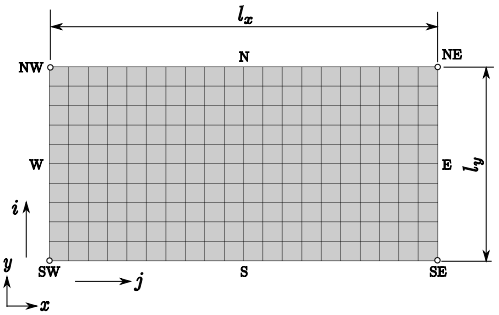

Figure 2.4: 2D unit cell meshed with 4-node bi-linear plane stress elements.

to the displacement fields (DF) listed in Table 2.1. For DF1 to DF4, 4-noded bi-linear plane stress elements (CPS4 in ABAQUS) with an edge length of 1 mm are used and for DF5 and DF6 the edge length of the elements (CPS4) is reduced to 0.25 mm

The results for DF1 to DF6 are depicted in Figure 2.5. The applied periodic deformation field results in a periodic stress state in the 2D unit cell. The boundary S of the unit cell consists of the four sides W,S,E, and N. With the normal vector $\underset{\sim}{\boldsymbol{n}}$ of an infinitesimally small element ds on the boundary the corresponding stress vector $\underset{\sim}{\boldsymbol{\sigma}}_n$ acting on ds can be calculated. As a result of the periodicity of the displacement field the stress vectors of corresponding elements ds on opposite sides of the unit cell must cancel each other. In the discretized model, the nodal reaction forces at the boundary side nodes can be interpreted as being approximately proportional to the stress vectors. At the corner nodes of the unit cell, reaction forces appear that correspond to the stress fields within the corner elements. These reaction forces do not have an immediate physical meaning. However, they can be interpreted as being proportional to the superposition of the stress vectors acting on the two free sides of the corner elements. Thus, the forces acting in the corner nodes are artefacts from the F.E. discretization. For the nodal reaction forces and the forces acting

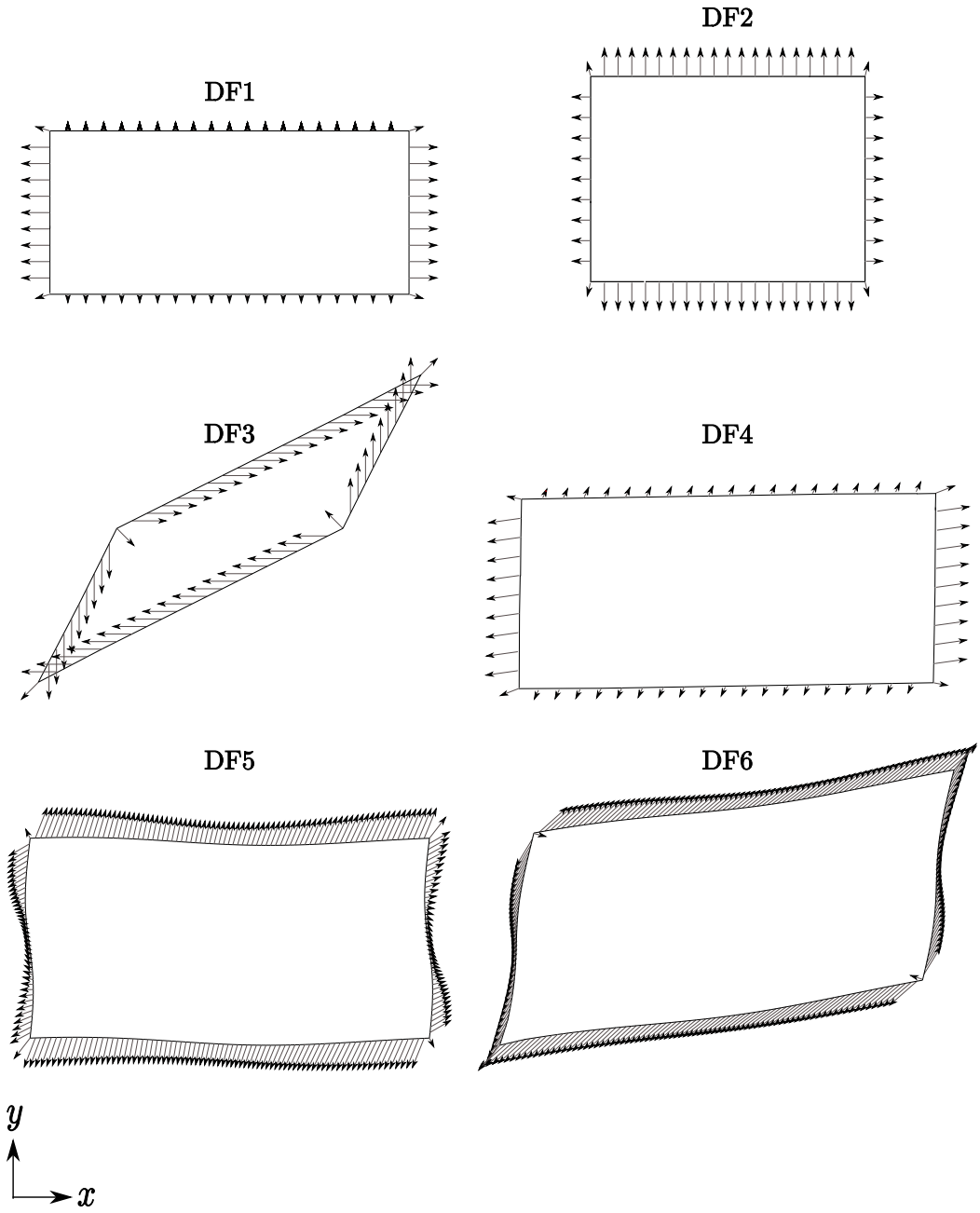

Figure 2.5: Deformed unit cell subjected to DF1 to DF6.

on opposite sides of the cell of the Finite Element model one finds:

$$\underset{\sim}{\boldsymbol{F}}_{\mathrm{SW}} + \underset{\sim}{\boldsymbol{F}}_{\mathrm{SE}} + \underset{\sim}{\boldsymbol{F}}_{\mathrm{NE}} + \underset{\sim}{\boldsymbol{F}}_{\mathrm{NW}} \approx \underset{\sim}{\mathbf{0}} \tag{2.13}$$

$$\underset{\sim}{\boldsymbol{F}}_{\mathrm{N}} \approx -\underset{\sim}{\boldsymbol{F}}_{\mathrm{S}} \tag{2.14}$$

$$\underset{\sim}{\boldsymbol{F}}_{\mathrm{E}} \approx -\underset{\sim}{\boldsymbol{F}}_{\mathrm{W}} \tag{2.15}$$

Equation (2.13) is the result of the periodicity of the stress vectors in the vicinity of the corner nodes. The results given in Equations (2.13) to (2.15) are comparable with Equations (2.8) to (2.9). The difference between the nodal forces on opposite sides is small and depends on the discretization used for the unit cell.

3 Accompanying Linear Eigenvalue Analysis

The present work deals with buckling type instabilities of periodic structures. Subjected to compressive loading thin or slender structural members can become unstable at a critical point on the load-displacement path. This point can represent a bifurcation of the equilibrium path, which corresponds to buckling of beams and shells, for example. There are various methods for predicting the critical point at which the structure becomes unstable. A description of these methods can be found in [11]. This chapter gives a brief outline of one of these methods, namely the accompanying linear eigenvalue analysis.

3.1 Eigenvalue Buckling Prediction of ABAQUS

The eigenvalue buckling prediction implemented in ABAQUS is typically used for structures with an almost linear prebuckling response. The critical load for which buckling occurs is estimated as a multiplier of a set of perturbation loads. These perturbation loads are added to the base state loads. The initial material stiffness is used in the derivation of the stiffness matrices.

At the critical state one finds, by using the static stability criterion:

$$\underset{\approx}{\underset{\approx}{\boldsymbol{K}}}\delta\underset{\sim}{\boldsymbol{u}} = \underset{\sim}{\boldsymbol{0}}, \tag{3.1}$$

where $\underset{\approx}{\underset{\approx}{\boldsymbol{K}}}$ is the tangent stiffness matrix corresponding to the current loading pattern of the structure and $\delta\underset{\sim}{\boldsymbol{u}}$ is the nontrivial displacement solution of the discretized Finite Element model. The loading pattern for the critical state $\underset{\sim}{\boldsymbol{F}}_{\text{crit}}$ can consist of concentrated nodal forces, prescribed non-zero displacements, thermal loadings and/or distributed loads.

As mentioned above ABAQUS calculates the critical buckling load $\underset{\sim}{\boldsymbol{F}}_{\text{crit}}$ relative to a base state [1]. The base state can result from any type of loading history and is the response of the structure to the base state loading pattern $\underset{\sim}{\boldsymbol{F}}_{\text{pre}}$ (pre-loading pattern). In the eigenvalue buckling prediction step a perturbation loading pattern $\underset{\sim}{\boldsymbol{F}}_{\text{pert}}$ is defined. $\underset{\sim}{\boldsymbol{F}}_{\text{pre}}$ and $\underset{\sim}{\boldsymbol{F}}_{\text{pert}}$ can, like $\underset{\sim}{\boldsymbol{F}}_{\text{crit}}$, consist of concentrated nodal forces, prescribed nonzero displacements, thermal loadings, and/or distributed loads. The aim of the buckling prediction is to find a multiplier λ for scaling $\underset{\sim}{\boldsymbol{F}}_{\text{pert}}$ in order to receive the critical buckling load:

$$\underset{\sim}{\boldsymbol{F}}_{\text{crit}} = \underset{\sim}{\boldsymbol{F}}_{\text{pre}} + \lambda\underset{\sim}{\boldsymbol{F}}_{\text{pert}} \tag{3.2}$$

This leads to the following eigenvalue problem (for a more detailed description see [1]) :

$$(\underset{\approx}{\boldsymbol{K}}_0 + \lambda_i \underset{\approx}{\boldsymbol{K}}_\Delta)\delta\underset{\sim}{\boldsymbol{u}}_i = \underset{\sim}{\boldsymbol{0}} \tag{3.3}$$

with $\underset{\approx}{\boldsymbol{K}}_0$ being the base state stiffness matrix due to the applied pre-loading pattern $\underset{\sim}{\boldsymbol{F}}_{\text{pre}}$ and $\underset{\approx}{\boldsymbol{K}}_\Delta$ being the incremental stiffness matrix due to the applied perturbation loading pattern $\underset{\sim}{\boldsymbol{F}}_{\text{pert}}$ of the ABAQUS buckle step. λ_i are the eigenvalues and $\delta\underset{\sim}{\boldsymbol{u}}_i$ are the corresponding eigenvectors where i refers to the number of the buckling mode. For calculating the critical load only the lowest eigenvalue λ_1 is of interest. Therefore, one can write:

$$\underset{\sim}{\boldsymbol{F}}_{\text{crit}} = \underset{\sim}{\boldsymbol{F}}_{\text{pre}} + \lambda_1 \underset{\sim}{\boldsymbol{F}}_{\text{pert}} \tag{3.4}$$

3.2 Accompanying Linear Eigenvalue Analysis Using ABAQUS

If the structure exhibits strong geometrically nonlinear behavior and the base state is far from the critical state, the critical buckling load and the corresponding buckling mode may be estimated incorrectly by the eigenvalue buckling prediction implemented in ABAQUS. To overcome this problem an incremental procedure is developed, in which the current base state loading pattern ${}^{i+1}\underset{\sim}{\boldsymbol{F}}_{\text{pre}}$ of the structure is calculated as a function of the base state loading pattern ${}^{i}\underset{\sim}{\boldsymbol{F}}_{\text{pre}}$ of the previous increment and the applied perturbation loading pattern $\underset{\sim}{\boldsymbol{F}}_{\text{pert}}$. This incremental procedure is referred to as accompanying linear eigenvalue analysis.

The accompanying linear eigenvalue analysis with ABAQUS is implemented using Python. The flow diagram of the accompanying linear eigenvalue analysis is shown in Figure 3.1. The program reads the geometric data (nodes, elements, boundary conditions) from a user provided .txt file. The geometry file must have the same structure as an ABAQUS input file. To generate the actual ABAQUS input file the Python script attaches two load steps at the end of the .txt file and stores the new file as an .inp file. The first step is a pre-loading step, in which the structure is subjected to a pre-load calculated using the following equation:

$${}^{i+1}\underset{\sim}{\boldsymbol{F}}_{\text{pre}} = {}^{i}\underset{\sim}{\boldsymbol{F}}_{\text{pre}} + k_r \, {}^{i}\lambda_1 \underset{\sim}{\boldsymbol{F}}_{\text{pert}} \tag{3.5}$$

with k_r as reduction factor and λ_1 as lowest eigenvalue of the buckling analysis. k_r is needed due to the fact that the critical load may be overestimated if the structure exhibits strongly nonlinear behavior . For all accompanying eigenvalue analysis used in the present

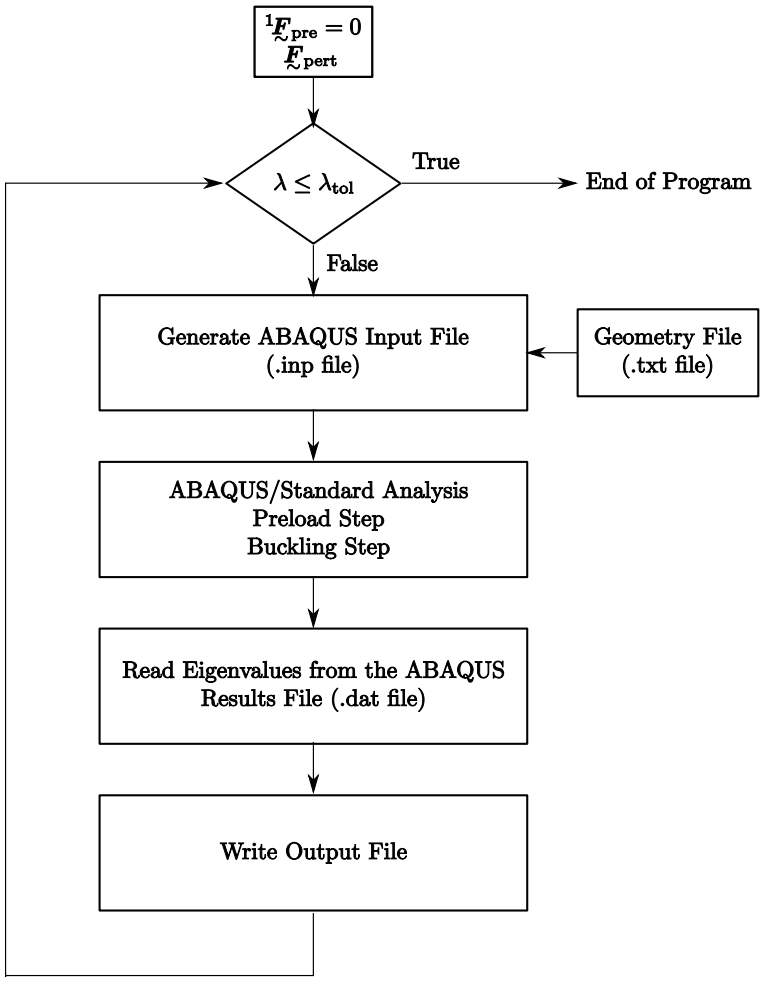

Figure 3.1: Accompanying linear eigenvalue analysis for a buckling type instability problem.

work, k_r is set to 0.7. For the first eigenvalue analysis step ${}^{1}\underset{\sim}{\boldsymbol{F}}_{\text{pre}} = 0.0$. The second step is an ABAQUS buckle step with $\underset{\sim}{\boldsymbol{F}}_{\text{pert}}$ as the corresponding perturbation load of the buckle step. $\underset{\sim}{\boldsymbol{F}}_{\text{pert}}$ is kept constant during the accompanying eigenvalue analysis and has to be specified by the user. If the eigenvalue of the current analysis step is greater than a user defined limit of λ_{tol}, then λ_1 is used to calculate ${}^{i+1}\underset{\sim}{\boldsymbol{F}}_{\text{pre}}$, and another preload/buckling analysis is started. The accompanying eigenvalue analysis proceeds until $\lambda_1 \leq \lambda_{\text{tol}}$. If $\lambda_1 \leq \lambda_{\text{tol}}$ and λ_{tol} is small enough one finds for the critical buckling load :

$$\underset{\sim}{\boldsymbol{F}}_{\text{crit}} \approx {}^{i}\underset{\sim}{\boldsymbol{F}}_{\text{pre}}. \tag{3.6}$$

.

4 Microscopic Onset-of-Failure

The ultimate failure mechanism of a ductile solid with a periodic microstructure can be related to a buckling type instability, see [27]. Therefore, the critical point on the loading path can be related to the occurrence of a bifurcation in the fundamental solution. The microscopic onset-of-failure concept presented in this chapter uses the Bloch Wave representation of the buckling eigenmode. By applying the Bloch Wave representation of the buckling eigenmode to periodic structures, the numerical effort for detecting the critical point on the loading path can be reduced significantly . The general mathematical theory of the microscopic onset-of-failure concept for periodic microstructures, presented in [27], is briefly described in Section 4.1, and the corresponding Finite element representation is presented in Section 4.2. In [27] the onset-of-failure concept and the corresponding Finite element discretization is presented for the case of a 2D unit cell, and in [17] this concept is applied to an open cell foam represented by a space-filling Kelvin Cell. In this chapter the microscopic onset-of-failure concept is given for a 2D unit cell. The 3D case emerges from the 2D case by extending the ranges of the used indices from $(1 \div 2)$ to $(1 \div 3)$.

4.1 General Theory

4.1.1 Total Lagrangian Formulation

For the problem description the total Lagrangian formulation is used. Therefore, the undeformed, stress free state is used as the reference state. Figure 4.1 shows a perfectly periodic micro structure on a domain V with boundary δV in its undeformed state. D is the characteristic cell (the fundamental building block) of this micro structure.

In the total Lagrangian formulation the initial position of a material point (p) is defined by the initial position vector $\underset{\sim}{\boldsymbol{X}}$ whereas the current position (p') of the same material point in the deformed configuration is identified by the current position vector $\underset{\sim}{\boldsymbol{x}}$ (see Figure 4.2).

The position vector of the current deformation state is a function of the initial position vector, namely:

$$\underset{\sim}{\boldsymbol{x}} = \underset{\sim}{\boldsymbol{\varphi}}(\underset{\sim}{\boldsymbol{X}}) \tag{4.1}$$

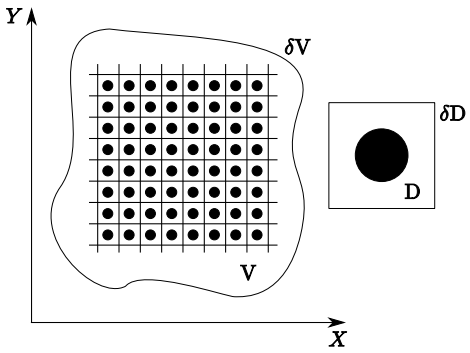

Figure 4.1: Infinite solid with a perfectly periodic micro structure and its fundamental building block (unit cell). Based on [27].

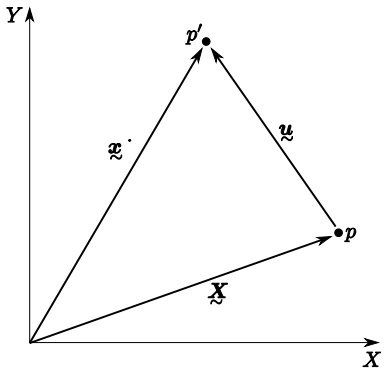

Figure 4.2: Position vectors of a material point in the undeformed and in the deformed state.

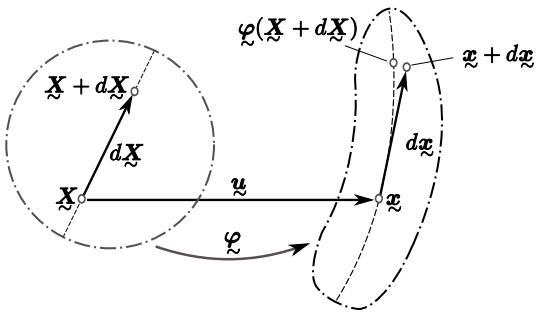

Figure 4.3: Line element in undeformed and deformed configuration. Based on [11]

With Equation (4.1) the displacement vector for the material point p can be written as:

$$\underset{\sim}{\boldsymbol{u}} = \underset{\sim}{\boldsymbol{x}} - \underset{\sim}{\boldsymbol{X}} = \underset{\sim}{\boldsymbol{\varphi}}(\underset{\sim}{\boldsymbol{X}}) - \underset{\sim}{\boldsymbol{X}} \tag{4.2}$$

In the initial configuration a small line element is defined by the vector $d\underset{\sim}{\boldsymbol{X}}$ with the starting point $\underset{\sim}{\boldsymbol{X}}$ and the ending point $\underset{\sim}{\boldsymbol{X}} + d\underset{\sim}{\boldsymbol{X}}$. For the same line element in the deformed configuration one can write (see Figure 4.3):

$$d\underset{\sim}{\boldsymbol{x}} = \underset{\sim}{\boldsymbol{\varphi}}(\underset{\sim}{\boldsymbol{X}} + d\underset{\sim}{\boldsymbol{X}}) - \underset{\sim}{\boldsymbol{\varphi}}(\underset{\sim}{\boldsymbol{X}}) \tag{4.3}$$

By expanding $\underset{\sim}{\boldsymbol{\varphi}}(\underset{\sim}{\boldsymbol{X}} + d\underset{\sim}{\boldsymbol{X}})$ in Equation (4.3) in a Taylor series one receives for $d\underset{\sim}{\boldsymbol{x}}$:

$$d\underset{\sim}{\boldsymbol{x}} \approx \frac{\partial \underset{\sim}{\boldsymbol{\varphi}}}{\partial \underset{\sim}{\boldsymbol{X}}} d\underset{\sim}{\boldsymbol{X}} = \underset{\approx}{\boldsymbol{F}} d\underset{\sim}{\boldsymbol{X}} \tag{4.4}$$

where $\underset{\approx}{\boldsymbol{F}}$ is the so called deformation gradient and defined as:

$$F_{ij} = \frac{\partial x_i}{\partial X_j} \quad \text{or} \quad \underset{\approx}{\boldsymbol{F}} = \frac{\partial \underset{\sim}{\boldsymbol{\varphi}}}{\partial \underset{\sim}{\boldsymbol{X}}} = \frac{\partial \underset{\sim}{\boldsymbol{x}}}{\partial \underset{\sim}{\boldsymbol{X}}} \tag{4.5}$$

For the 2D case one finds for $\underset{\approx}{\boldsymbol{F}}$:

$$\underset{\approx}{\boldsymbol{F}} = \begin{bmatrix} \frac{\partial x}{\partial X} & \frac{\partial x}{\partial Y} \\ \frac{\partial y}{\partial X} & \frac{\partial y}{\partial Y} \end{bmatrix} \tag{4.6}$$

The deformation gradient $\underset{\approx}{\boldsymbol{F}}$ defined at $\underset{\sim}{\boldsymbol{X}}$ describes the deformation field in the neighborhood of each point in a linearized sense.

4.1.2 The Incremental Tangent Moduli Tensor

In [27] the incrementally linear constitutive law for rate-independent materials is used. In index notation it can be written as:

$$\dot{P}_{ij}(\Lambda, \underset{\sim}{\boldsymbol{X}}) = L_{ijkl}(\Lambda, \underset{\sim}{\boldsymbol{X}})\dot{F}_{kl} \tag{4.7}$$

with

$$\dot{F}_{kl} = \dot{u}_{k,l} \tag{4.8}$$

where $\dot{\boldsymbol{P}}$ is the rate of the first Piola-Kirchhoff stress tensor and $\dot{\boldsymbol{F}}$ is the rate of the deformation gradient. The incrementally linear constitutive law depends on the loading state, which is expressed by a scalar quantity Λ called the load parameter. $\dot{\boldsymbol{F}}$ is a function of the displacement rate $\dot{\underset{\sim}{\boldsymbol{u}}}$. For the assumed quasi-static loading conditions all derivatives are taken with respect to any time-like parameter which increases monotonically with the loading process.

$\boldsymbol{L}$ is the incremental tangent moduli tensor. It depends on the material properties and the current equilibrium state described by a set of internal variables. $\boldsymbol{L}$ describes the material response in the neighborhood of $\underset{\sim}{\boldsymbol{X}}$ and is a periodic function with the same periodicity as the micro structure.

$$\boldsymbol{L}(\Lambda, X, Y) = \boldsymbol{L}(\Lambda, X + n_1 h_1, Y + n_2 h_2) \tag{4.9}$$

where n_i are arbitrary integers and h_i are the unit cell dimensions. Many rate-independent materials satisfy the major symmetry condition for the incremental moduli tensor $\boldsymbol{L}$:

$$L_{ijkl}(\Lambda, \underset{\sim}{\boldsymbol{X}}) = L_{klij}(\Lambda, \underset{\sim}{\boldsymbol{X}}) \tag{4.10}$$

We assume that the loading process produces a unique response. This loading path will be referred to as "principle equilibrium path". Any of these principle equilibrium loading paths can be parametrized with the load parameter Λ. All internal variables and stresses in the neighborhood of $\underset{\sim}{\boldsymbol{X}}$ are depending on Λ. For that reason the incremental moduli tensor $\boldsymbol{L}$ is only a function of the load parameter Λ and the initial position vector $\underset{\sim}{\boldsymbol{X}}$. This was already implicitly assumed in Equation (4.9) and (4.10).

4.1.3 Hill's Stability Criterion

Hill [18] was the first to deal with stability criteria for elasto-plastic solids on a mathematical foundation. Hill's stability criterion is based on the positive definiteness of a functional $\mathcal{F}_{\mathrm{V}}$, which, defined on a domain V, is quadratic in the virtual displacement rate field $\delta\dot{\underset{\sim}{\boldsymbol{u}}}$ (from [27]),

$$\mathcal{F}_{\mathrm{V}} = \int_V \delta\dot{\bar{u}}_{i,j} L_{ijkl}(\Lambda, \underset{\sim}{\boldsymbol{X}}) \delta\dot{u}_{k,l} dV \tag{4.11}$$

where $\delta\dot{\underset{\sim}{\boldsymbol{u}}}$ is the complex conjugate of $\delta\dot{\underset{\sim}{\boldsymbol{u}}}$. The minimum eigenvalue $\lambda(\Lambda)$ of this functional is defined as:

$$\lambda(\Lambda) = \min(\mathcal{F}_{\mathrm{V}}(\Lambda, \delta\dot{\underset{\sim}{\boldsymbol{u}}}) / \|\delta\dot{\underset{\sim}{\boldsymbol{u}}}\|_V^2) \tag{4.12}$$

with

$$\|\delta\dot{\underset{\sim}{\boldsymbol{u}}}\|_V^2 = \int_V \delta\dot{\bar{u}}_{m,n} \delta\dot{u}_{m,n} dV \tag{4.13}$$

As long as the minimum eigenvalue $\lambda(\Lambda)$ is positive, the deformed state, which depends on Λ, is stable. $\delta\dot{\underset{\sim}{\boldsymbol{u}}}$ must be continuous in V and vanish on those points of δV (see Figure 4.1) where the kinematic boundary conditions are applied. The major symmetry of the incremental moduli tensor $\boldsymbol{L}$ guarantees that all eigenvalues of $\mathcal{F}_V$ are real. Equations (4.11) to (4.13) are valid for solids of finite size. The corresponding equation for solids of infinite extent in $\Re^2$ is given by (from [27]):

$$(L_{ijkl}(\Lambda, \underset{\sim}{\boldsymbol{X}}) \delta\dot{u}_{k,l} - \lambda(\Lambda) \delta\dot{u}_{i,j})_{,j} = 0 \tag{4.14}$$

The extension to an infinite sized solid can be established by using only locally integrable, bounded functions $\delta\dot{\underset{\sim}{\boldsymbol{u}}}$ and increasing the size of the domain V to $\Re^2$.

It was shown by [13] that the eigenmodes $\delta\dot{\underset{\sim}{\boldsymbol{u}}}(\Lambda)$ of Equation (4.14) can be expressed as:

$$\delta\dot{\underset{\sim}{\boldsymbol{u}}} = \underset{\sim}{\boldsymbol{p}} \exp[i(\frac{m_1}{h_1} X + \frac{m_2}{h2} Y)] \tag{4.15}$$

with $\underset{\sim}{\boldsymbol{p}}$ as an arbitrary periodic function defined on the domain D, and $\underset{\sim}{\boldsymbol{p}}\exp[i(\frac{m_1}{h_1}X + \frac{m_2}{h2}Y)]$ as the Bloch Wave representation of the buckling eigenmodes. Because of the periodicity, the search for the minimum eigenvalue λ of $\mathcal{F}_{\mathrm{V}}$ for all bounded functions $\delta\dot{\underset{\sim}{\boldsymbol{u}}}$ is reduced to the search of the minimum eigenvalue of the functional, $\mathcal{F}_{\mathrm{D}}$ defined on D. For the

minimum eigenvalue corresponding to this functional one receives with $\underset{\sim}{\boldsymbol{m}} = \{m_1, m_2\}^{\mathrm{T}}$ as vector of the wave numbers:

$$\lambda(\Lambda) = \inf_{\underset{\sim}{\boldsymbol{m}}}[\gamma(\Lambda, \underset{\sim}{\boldsymbol{m}})] \tag{4.16}$$

with (see [27])

$$\gamma(\Lambda, \underset{\sim}{\boldsymbol{m}}) = \min_{\underset{\sim}{\boldsymbol{p}}}[\mathcal{F}_{\mathrm{D}}(\Lambda, \underset{\sim}{\boldsymbol{p}}\exp[i(\frac{m_1}{h_1}X + \frac{m_2}{h2}Y)])/\|\underset{\sim}{\boldsymbol{p}}\exp[i(\frac{m_1}{h_1}X + \frac{m_2}{h2}Y)]\|^2_{\mathrm{D}}]. \tag{4.17}$$

$\inf(A)$ is the infimum (greatest lower bound) of a subset A containing real numbers and is defined as the biggest real number that is smaller than, or equal to, all numbers of the subset A. If A has no lower bound then $\inf(A) = -\infty$, or if A is empty than $\inf(A) = \infty$ (by definition). If A has a smallest element, e.g., $\inf\{3, 7, 9\} = 3$ then the smallest element is the infimum of the subset A. The infimum of a set of real numbers A does not have to belong to the set, e.g., $\inf\{y \in \Re : 0.2 < y < 1\} = 0.2$.

Integration in Equations (4.11) and (4.13) is now performed over the domain D instead of the larger domain V. To find the minimum eigenvalue one has to scan over all possible periodic functions $\underset{\sim}{\boldsymbol{p}}$ on the domain D and over all combinations of m_1 and m_2. For $\forall m_i = 0$, γ may have a singular point. For that reason the inf-symbol was used for the minimization over $\underset{\sim}{\boldsymbol{m}}$.

4.1.4 Solution Procedure

The solution procedure starts with the undeformed solid in a stress free state. At this point of the loading path $\lambda(\Lambda) > 0$. The load parameter Λ is now increased monotonically. While increasing Λ one can see that $\lambda(\Lambda)$ decreases. If $\lambda(\Lambda_{\mathrm{c}}) = 0$ the critical state is established. Λ_{c} is the critical load parameter corresponding to this state. At this point of the loading path a bifurcation of the fundamental solution occurs. At the critical state the following conditions must be satisfied (see also [27]):

$$\begin{aligned} \lambda(\Lambda_{\mathrm{c}}) &= 0, \qquad \Lambda_{\mathrm{c}} = \inf_{\underset{\sim}{\boldsymbol{m}}}[\Lambda_{\mathrm{m}}(\underset{\sim}{\boldsymbol{m}})] \\ \gamma(\Lambda_{\mathrm{m}}(\underset{\sim}{\boldsymbol{m}}), \underset{\sim}{\boldsymbol{m}}) &= 0, \qquad \gamma(\Lambda, \underset{\sim}{\boldsymbol{m}}) > 0 \qquad \text{for} \quad 0 \le \Lambda < \Lambda_{\mathrm{m}} \end{aligned} \tag{4.18}$$

with Λ_m being the lowest value for which $\gamma(\Lambda(\underset{\sim}{\boldsymbol{m}}), \underset{\sim}{\boldsymbol{m}}) = 0$ is possible for fixed $\underset{\sim}{\boldsymbol{m}}$. The search for Λ_c is equal to the search of the lowest point on the surface $\Lambda_m(\underset{\sim}{\boldsymbol{m}})$ in a Λ_m versus m_1, m_2 graph. The onset-of-failure surface is now defined as the locus of all macroscopic stresses or strains corresponding to Λ_c on all possible loading paths emerging from the undeformed basis state.

With Equation (4.15) one can see that in the neighborhood of $\forall m_i = 0$ two different modes coexist: the strictly periodic mode for $\forall m_i = 0$, $\delta\dot{\underset{\sim}{\boldsymbol{u}}} = \underset{\sim}{\boldsymbol{p}}$ and the long wave length mode for one $m_i \to 0$, $\delta\dot{\underset{\sim}{\boldsymbol{u}}} \neq \underset{\sim}{\boldsymbol{p}}$. This is the physical reason for the singularity in the neighborhood of $\forall m_i = 0$ on the surface $\Lambda_m(\underset{\sim}{\boldsymbol{m}})$.

4.1.5 Eigenmodes

As mentioned above Λ_c is the lowest point of the surface $\Lambda_m(\underset{\sim}{\boldsymbol{m}})$:

$$\Lambda_c = \Lambda_m(\underset{\sim}{\boldsymbol{m}}_c) \tag{4.19}$$

For $\forall m_{ic} \neq 0$ the corresponding eigenmodes are local and show a periodicity that involves multiple base cells. If one $m_{ic} \to 0$ is a regular point on the surface $\Lambda_m(m_i)$ the existing mode is still local, but if the limit of one $m_{ic} \to 0$ has a singularity on this surface the corresponding mode is global in nature. If there exists a global buckling mode it can be detected by a computationally less expensive procedure which will be described in Chapter 5.

For $\forall m_{ic} = 0$ the eigenmode is strictly periodic to the cell. For this case the Bloch Wave analysis program has to be adapted in a way that this singularity can be handled without problems (see Appendix A.3).

4.2 F.E.M. Discretization

This section deals with the most general case of 3D unit cells. The used unit cells are discretized using displacement finite elements. One may use structural or continuum elements for discretization. With the present implementation of the Bloch Wave Analysis Program these two element types must not be mixed within one unit cell.

Appropriate periodic boundary conditions (see Section 2.1) must be applied to the cell. The calculation of the principal load path is done by using a standard incremental Newton-

Raphson algorithm. For each equilibrium state along the loading path ABAQUS provides the stiffness matrices[1] of all elements in the unit cell. The unconstrained, incremental tangent stiffness matrix of the unit cell $\underset{\approx}{\boldsymbol{K}}(\Lambda)$ can be assembled in a straight forward manner.

As shown in Section 4.1 the critical state is established when the quadratic stability functional $\mathcal{F}_{\mathrm{D}}(\Lambda, \delta\underset{\sim}{\boldsymbol{u}})$ looses its positive definiteness, i.e., its minimum eigenvalue $\lambda(\Lambda_{\mathrm{c}}) = 0$. Λ_{c} is the lowest value of the load parameter Λ for which a critical state is found to occur. Along the loading path one finds:

$$\lambda(\Lambda) > 0 \qquad \text{for} \qquad 0 \leq \Lambda < \Lambda_{\mathrm{c}} \tag{4.20}$$

In [27] the quadratic form F_{D} corresponding to $\mathcal{F}_{\mathrm{D}}$ is used for the finite element discretization. The critical load parameter is reached, if $F_{\mathrm{D}}(\Lambda, \delta\underset{\sim}{\boldsymbol{u}})$ has a zero eigenvalue, where

$$F_{\mathrm{D}}(\Lambda, \delta\underset{\sim}{\boldsymbol{u}}) = \delta\bar{\underset{\sim}{\boldsymbol{u}}}^{\mathrm{T}}\underset{\approx}{\boldsymbol{K}}(\Lambda)\delta\underset{\sim}{\boldsymbol{u}} \tag{4.21}$$

with $\delta\underset{\sim}{\boldsymbol{u}}$ as the nodal displacement perturbation vector corresponding to the critical eigenmode of the structure and $\underset{\approx}{\boldsymbol{K}}(\Lambda)$ as the unconstrained, incremental tangent stiffness matrix corresponding to the discretization of the unit cell. $\underset{\approx}{\boldsymbol{K}}(\Lambda)$ depends only on the dimensionless load parameter Λ. $\delta\bar{\underset{\sim}{\boldsymbol{u}}}$ is the conjugate complex of $\delta\underset{\sim}{\boldsymbol{u}}$. Using the Bloch Wave representation of the buckling eigenmode the critical eigenmode (see Section 4.1) of a periodic micro structure can be expressed as

$$\delta\underset{\sim}{\boldsymbol{u}}(\underset{\sim}{\boldsymbol{X}}) = \underset{\sim}{\boldsymbol{U}}(\underset{\sim}{\boldsymbol{X}})\exp[i(\frac{m_1}{h_1}X + \frac{m_2}{h_2}Y + \frac{m_3}{h_3}Z)] \tag{4.22}$$

Where $\underset{\sim}{\boldsymbol{U}}(\underset{\sim}{\boldsymbol{X}})$ is a periodic function with the same periodicity as the unit cell:

$$\underset{\sim}{\boldsymbol{U}}(X + n_1h_1, Y + n_2h_2, Z + n_3h_3) = \underset{\sim}{\boldsymbol{U}}(X, Y, Z) \tag{4.23}$$

where h_i are the cell dimensions and n_i are arbitrary integers.

Therefore, the search for the critical state requires the consideration of all possible dimen-

[1] ABAQUS-Syntax (Version 6.7.4):
*STEP
*STATIC
...
*ELEMENT MATRIX OUTPUT, ELSET= myelementset ,STIFFNESS=YES, OUTPUT FILE=USER DEFINED, FILE NAME=mymtxfile , FREQUENCY = 1,
*END STEP

sionless wave numbers m_i. For large stiffness matrices and a reasonably fine scanning grid for the wave numbers this procedure can be daunting. An algorithm to reduce the size of the stiffness matrix is presented in [27] and [17], and will be outlined in the following.

The components of the nodal displacement perturbation vector $\delta\underset{\sim}{\boldsymbol{u}}$ are not independent of each other. They must satisfy the relationship given in Equation (4.23). It was observed that only the deformations of the boundary nodes need to be coupled in the Bloch Wave calculations, therefore the internal nodes can be condensed out. The index notation of the matrices is taken according to the indices used in [17], where $\bullet_1$ denotes independent (master) nodal quantities, $\bullet_2$ describes dependent (slave) nodal quantities on the unit cell boundary and $\bullet_{\mathrm{I}}$ characterizes dependent nodal quantities assigned to interior nodes.

With $\delta\underset{\sim}{\boldsymbol{u}} = \{\delta\underset{\sim}{\boldsymbol{u}}_1, \delta\underset{\sim}{\boldsymbol{u}}_2, \delta\underset{\sim}{\boldsymbol{u}}_{\mathrm{I}}\}$ and with $\delta\underset{\sim}{\boldsymbol{F}} = \{\delta\underset{\sim}{\boldsymbol{F}}_1, \delta\underset{\sim}{\boldsymbol{F}}_2, \delta\underset{\sim}{\boldsymbol{F}}_{\mathrm{I}}\}$ as corresponding force vector the incremental equilibrium condition

$$\underset{\approx}{\boldsymbol{K}}(\Lambda)\delta\underset{\sim}{\boldsymbol{u}} = \delta\underset{\sim}{\boldsymbol{F}} \tag{4.24}$$

can be written as

$$\begin{bmatrix} \underset{\approx}{\boldsymbol{K}}_{11} & \underset{\approx}{\boldsymbol{K}}_{12} & \underset{\approx}{\boldsymbol{K}}_{1\mathrm{I}} \\ \underset{\approx}{\boldsymbol{K}}_{21} & \underset{\approx}{\boldsymbol{K}}_{22} & \underset{\approx}{\boldsymbol{K}}_{2\mathrm{I}} \\ \underset{\approx}{\boldsymbol{K}}_{\mathrm{I}1} & \underset{\approx}{\boldsymbol{K}}_{\mathrm{I}2} & \underset{\approx}{\boldsymbol{K}}_{\mathrm{II}} \end{bmatrix} \begin{pmatrix} \delta\underset{\sim}{\boldsymbol{u}}_1 \\ \delta\underset{\sim}{\boldsymbol{u}}_2 \\ \delta\underset{\sim}{\boldsymbol{u}}_{\mathrm{I}} \end{pmatrix} = \begin{pmatrix} \delta\underset{\sim}{\boldsymbol{F}}_1 \\ \delta\underset{\sim}{\boldsymbol{F}}_2 \\ \delta\underset{\sim}{\boldsymbol{F}}_{\mathrm{I}} \end{pmatrix} . \tag{4.25}$$

The partition of the tangent stiffness matrix $\underset{\approx}{\boldsymbol{K}}(\Lambda)$ is implied by the partition of the nodal displacement vector $\delta\underset{\sim}{\boldsymbol{u}}$. $\delta\underset{\sim}{\boldsymbol{u}}_1$ is the displacement perturbation vector of the master nodes for the Bloch Wave method (BW master) and $\delta\underset{\sim}{\boldsymbol{u}}_2$ is the corresponding displacement perturbation vector for the slaved nodes (BW slave). These BW master and BW slave nodes can be different from those defined for the periodic boundary conditions. The displacement perturbation vector of the internal nodes is represented by the vector $\delta\underset{\sim}{\boldsymbol{u}}_{\mathrm{I}}$. With $\delta\underset{\sim}{\boldsymbol{F}}_{\mathrm{I}} = \underset{\sim}{\boldsymbol{0}}$ the internal displacement vector can be evaluated from (4.25) as

$$\delta\underset{\sim}{\boldsymbol{u}}_{\mathrm{I}} = -\underset{\approx}{\boldsymbol{K}}_{\mathrm{II}}^{-1}[\underset{\approx}{\boldsymbol{K}}_{\mathrm{I}1}\delta\underset{\sim}{\boldsymbol{u}}_1 + \underset{\approx}{\boldsymbol{K}}_{\mathrm{I}2}\delta\underset{\sim}{\boldsymbol{u}}_2] \tag{4.26}$$

Substituting (4.26) in (4.25) one receives:

$$\begin{bmatrix} \hat{\underset{\approx}{\boldsymbol{K}}}_{11} & \hat{\underset{\approx}{\boldsymbol{K}}}_{12} \\ \hat{\underset{\approx}{\boldsymbol{K}}}_{21} & \hat{\underset{\approx}{\boldsymbol{K}}}_{22} \end{bmatrix} \begin{pmatrix} \delta\underset{\sim}{\boldsymbol{u}}_1 \\ \delta\underset{\sim}{\boldsymbol{u}}_2 \end{pmatrix} = \begin{pmatrix} \delta\underset{\sim}{\boldsymbol{F}}_1 \\ \delta\underset{\sim}{\boldsymbol{F}}_2 \end{pmatrix} \tag{4.27}$$

with

$$\hat{\underset{\approx}{\boldsymbol{K}}}_{11} = \underset{\approx}{\boldsymbol{K}}_{11} - \underset{\approx}{\boldsymbol{K}}_{1\mathrm{I}} \underset{\approx}{\boldsymbol{K}}_{\mathrm{II}}^{-1} \underset{\approx}{\boldsymbol{K}}_{\mathrm{I}1} \tag{4.28}$$

$$\hat{\underset{\approx}{\boldsymbol{K}}}_{12} = \underset{\approx}{\boldsymbol{K}}_{12} - \underset{\approx}{\boldsymbol{K}}_{1\mathrm{I}} \underset{\approx}{\boldsymbol{K}}_{\mathrm{II}}^{-1} \underset{\approx}{\boldsymbol{K}}_{\mathrm{I}2} \tag{4.29}$$

$$\hat{\underset{\approx}{\boldsymbol{K}}}_{21} = \underset{\approx}{\boldsymbol{K}}_{21} - \underset{\approx}{\boldsymbol{K}}_{2\mathrm{I}} \underset{\approx}{\boldsymbol{K}}_{\mathrm{II}}^{-1} \underset{\approx}{\boldsymbol{K}}_{\mathrm{I}1} \tag{4.30}$$

$$\hat{\underset{\approx}{\boldsymbol{K}}}_{22} = \underset{\approx}{\boldsymbol{K}}_{22} - \underset{\approx}{\boldsymbol{K}}_{2\mathrm{I}} \underset{\approx}{\boldsymbol{K}}_{\mathrm{II}}^{-1} \underset{\approx}{\boldsymbol{K}}_{\mathrm{I}2} \quad . \tag{4.31}$$

The displacements of the master vector $\delta\underset{\sim}{\boldsymbol{u}}_1$ and the slave vector $\delta\underset{\sim}{\boldsymbol{u}}_2$ are coupled via Equation (4.22). Therefore, $\delta\underset{\sim}{\boldsymbol{u}}_2$ can be written as:

$$\delta\underset{\sim}{\boldsymbol{u}}_2 = \underset{\approx}{\boldsymbol{\nu}} \delta\underset{\sim}{\boldsymbol{u}}_1 \quad . \tag{4.32}$$

The matrix $\underset{\approx}{\boldsymbol{\nu}}$ couples the displacements of the master and slave nodes in the Bloch Wave analysis. The non zero entries of this matrix are functions of the wave numbers m_i. The matrix will be referred to as "wave matrix". In the following subsections the wave matrix and the coupling equations will be given for a 2D and a 3D unit cell, respectively.

With Equation (4.32) and

$$\delta\bar{\underset{\sim}{\boldsymbol{u}}}_2^{\mathrm{T}} = \delta\bar{\underset{\sim}{\boldsymbol{u}}}_1^{\mathrm{T}} \bar{\underset{\approx}{\boldsymbol{\nu}}}^{\mathrm{T}} \tag{4.33}$$

one can show that, at the loss of positive definiteness of the quadratic form, F_{D} can be equivalently expressed involving only $\delta\underset{\sim}{\boldsymbol{u}}_1$:

$$F_{\mathrm{D}}(\Lambda, \underset{\sim}{\boldsymbol{m}}) = \delta\bar{\underset{\sim}{\boldsymbol{u}}}_1^{\mathrm{T}} \mathring{\underset{\approx}{\boldsymbol{K}}} \delta\underset{\sim}{\boldsymbol{u}}_1 \tag{4.34}$$

where

$$\mathring{\underset{\approx}{\boldsymbol{K}}} = \hat{\underset{\approx}{\boldsymbol{K}}}_{11} + \hat{\underset{\approx}{\boldsymbol{K}}}_{12} \underset{\approx}{\boldsymbol{\nu}} + \bar{\underset{\approx}{\boldsymbol{\nu}}}^{\mathrm{T}} \hat{\underset{\approx}{\boldsymbol{K}}}_{21} + \bar{\underset{\approx}{\boldsymbol{\nu}}}^{\mathrm{T}} \hat{\underset{\approx}{\boldsymbol{K}}}_{22} \underset{\approx}{\boldsymbol{\nu}}. \tag{4.35}$$

For the special case of $\forall m_i = 0$, Equation (4.34) must be constrained against rigid body translation (see Appendix A.3). F_{D} loses its positive definiteness when the Hermitian matrix $\mathring{\underset{\approx}{\boldsymbol{K}}}$ becomes positive semi definite (its lowest eigenvalue is equal to zero).

The algorithm for detecting the critical state proceeds the following way: For each increment, $\mathring{\underset{\approx}{\boldsymbol{K}}}$ is constructed for all combinations of the wave numbers m_1, m_2, and m_3 on a reasonably fine grid. If there exists a critical combination of these wave numbers

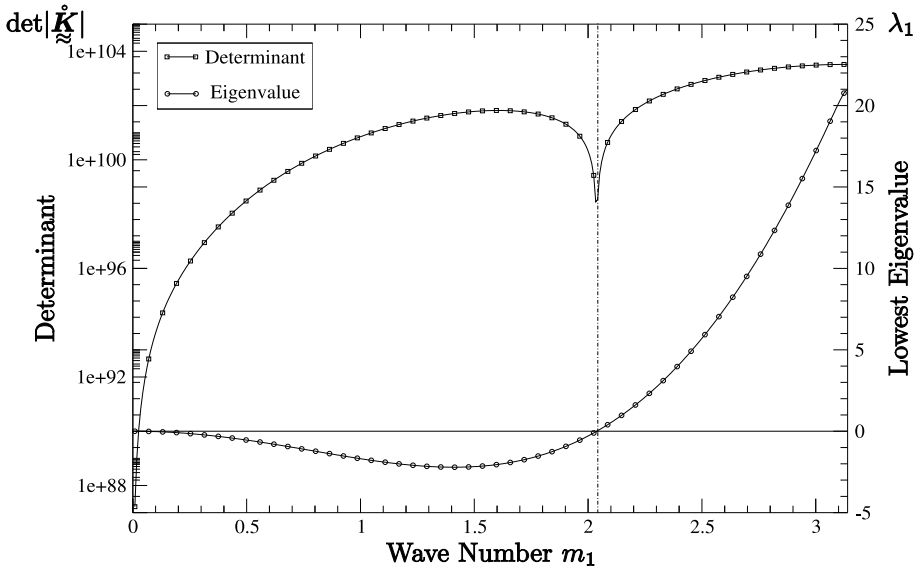

Figure 4.4: Determinant and lowest eigenvalue of the reduced stiffness matrix plotted against the wave number.

(m_{1c}, m_{2c}, m_{3c}) for which the lowest eigenvalue of $\mathring{\underset{\approx}{K}}$ is zero, the critical state is established. The critical load parameter Λ_c is the lowest value of Λ for which this criterion is fulfilled.

In [17] the stability criterion is formulated using $\det|\mathring{\underset{\approx}{K}}| = 0$. Similar to the method described above the reduced stiffness matrix $\mathring{\underset{\approx}{K}}$ is constructed for all possible combinations of the wave numbers m_1, m_2 and m_3 for each increment. If the critical state is established then a critical combination of these wave numbers exists (m_{1c}, m_{2c}, m_{3c}) and $\det|\mathring{\underset{\approx}{K}}| = 0$ is fulfilled. In practice this method appears to work only for reduced stiffness matrices for which the determinant changes its sign at (m_{1c}, m_{2c}, m_{3c}) when the critical state $(\Lambda = \Lambda_c)$ is reached.

Figure 4.4 shows the progression of the determinant $\det|\mathring{\underset{\approx}{K}}|$ and the lowest eigenvalue λ of the reduced stiffness matrix over the wave number m_1 for a Kelvin Cell (see Section 6) subjected to compressive loading in rise direction. The values of the determinant are rather high. Due to the imperfect numerical resolution of the scan of the m_1 range, $\det|\mathring{\underset{\approx}{K}}| = 0$ (no change in sign of $\det|\mathring{\underset{\approx}{K}}|$) is not reached within the whole analysis, although the determinant has a significant drop around the critical wave number. The apex in the determinant progression is found to occur for a vanishing lowest eigenvalue of the reduced stiffness matrix, $\lambda_1 = 0$ (see Section 4.4). The reason for this behavior can be found in the structural symmetry of the Kelvin Cell. The two principal directions normal to

the rise direction are equivalent in their mechanical behavior. Therefore, the first two eigenvalues change their signs simultaneously. For this reason $\det|\mathring{\underset{\approx}{\boldsymbol{K}}}|$ always remains positive. Thus, the search for the critical state is implemented based on the criterion of the lowest eigenvalue being zero (changing its sign).

4.2.1 Wave Matrix of a 2D Unit Cell

In Figure 4.5 a 2D unit cell is shown. The naming convention for the side and corner node sets is taken from [10]. W (West), E (East) and SW (South West) are the master node sets for the Bloch Wave analysis (BWA). The arrows show which node sets (BWA slaved node sets) are coupled to these BWA master node sets . In the following sections the variables, listed below will be used:

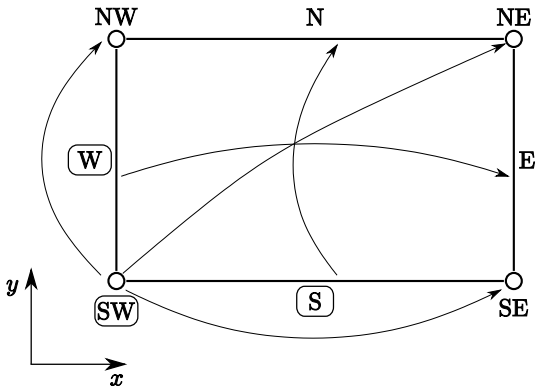

Figure 4.5: 2D Unit Cell.

n_{dof}	...	Nodal degrees of freedom, $n_{\mathrm{dof}} = 6$, $n_{\mathrm{dof}} = 5$, $n_{\mathrm{dof}} = 3$, or $n_{\mathrm{dof}} = 2$ depending on the element type and the dimensionality of the problem.
n_{W}	...	Number of nodes on the west side of the cell
n_{E}	...	Number of nodes on the east side of the cell
n_{S}	...	Number of nodes on the south side of the cell
n_{N}	...	Number of nodes on the north side of the cell
n_{cm}	...	Number of master corner nodes (1 or 0)
n_{cs}	...	Number of slaved corner nodes
m_{W}	...	Number of master degrees of freedom on the west side
m_{S}	...	Number of master DOFs on the south side
m_{SW}	...	Number of master DOFs in the south west corner
s_{E}	...	Number of slaved DOFs on the east side
s_{N}	...	Number of slaved DOFs on the north side
s_{c}	...	Number of slaved corner DOFs
m	...	Number of master DOFs of the cell
s	...	Number of slaved DOFs of the cell

Note, that with the current implementation of the program structural and continuum elements must not be mixed. Each node on the slaved side must have a master node on the opposite side of the cell whereas it is not necessary that each node on the master side has a corresponding slave node. An example for this case will be given in Section 4.2.2. This leads to the following relations for the 2D cell:

$$n_{\mathrm{W}} \geq n_{\mathrm{E}} \tag{4.36}$$

$$n_{\mathrm{S}} \geq n_{\mathrm{N}} \tag{4.37}$$

The same scheme can be applied for the corner nodes. If the cell has a master node in the SW corner ($n_{\mathrm{cm}} = 1$) at least two of the other three corner nodes (SE, NE, NW) must

exist. For the number of slaved corner nodes therefore, one can write:

$$n_{\mathrm{cs}} = 2, \qquad \text{or} \qquad n_{\mathrm{cs}} = 3. \tag{4.38}$$

If SW exists, other values for n_{cs} are not possible in the 2D case. If SW does not exist ($n_{\mathrm{cm}} = 0$), then the other corner nodes in the cell must not (!) exist. Therefore, $n_{\mathrm{cs}} = 0$.

The number of master DOFs m and slaved DOFs s in the unit cell can be evaluated as:

$$m = m_{\mathrm{W}} + m_{\mathrm{S}} + m_{\mathrm{SW}} \tag{4.39}$$

$$s = s_{\mathrm{E}} + s_{\mathrm{N}} + s_{\mathrm{c}} \tag{4.40}$$

where

$$\begin{aligned} m_{\mathrm{W}} &= s_{\mathrm{E}} = n_{\mathrm{E}} n_{\mathrm{dof}} \\ m_{\mathrm{S}} &= s_{\mathrm{N}} = n_{\mathrm{N}} n_{\mathrm{dof}} \\ m_{\mathrm{SW}} &= n_{\mathrm{cm}} n_{\mathrm{dof}} \\ s_{\mathrm{c}} &= n_{\mathrm{cs}} n_{\mathrm{dof}} \end{aligned} \tag{4.41}$$

Those nodes on the master sides, that do not have a corresponding slave node, are counted as internal nodes.

With $\delta\underset{\sim}{\boldsymbol{u}}_1 = \{\delta\underset{\sim}{\boldsymbol{u}}_{\mathrm{W}}, \delta\underset{\sim}{\boldsymbol{u}}_{\mathrm{S}}, \delta\underset{\sim}{\boldsymbol{u}}_{\mathrm{SW}}\}^{\mathrm{T}}$ as the displacement perturbation vector of the master nodes and $\delta\underset{\sim}{\boldsymbol{u}}_2 = \{\delta\underset{\sim}{\boldsymbol{u}}_{\mathrm{E}}, \delta\underset{\sim}{\boldsymbol{u}}_{\mathrm{N}}, \delta\underset{\sim}{\boldsymbol{u}}_{\mathrm{SE}}, \delta\underset{\sim}{\boldsymbol{u}}_{\mathrm{NW}}, \delta\underset{\sim}{\boldsymbol{u}}_{\mathrm{NE}}\}^{\mathrm{T}}$ as the displacement perturbation vector of the slaved nodes, the Bloch Wave relations between the boundary nodes can be written as:

$$\begin{aligned} \delta\underset{\sim}{\boldsymbol{u}}_{\mathrm{E}} &= \exp[im_1]\delta\underset{\sim}{\boldsymbol{u}}_{\mathrm{W}} \\ \delta\underset{\sim}{\boldsymbol{u}}_{\mathrm{N}} &= \exp[im_2]\delta\underset{\sim}{\boldsymbol{u}}_{\mathrm{S}} \\ \delta\underset{\sim}{\boldsymbol{u}}_{\mathrm{SE}} &= \exp[im_1]\delta\underset{\sim}{\boldsymbol{u}}_{\mathrm{SW}} \\ \delta\underset{\sim}{\boldsymbol{u}}_{\mathrm{NW}} &= \exp[im_2]\delta\underset{\sim}{\boldsymbol{u}}_{\mathrm{SW}} \\ \delta\underset{\sim}{\boldsymbol{u}}_{\mathrm{NE}} &= \exp[i(m_1+m_2)]\delta\underset{\sim}{\boldsymbol{u}}_{\mathrm{SW}} \end{aligned} \tag{4.42}$$

With (4.42) and (4.32) one finds for the wave matrix $\underset{\approx}{\boldsymbol{\nu}}$:

$$\underset{\approx}{\boldsymbol{\nu}} = \begin{bmatrix} \underset{\approx}{\boldsymbol{I}}_1 \exp[im_1] & \underset{\approx}{\mathbf{0}} & \underset{\approx}{\mathbf{0}} \\ \underset{\approx}{\mathbf{0}} & \underset{\approx}{\boldsymbol{I}}_2 \exp[im_2] & \underset{\approx}{\mathbf{0}} \\ \underset{\approx}{\mathbf{0}} & \underset{\approx}{\mathbf{0}} & \underset{\approx}{\boldsymbol{I}}_3 \exp[im_1] \\ \underset{\approx}{\mathbf{0}} & \underset{\approx}{\mathbf{0}} & \underset{\approx}{\boldsymbol{I}}_3 \exp[im_2] \\ \underset{\approx}{\mathbf{0}} & \underset{\approx}{\mathbf{0}} & \underset{\approx}{\boldsymbol{I}}_3 \exp[i(m_1+m_2)] \end{bmatrix} \tag{4.43}$$

where

$$\begin{aligned} \dim(\underset{\approx}{\boldsymbol{\nu}}) &= (s \times m) \\ \dim(\underset{\approx}{\boldsymbol{I}}_1) &= (s_{\mathrm{E}} \times m_{\mathrm{W}}), \quad s_{\mathrm{E}} = m_{\mathrm{W}} \\ \dim(\underset{\approx}{\boldsymbol{I}}_2) &= (s_{\mathrm{N}} \times m_{\mathrm{S}}), \quad s_{\mathrm{N}} = m_{\mathrm{S}} \\ \dim(\underset{\approx}{\boldsymbol{I}}_3) &= (m_{\mathrm{SW}} \times m_{\mathrm{SW}}) \end{aligned} \tag{4.44}$$

with $\underset{\approx}{\boldsymbol{I}}_i$ as identity matrices with the given dimensions.

4.2.2 Wave Matrix of a 3D Unit Cell

The naming convention for the node sets of the 3D unit cell is taken from [10]. Figure 4.6 shows a 3D unit cell. W (West), S (South), B(Bottom), SW (South West), SB (South Bottom), WB (West Bottom) and SWB (South West Bottom) are the master node sets for the Bloch Wave analysis. For clarity, only the coupling conditions between the corner nodes are marked with arrows.

With $\delta\underset{\sim}{\boldsymbol{u}}_1 = \{\delta\underset{\sim}{\boldsymbol{u}}_{\mathrm{W}}, \delta\underset{\sim}{\boldsymbol{u}}_{\mathrm{S}}, \delta\underset{\sim}{\boldsymbol{u}}_{\mathrm{B}}, \delta\underset{\sim}{\boldsymbol{u}}_{\mathrm{SB}}, \delta\underset{\sim}{\boldsymbol{u}}_{\mathrm{WB}}, \delta\underset{\sim}{\boldsymbol{u}}_{\mathrm{SW}}, \delta\underset{\sim}{\boldsymbol{u}}_{\mathrm{SWB}}\}^{\mathrm{T}}$ as the displacement perturbation vector of the master nodes and

$$\begin{aligned} \delta\underset{\sim}{\boldsymbol{u}}_2 = \{&\delta\underset{\sim}{\boldsymbol{u}}_{\mathrm{E}}, \delta\underset{\sim}{\boldsymbol{u}}_{\mathrm{N}}, \delta\underset{\sim}{\boldsymbol{u}}_{\mathrm{T}}, \delta\underset{\sim}{\boldsymbol{u}}_{\mathrm{NB}}, \delta\underset{\sim}{\boldsymbol{u}}_{\mathrm{ST}}, \delta\underset{\sim}{\boldsymbol{u}}_{\mathrm{NT}}, \delta\underset{\sim}{\boldsymbol{u}}_{\mathrm{EB}}, \delta\underset{\sim}{\boldsymbol{u}}_{\mathrm{WT}}, \delta\underset{\sim}{\boldsymbol{u}}_{\mathrm{ET}}, \delta\underset{\sim}{\boldsymbol{u}}_{\mathrm{SE}}, \delta\underset{\sim}{\boldsymbol{u}}_{\mathrm{NW}}, \\ &\delta\underset{\sim}{\boldsymbol{u}}_{\mathrm{NE}}, \delta\underset{\sim}{\boldsymbol{u}}_{\mathrm{SEB}}, \delta\underset{\sim}{\boldsymbol{u}}_{\mathrm{NEB}}, \delta\underset{\sim}{\boldsymbol{u}}_{\mathrm{NWB}}, \delta\underset{\sim}{\boldsymbol{u}}_{\mathrm{SWT}}, \delta\underset{\sim}{\boldsymbol{u}}_{\mathrm{SET}}, \delta\underset{\sim}{\boldsymbol{u}}_{\mathrm{NET}}, \delta\underset{\sim}{\boldsymbol{u}}_{\mathrm{NWT}}\}^{\mathrm{T}} \end{aligned} \tag{4.45}$$

as the displacement perturbation vector of the slaved nodes, the Bloch Wave relations

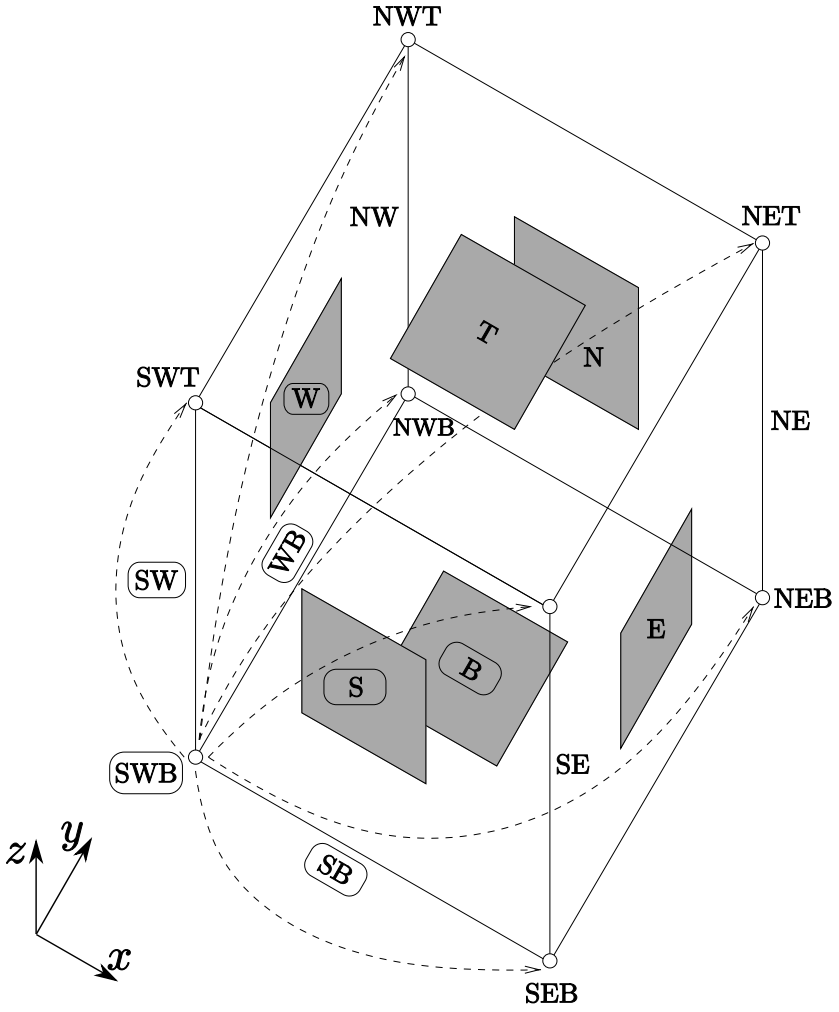

Figure 4.6: 3D Unit Cell. Coupling conditions between corner nodes marked with arrows.

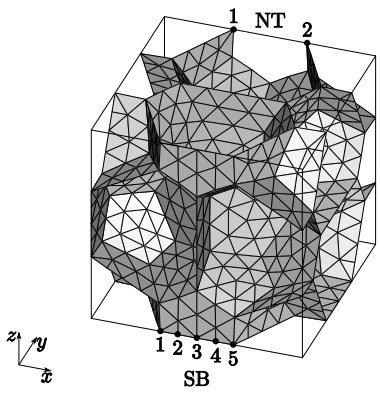

Figure 4.7: Weaire-Phelan unit cell showing different numbers of edge nodes. From Bitsche 2005 [6](modified).

between the boundary nodes can be written as:

$$
\begin{aligned}
&\delta\underset{\sim}{\boldsymbol{u}}_{\mathrm{E}} = \exp[im_1]\delta\underset{\sim}{\boldsymbol{u}}_{\mathrm{W}},\ \delta\underset{\sim}{\boldsymbol{u}}_{\mathrm{N}} = \exp[im_2]\delta\underset{\sim}{\boldsymbol{u}}_{\mathrm{S}},\ \delta\underset{\sim}{\boldsymbol{u}}_{\mathrm{T}} = \exp[im_3]\delta\underset{\sim}{\boldsymbol{u}}_{\mathrm{B}}\\
&\delta\underset{\sim}{\boldsymbol{u}}_{\mathrm{NB}} = \exp[im_2]\delta\underset{\sim}{\boldsymbol{u}}_{\mathrm{SB}},\ \delta\underset{\sim}{\boldsymbol{u}}_{\mathrm{ST}} = \exp[im_3]\delta\underset{\sim}{\boldsymbol{u}}_{\mathrm{SB}},\ \delta\underset{\sim}{\boldsymbol{u}}_{\mathrm{NT}} = \exp[i(m_2+m_3)]\delta\underset{\sim}{\boldsymbol{u}}_{\mathrm{SB}}\\
&\delta\underset{\sim}{\boldsymbol{u}}_{\mathrm{EB}} = \exp[im_1]\delta\underset{\sim}{\boldsymbol{u}}_{\mathrm{WB}},\ \delta\underset{\sim}{\boldsymbol{u}}_{\mathrm{WT}} = \exp[im_3]\delta\underset{\sim}{\boldsymbol{u}}_{\mathrm{WB}},\ \delta\underset{\sim}{\boldsymbol{u}}_{\mathrm{ET}} = \exp[i(m_1+m_3)]\delta\underset{\sim}{\boldsymbol{u}}_{\mathrm{WB}}\\
&\delta\underset{\sim}{\boldsymbol{u}}_{\mathrm{SE}} = \exp[im_1]\delta\underset{\sim}{\boldsymbol{u}}_{\mathrm{SW}},\ \delta\underset{\sim}{\boldsymbol{u}}_{\mathrm{NW}} = \exp[im_2]\delta\underset{\sim}{\boldsymbol{u}}_{\mathrm{SW}},\ \delta\underset{\sim}{\boldsymbol{u}}_{\mathrm{NE}} = \exp[i(m_1+m_2)]\delta\underset{\sim}{\boldsymbol{u}}_{\mathrm{SW}}\\
&\delta\underset{\sim}{\boldsymbol{u}}_{\mathrm{SEB}} = \exp[im_1]\delta\underset{\sim}{\boldsymbol{u}}_{\mathrm{SWB}}, \qquad \delta\underset{\sim}{\boldsymbol{u}}_{\mathrm{NEB}} = \exp[i(m_1+m_2)]\delta\underset{\sim}{\boldsymbol{u}}_{\mathrm{SWB}}\\
&\delta\underset{\sim}{\boldsymbol{u}}_{\mathrm{NWB}} = \exp[im_2]\delta\underset{\sim}{\boldsymbol{u}}_{\mathrm{SWB}}, \qquad \delta\underset{\sim}{\boldsymbol{u}}_{\mathrm{SWT}} = \exp[im_3]\delta\underset{\sim}{\boldsymbol{u}}_{\mathrm{SWB}},\\
&\delta\underset{\sim}{\boldsymbol{u}}_{\mathrm{SET}} = \exp[i(m_1+m_3)]\delta\underset{\sim}{\boldsymbol{u}}_{\mathrm{SWB}},\ \delta\underset{\sim}{\boldsymbol{u}}_{\mathrm{NET}} = \exp[i(m_1+m_2+m_3)]\delta\underset{\sim}{\boldsymbol{u}}_{\mathrm{SWB}}\\
&\delta\underset{\sim}{\boldsymbol{u}}_{\mathrm{NWT}} = \exp[i(m_2+m_3)]\delta\underset{\sim}{\boldsymbol{u}}_{\mathrm{SWB}}
\end{aligned}
\tag{4.46}
$$

These relations are only valid if the displacement vectors of the slaved node sets have the same length as the displacement vectors of the master node sets. For the face and corner node sets this is always true. But for the edges the three slave node sets belonging to one master node set can have different length. As an example for this problem a Weaire-Phelan Cell is shown in Figure 4.7.

The length of the master node set SB is given as

$$
m_{\mathrm{SB}} = \min[\max(n_{\mathrm{NB}}, n_{\mathrm{ST}}, n_{\mathrm{NT}}), n_{\mathrm{SB}}]n_{\mathrm{dof}}, \tag{4.47}
$$

with n_{NB}, n_{ST}, and n_{NT} as the number of nodes on the slaved edges and n_{SB} as the

number of nodes on the master edge.

From Figure 4.7 one can find the following relations

$$\begin{aligned} m_{\mathrm{SB}} &> n_{\mathrm{NB}}, \\ m_{\mathrm{SB}} &= n_{\mathrm{ST}}, \\ m_{\mathrm{SB}} &> n_{\mathrm{NT}}. \end{aligned} \tag{4.48}$$

The Bloch Wave relations between, for example, SB and NT of the Weaire-Phelan Cell (nodes marked in Figure 4.7) can be rewritten as:

$$\begin{pmatrix} \delta \underset{\sim}{\boldsymbol{u}}_{\mathrm{NT1}} \\ \delta \underset{\sim}{\boldsymbol{u}}_{\mathrm{NT2}} \end{pmatrix} = \exp[i(m_2 + m_3)] \begin{bmatrix} \underset{\approx}{\boldsymbol{I}} & \underset{\approx}{\boldsymbol{0}} & \underset{\approx}{\boldsymbol{0}} & \underset{\approx}{\boldsymbol{0}} & \underset{\approx}{\boldsymbol{0}} \\ \underset{\approx}{\boldsymbol{0}} & \underset{\approx}{\boldsymbol{0}} & \underset{\approx}{\boldsymbol{0}} & \underset{\approx}{\boldsymbol{0}} & \underset{\approx}{\boldsymbol{I}} \end{bmatrix} \begin{pmatrix} \delta \underset{\sim}{\boldsymbol{u}}_{\mathrm{SB1}} \\ \delta \underset{\sim}{\boldsymbol{u}}_{\mathrm{SB2}} \\ \delta \underset{\sim}{\boldsymbol{u}}_{\mathrm{SB3}} \\ \delta \underset{\sim}{\boldsymbol{u}}_{\mathrm{SB4}} \\ \delta \underset{\sim}{\boldsymbol{u}}_{\mathrm{SB5}} \end{pmatrix} \tag{4.49}$$

with

$$\dim(\underset{\approx}{\boldsymbol{I}}) = (n_{\mathrm{dof}} \times n_{\mathrm{dof}}) \tag{4.50}$$

With the Bloch Wave relations (Equations (4.46)) and the concept for the edge node sets, presented with Equations (4.47) and (4.49), the construction of $\underset{\approx}{\boldsymbol{\nu}}$ is straight forward. Because of its size the Wave Matrix $\underset{\approx}{\boldsymbol{\nu}}$ is not given explicitly in this section.

5 Macroscopic Onset-of-Failure

5.1 General Theory

The general theory for the macroscopic onset-of-failure surface is presented in [27] and will be briefly summarized in the following. According to Equation (4.7) the "homogenized" constitutive material law can be written as:

$$\langle \dot{P}_{ij} \rangle = L^{\mathrm{H}}_{ijkl}(\Lambda) \langle \dot{F}_{kl} \rangle, \quad \langle f \rangle \equiv \frac{1}{\mathrm{volD}} \int_{\mathrm{D}} f dV \tag{5.1}$$

The homogenized tangent moduli tensor L^{H}_{ijkl} relates the volume averaged first Piola-Kirchhoff stress rate tensor $\langle \dot{P}_{ij} \rangle$ to the volume averaged rate of the deformation gradient $\langle \dot{F}_{kl} \rangle$. For solids with a periodic micro structure, Equation (5.1) is unambiguous and consistent. For this class of solids the homogenized moduli tensor is given by:

$$\langle \dot{F}_{ij} \rangle L^{\mathrm{H}}_{ijkl}(\Lambda) \langle \dot{F}_{kl} \rangle = \min_{\boldsymbol{p}} \left(\frac{1}{\mathrm{volD}} \int_{\mathrm{D}} (\langle \dot{F}_{ij} \rangle + p_{i,j}) L_{ijkl}(\Lambda, \underset{\sim}{\boldsymbol{X}}) (\langle \dot{F}_{kl} \rangle + p_{k,l}) dV \right). \tag{5.2}$$

$\boldsymbol{p}$ is any periodic function with the same periodicity as the unit cell, and $\langle \dot{\boldsymbol{F}} \rangle$ is an arbitrary rank two tensor. Similar to the microscopic stability criterion one can define the macroscopic stability criterion as (from [27]):

$$B(\Lambda) = \min_{\underset{\sim}{\boldsymbol{a}}, \underset{\sim}{\boldsymbol{n}}} \Gamma(\Lambda, \underset{\sim}{\boldsymbol{a}}, \underset{\sim}{\boldsymbol{n}}) \tag{5.3}$$

with

$$\Gamma(\Lambda, \underset{\sim}{\boldsymbol{a}}, \underset{\sim}{\boldsymbol{n}}) \equiv a_i n_j L^{\mathrm{H}}_{ijkl}(\Lambda) a_k n_l, \quad \|\underset{\sim}{\boldsymbol{a}}\| = \|\underset{\sim}{\boldsymbol{n}}\| = 1 \tag{5.4}$$

The macroscopic critical load parameter can therefore be defined as lowest root of $B(\Lambda)$:

$$B(\Lambda_{\mathrm{h}}) = 0, \quad \Lambda_{\mathrm{h}} = \min_{\underset{\sim}{\boldsymbol{a}}, \underset{\sim}{\boldsymbol{n}}} \Lambda_{\mathrm{m}}(\underset{\sim}{\boldsymbol{a}}, \underset{\sim}{\boldsymbol{n}}) \tag{5.5}$$

where

$$\Gamma(\Lambda_{\mathrm{m}}(\underset{\sim}{\boldsymbol{a}}, \underset{\sim}{\boldsymbol{n}}), \underset{\sim}{\boldsymbol{a}}, \underset{\sim}{\boldsymbol{n}}) = 0, \qquad \Gamma(\Lambda, \underset{\sim}{\boldsymbol{a}}, \underset{\sim}{\boldsymbol{n}}) > 0 \quad \text{for} \quad 0 \leq \Lambda < \Lambda_{\mathrm{m}} \tag{5.6}$$

Λ_{m} is the lowest value for which $\Gamma(\Lambda, \underset{\sim}{\boldsymbol{a}}, \underset{\sim}{\boldsymbol{n}}) = 0$ is possible for fixed $\underset{\sim}{\boldsymbol{a}}, \underset{\sim}{\boldsymbol{n}}$. $\boldsymbol{L}^{\mathrm{H}}$ only exists if the boundary value problem of the loaded unit cell has a unique solution, thus the first buckling mode found to occur must not be equal to the strictly periodic mode ($\forall m_i = 0$).

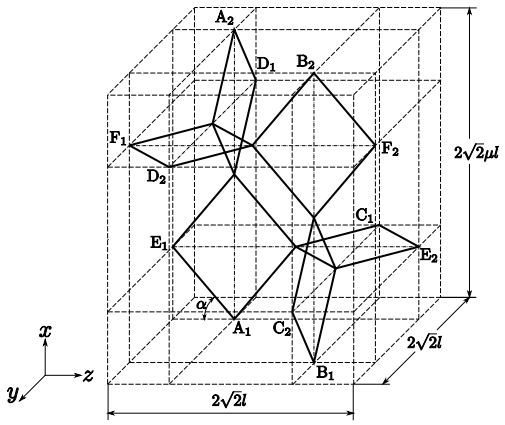

Figure 5.1: Kelvin Cell.

The macroscopic onset of failure surface always lies within its microscopic counterpart ([27]). In the case of a unique solution ($\boldsymbol{L}^{\mathrm{H}}$ exists) the critical loads found by this two different concepts are coupled through the following equation (see [27]):

$$\Lambda_{\mathrm{h}} = \inf_{\underset{\sim}{\boldsymbol{m}} \to 0} \Lambda_{\mathrm{m}}(\underset{\sim}{\boldsymbol{m}}) \tag{5.7}$$

5.2 F.E.M. Discretization

Section 2.2.1 in [17] describes the method for obtaining the homogenized tangent moduli $\boldsymbol{L}^{\mathrm{H}}$ for the Kelvin Cell model of an open cell foam. This method will be described in this section and expanded to arbitrary unit cells.

In [17] special functions $\overset{ij}{\underset{\sim}{\chi}}$ are constructed for all degrees of freedom (six in the case of the Kelvin Cell, see Figure 5.1) of all nodes in the unit cell. These functions are related to the unit normal (ε_{ii}, no sum) and shear (ε_{ij}, $i \neq j$) strains and will be referred to as "strain functions".

$$\overset{ij}{\underset{\sim}{\chi}} = \{\overset{ij}{\underset{\sim}{\chi}}_1, \overset{ij}{\underset{\sim}{\chi}}_2, \overset{ij}{\underset{\sim}{\chi}}_{\mathrm{I}}\}^{\mathrm{T}} \tag{5.8}$$

with $(i,j) = 1,2,3$ in the 3D case or $(i,j) = 1,2$ in the 2D case. $\overset{ij}{\underset{\sim}{\chi}}_1$ are the strain functions defined for those master nodes of the unit cell which correspond to the master nodes used in the Bloch Wave analysis. $\overset{ij}{\underset{\sim}{\chi}}_2$ belong to the slaved nodes (BW slave) and $\overset{ij}{\underset{\sim}{\chi}}_{\mathrm{I}}$ are the special functions belonging to the remaining internal nodes of the cell. For each node with

the node number n one can write:

$$\underset{\sim}{\overset{ij}{\boldsymbol{\chi}}}(n) = \begin{bmatrix} \overset{ij}{\chi}_k \\ \overset{ij}{\chi}_r \end{bmatrix}, \quad k = 1,2,3 \quad \text{and} \quad r = 4,5,6 \tag{5.9}$$

for the 3D case and

$$\underset{\sim}{\overset{ij}{\boldsymbol{\chi}}}(n) = \begin{bmatrix} \overset{ij}{\chi}_k \\ \overset{ij}{\chi}_r \end{bmatrix}, \quad k = 1,2 \quad \text{and} \quad r = 3 \tag{5.10}$$

for the 2D case, with $\underset{\sim}{\overset{ij}{\boldsymbol{\chi}}}_k$ representing the displacements and $\underset{\sim}{\overset{ij}{\boldsymbol{\chi}}}_r$ the rotations. The existence of the strain functions for the rotational DOFs $\underset{\sim}{\overset{ij}{\boldsymbol{\chi}}}_r$ depends on the finite elements used in the unit cell model. For the displacement degrees of freedom one can write (see also [17])

$$\overset{ij}{\chi}_k = \delta_{ik} X_j + \overset{ij}{v}_k, \quad \delta_{ik} = \begin{cases} 1 & \text{if} \quad i = k \\ 0 & \text{if} \quad i \neq k \end{cases} \tag{5.11}$$

where $\underset{\sim}{\boldsymbol{X}}$ is the position vector of the nodes corresponding to the undeformed state, δ_{ik} is the Kronecker delta and $\overset{ij}{v}_k$ are periodic functions with the same periodicity as the unit cell, leading to

$$\overset{ij}{v}_k\,|_2 = \overset{ij}{v}_k\,|_1. \tag{5.12}$$

In [17] $\bullet|_1$ and $\bullet|_2$ refer to opposite sides of the unit cell. In the present work $\bullet|_1$ is used for the BW master and $\bullet|_2$ for the BW slave. The special functions of the master and slave nodes are coupled with the following equations:

$$\overset{ij}{\chi}_k\,|_2 = \overset{ij}{\chi}_k\,|_1 + \delta_{ik} h_j \tag{5.13}$$

$$\overset{ij}{\chi}_r\,|_2 = \overset{ij}{\chi}_r\,|_1 \tag{5.14}$$

where h_j is the unit cell dimension in j-direction.

In the case of [17] the master and slave vector for the strain functions has the same length. For arbitrary cells this has not to be the case. Figure 5.2 shows a 2D unit cell. One can see, that the master vector of the strain functions $\underset{\sim}{\overset{ij}{\boldsymbol{\chi}}}_1 = \{\underset{\sim}{\overset{ij}{\boldsymbol{\chi}}}_{\mathrm{W}}, \underset{\sim}{\overset{ij}{\boldsymbol{\chi}}}_{\mathrm{S}}, \underset{\sim}{\overset{ij}{\boldsymbol{\chi}}}_{\mathrm{SW}}\}^{\mathrm{T}}$ is shorter than

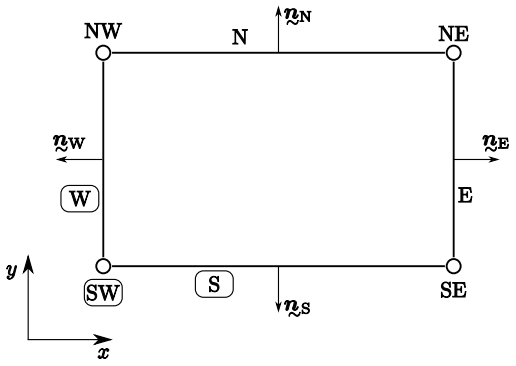

Figure 5.2: Master and slave node sets and edge normals on a 2D unit cell.

the corresponding vector of the slaved nodes $\overset{ij}{\underset{\sim}{\chi}}_1 = \{\overset{ij}{\underset{\sim}{\chi}}_{\mathrm{E}}, \overset{ij}{\underset{\sim}{\chi}}_{\mathrm{N}}, \overset{ij}{\underset{\sim}{\chi}}_{\mathrm{SE}}, \overset{ij}{\underset{\sim}{\chi}}_{\mathrm{NW}}, \overset{ij}{\underset{\sim}{\chi}}_{\mathrm{NE}}\}^{\mathrm{T}}$. The second term $\delta_{ik}h_j$ in Equation (5.13) is only active for surfaces (edges) with normals acting in j-direction. For the 2D unit cell the edge normals $\underset{\sim}{n}_{\mathrm{W}}$, $\underset{\sim}{n}_{\mathrm{S}}$, $\underset{\sim}{n}_{\mathrm{E}}$, and $\underset{\sim}{n}_{\mathrm{N}}$ are displayed in Figure 5.2.

For the unit cell displayed in Figure 5.2 the relations between the BW master and BW slave strain functions for the displacements will be given explicitly:

East coupled with West, normal acting in x-direction

$$\begin{aligned}
\overset{11}{\chi}_1|_{\mathrm{E}} &= \overset{11}{\chi}_1|_{\mathrm{W}} + h_1, & \overset{21}{\chi}_1|_{\mathrm{E}} &= \overset{21}{\chi}_1|_{\mathrm{W}} \\
\overset{11}{\chi}_2|_{\mathrm{E}} &= \overset{11}{\chi}_2|_{\mathrm{W}}, & \overset{21}{\chi}_2|_{\mathrm{E}} &= \overset{21}{\chi}_2|_{\mathrm{W}} + h_1 \\
\overset{12}{\chi}_1|_{\mathrm{E}} &= \overset{12}{\chi}_1|_{\mathrm{W}}, & \overset{22}{\chi}_1|_{\mathrm{E}} &= \overset{22}{\chi}_1|_{\mathrm{W}} \\
\overset{12}{\chi}_2|_{\mathrm{E}} &= \overset{12}{\chi}_2|_{\mathrm{W}}, & \overset{22}{\chi}_2|_{\mathrm{E}} &= \overset{22}{\chi}_2|_{\mathrm{W}}
\end{aligned} \tag{5.15}$$

North coupled with South, normal acting in y-direction

$$\begin{aligned}
\overset{11}{\chi}_1|_{\mathrm{N}} &= \overset{11}{\chi}_1|_{\mathrm{S}}, & \overset{21}{\chi}_1|_{\mathrm{N}} &= \overset{21}{\chi}_1|_{\mathrm{S}} \\
\overset{11}{\chi}_2|_{\mathrm{N}} &= \overset{11}{\chi}_2|_{\mathrm{S}}, & \overset{21}{\chi}_2|_{\mathrm{N}} &= \overset{21}{\chi}_2|_{\mathrm{S}} \\
\overset{12}{\chi}_1|_{\mathrm{N}} &= \overset{12}{\chi}_1|_{\mathrm{S}} + h_2, & \overset{22}{\chi}_1|_{\mathrm{N}} &= \overset{22}{\chi}_1|_{\mathrm{S}} \\
\overset{12}{\chi}_2|_{\mathrm{N}} &= \overset{12}{\chi}_2|_{\mathrm{S}}, & \overset{22}{\chi}_2|_{\mathrm{N}} &= \overset{22}{\chi}_2|_{\mathrm{S}} + h_2
\end{aligned} \tag{5.16}$$

SE coupled with SW, normals acting in x and $-y$-direction

$$\begin{array}{lcllcl}
\overset{11}{\chi}_1|_{\mathrm{SE}} &=& \overset{11}{\chi}_1|_{\mathrm{SW}} + h_1, & \overset{21}{\chi}_1|_{\mathrm{SE}} &=& \overset{21}{\chi}_1|_{\mathrm{SW}} \\
\overset{11}{\chi}_2|_{\mathrm{SE}} &=& \overset{11}{\chi}_2|_{\mathrm{SW}}, & \overset{21}{\chi}_2|_{\mathrm{SE}} &=& \overset{21}{\chi}_2|_{\mathrm{SW}} + h_1 \\
\overset{12}{\chi}_1|_{\mathrm{SE}} &=& \overset{12}{\chi}_1|_{\mathrm{SW}}, & \overset{22}{\chi}_1|_{\mathrm{SE}} &=& \overset{22}{\chi}_1|_{\mathrm{SW}} \\
\overset{12}{\chi}_2|_{\mathrm{SE}} &=& \overset{12}{\chi}_2|_{\mathrm{SW}}, & \overset{22}{\chi}_2|_{\mathrm{SE}} &=& \overset{22}{\chi}_2|_{\mathrm{SW}}
\end{array} \tag{5.17}$$

NW coupled with SW, normals acting in $-x$ and y-direction

$$\begin{array}{lcllcl}
\overset{11}{\chi}_1|_{\mathrm{NW}} &=& \overset{11}{\chi}_1|_{\mathrm{SW}}, & \overset{21}{\chi}_1|_{\mathrm{NW}} &=& \overset{21}{\chi}_1|_{\mathrm{SW}} \\
\overset{11}{\chi}_2|_{\mathrm{NW}} &=& \overset{11}{\chi}_2|_{\mathrm{SW}}, & \overset{21}{\chi}_2|_{\mathrm{NW}} &=& \overset{21}{\chi}_2|_{\mathrm{SW}} \\
\overset{12}{\chi}_1|_{\mathrm{NW}} &=& \overset{12}{\chi}_1|_{\mathrm{SW}} + h_2, & \overset{22}{\chi}_1|_{\mathrm{NW}} &=& \overset{22}{\chi}_1|_{\mathrm{SW}} \\
\overset{12}{\chi}_2|_{\mathrm{NW}} &=& \overset{12}{\chi}_2|_{\mathrm{SW}}, & \overset{22}{\chi}_2|_{\mathrm{NW}} &=& \overset{22}{\chi}_2|_{\mathrm{SW}} + h_2
\end{array} \tag{5.18}$$

NE coupled with SW, normals acting in x and y-direction

$$\begin{array}{lcllcl}
\overset{11}{\chi}_1|_{\mathrm{NE}} &=& \overset{11}{\chi}_1|_{\mathrm{SW}} + h_1, & \overset{21}{\chi}_1|_{\mathrm{NE}} &=& \overset{21}{\chi}_1|_{\mathrm{SW}} \\
\overset{11}{\chi}_2|_{\mathrm{NE}} &=& \overset{11}{\chi}_2|_{\mathrm{SW}}, & \overset{21}{\chi}_2|_{\mathrm{NE}} &=& \overset{21}{\chi}_2|_{\mathrm{SW}} + h_1 \\
\overset{12}{\chi}_1|_{\mathrm{NE}} &=& \overset{12}{\chi}_1|_{\mathrm{SW}} + h_2, & \overset{22}{\chi}_1|_{\mathrm{NE}} &=& \overset{22}{\chi}_1|_{\mathrm{SW}} \\
\overset{12}{\chi}_2|_{\mathrm{NE}} &=& \overset{12}{\chi}_2|_{\mathrm{SW}}, & \overset{22}{\chi}_2|_{\mathrm{NE}} &=& \overset{22}{\chi}_2|_{\mathrm{SW}} + h_2
\end{array} \tag{5.19}$$

This method can easily be adapted to 3D unit cells. By comparing Equations (5.15) to (5.19) with Equation (4.32) one can see that there exists an relation between the second term in Equation (5.13) and the $\underset{\approx}{\boldsymbol{\nu}}$-Matrix in Equation (4.32), namely:

> The normal is acting in the j-direction of a slaved node k if m_j of this node k is active in the wave matrix $\underset{\approx}{\boldsymbol{\nu}}$.

Therefore, the same information used to generate the $\underset{\approx}{\boldsymbol{\nu}}$-Matrix can be used to evaluate the second term in (5.13). Equation (5.13) can be written in matrix notation:

$$\overset{ij}{\underset{\sim}{\boldsymbol{\chi}}}_2 = \overset{ij}{\underset{\sim}{\boldsymbol{\chi}}}_{1,\mathrm{elong.}} + \overset{ij}{\underset{\sim}{\boldsymbol{\mathcal{H}}}} \tag{5.20}$$

with

$$\overset{ij}{\underset{\sim}{\chi}}_{1,\text{elong.}} = \underset{\approx}{\omega} \overset{ij}{\underset{\sim}{\chi}}_{1} \tag{5.21}$$

Thus, we can write for $\overset{ij}{\underset{\sim}{\chi}}_{2}$:

$$\overset{ij}{\underset{\sim}{\chi}}_{2} = \underset{\approx}{\omega} \overset{ij}{\underset{\sim}{\chi}}_{1} + \overset{ij}{\underset{\sim}{\mathcal{H}}} \tag{5.22}$$

For the 2D case one finds with $\overset{ij}{\underset{\sim}{\chi}}_{1,\text{elong.}} = \{\overset{ij}{\underset{\sim}{\chi}}_{\text{W}}, \overset{ij}{\underset{\sim}{\chi}}_{\text{S}}, \overset{ij}{\underset{\sim}{\chi}}_{\text{SW}}, \overset{ij}{\underset{\sim}{\chi}}_{\text{SW}}, \overset{ij}{\underset{\sim}{\chi}}_{\text{SW}}\}^{\text{T}}$ and $\overset{ij}{\underset{\sim}{\chi}}_{1} = \{\overset{ij}{\underset{\sim}{\chi}}_{\text{W}}, \overset{ij}{\underset{\sim}{\chi}}_{\text{S}}, \overset{ij}{\underset{\sim}{\chi}}_{\text{SW}}\}^{\text{T}}$ for the elongation matrix $\underset{\approx}{\omega}$:

$$\underset{\approx}{\omega} = \begin{bmatrix} \underset{\approx}{I} & \underset{\approx}{0} & \underset{\approx}{0} \\ \underset{\approx}{0} & \underset{\approx}{I} & \underset{\approx}{0} \\ \underset{\approx}{0} & \underset{\approx}{0} & \underset{\approx}{I} \\ \underset{\approx}{0} & \underset{\approx}{0} & \underset{\approx}{I} \\ \underset{\approx}{0} & \underset{\approx}{0} & \underset{\approx}{I} \end{bmatrix} \quad \text{with} \quad \dim(\underset{\approx}{I}) = (n_{\text{dof}} \times n_{\text{dof}}) \tag{5.23}$$

and $\underset{\sim}{I}$ being the identity matrix.

Applying Equation (5.8) to the unit cell with the internal degrees of freedom condensed out like in Equation (4.26) yields:

$$\begin{bmatrix} \hat{\underset{\approx}{K}}_{11} & \hat{\underset{\approx}{K}}_{12} \\ \hat{\underset{\approx}{K}}_{21} & \hat{\underset{\approx}{K}}_{22} \end{bmatrix} \begin{bmatrix} \overset{ij}{\underset{\sim}{\chi}}_{1} \\ \overset{ij}{\underset{\sim}{\chi}}_{2} \end{bmatrix} = \begin{bmatrix} \overset{ij}{\underset{\sim}{F}}_{1} \\ \overset{ij}{\underset{\sim}{F}}_{2} \end{bmatrix} \tag{5.24}$$

Expressing $\overset{ij}{\underset{\sim}{\chi}}_{2}$ with Equation (5.22) gives:

$$\begin{bmatrix} \hat{\underset{\approx}{K}}_{11} & \hat{\underset{\approx}{K}}_{12} \\ \hat{\underset{\approx}{K}}_{21} & \hat{\underset{\approx}{K}}_{22} \end{bmatrix} \begin{bmatrix} \underset{\approx}{I} & \underset{\approx}{0} \\ \underset{\approx}{0} & \underset{\approx}{\omega} \end{bmatrix} \begin{bmatrix} \overset{ij}{\underset{\sim}{\chi}}_{1} \\ \overset{ij}{\underset{\sim}{\chi}}_{1} \end{bmatrix} + \begin{bmatrix} \hat{\underset{\approx}{K}}_{11} & \hat{\underset{\approx}{K}}_{12} \\ \hat{\underset{\approx}{K}}_{21} & \hat{\underset{\approx}{K}}_{22} \end{bmatrix} \begin{bmatrix} \underset{\sim}{0} \\ \overset{ij}{\underset{\sim}{\mathcal{H}}} \end{bmatrix} = \begin{bmatrix} \overset{ij}{\underset{\sim}{F}}_{1} \\ \overset{ij}{\underset{\sim}{F}}_{2} \end{bmatrix} \tag{5.25}$$

Multiplying both sides with $[\underset{\approx}{\boldsymbol{I}}, \underset{\approx}{\boldsymbol{\omega}}^{\mathrm{T}}]$ produces:

$$[\underset{\approx}{\boldsymbol{I}}, \underset{\approx}{\boldsymbol{\omega}}^{\mathrm{T}}] \left\{ \begin{bmatrix} \hat{\underset{\approx}{\boldsymbol{K}}}_{11} & \hat{\underset{\approx}{\boldsymbol{K}}}_{12} \\ \hat{\underset{\approx}{\boldsymbol{K}}}_{21} & \hat{\underset{\approx}{\boldsymbol{K}}}_{22} \end{bmatrix} \begin{bmatrix} \underset{\approx}{\boldsymbol{I}} & \underset{\approx}{\boldsymbol{0}} \\ \underset{\approx}{\boldsymbol{0}} & \underset{\approx}{\boldsymbol{\omega}} \end{bmatrix} \begin{bmatrix} \overset{ij}{\underset{\sim}{\boldsymbol{\chi}}}_1 \\ \overset{ij}{\underset{\sim}{\boldsymbol{\chi}}}_1 \end{bmatrix} + \begin{bmatrix} \hat{\underset{\approx}{\boldsymbol{K}}}_{11} & \hat{\underset{\approx}{\boldsymbol{K}}}_{12} \\ \hat{\underset{\approx}{\boldsymbol{K}}}_{21} & \hat{\underset{\approx}{\boldsymbol{K}}}_{22} \end{bmatrix} \begin{bmatrix} \underset{\sim}{\boldsymbol{0}} \\ \overset{ij}{\underset{\sim}{\boldsymbol{\mathcal{H}}}} \end{bmatrix} \right\} = \underset{\approx}{\boldsymbol{I}} \overset{ij}{\underset{\sim}{\boldsymbol{F}}}_1 + \underset{\approx}{\boldsymbol{\omega}}^{\mathrm{T}} \overset{ij}{\underset{\sim}{\boldsymbol{F}}}_2 \tag{5.26}$$

All forces and moments acting on the unit cell fulfill the equilibrium conditions for peridoic unit cells given in Section 2.2, thus the right side of Equation (5.26) vanishes.

$$\underset{\approx}{\boldsymbol{I}} \overset{ij}{\underset{\sim}{\boldsymbol{F}}}_1 + \underset{\approx}{\boldsymbol{\omega}}^{\mathrm{T}} \overset{ij}{\underset{\sim}{\boldsymbol{F}}}_2 = \underset{\sim}{\boldsymbol{0}} \tag{5.27}$$

Equation (5.26) therefore has the solution:

$$\overset{ij}{\underset{\sim}{\boldsymbol{\chi}}}_1 = -\left(\hat{\underset{\approx}{\boldsymbol{K}}}_{\mathbf{11}} + \hat{\underset{\approx}{\boldsymbol{K}}}_{\mathbf{12}} \underset{\approx}{\boldsymbol{\omega}} + \underset{\approx}{\boldsymbol{\omega}}^{\mathrm{T}} \hat{\underset{\approx}{\boldsymbol{K}}}_{\mathbf{21}} + \underset{\approx}{\boldsymbol{\omega}}^{\mathrm{T}} \hat{\underset{\approx}{\boldsymbol{K}}}_{\mathbf{22}} \underset{\approx}{\boldsymbol{\omega}} \right)^{-1} \left(\hat{\underset{\approx}{\boldsymbol{K}}}_{\mathbf{12}} + \underset{\approx}{\boldsymbol{\omega}}^{\mathrm{T}} \hat{\underset{\approx}{\boldsymbol{K}}}_{\mathbf{22}} \right) \overset{ij}{\underset{\sim}{\boldsymbol{\mathcal{H}}}} \tag{5.28}$$

For the strain functions of the internal degrees of freedom one receives with Equation (4.26) (replace $\delta\underset{\sim}{\boldsymbol{u}}$ with $\overset{ij}{\underset{\sim}{\boldsymbol{\chi}}}$):

$$\overset{ij}{\underset{\sim}{\boldsymbol{\chi}}}_{\mathrm{I}} = -\underset{\approx}{\boldsymbol{K}}_{\mathrm{II}}^{-1} [\underset{\approx}{\boldsymbol{K}}_{\mathrm{I1}} \overset{ij}{\underset{\sim}{\boldsymbol{\chi}}}_1 + \underset{\approx}{\boldsymbol{K}}_{\mathrm{I2}} \overset{ij}{\underset{\sim}{\boldsymbol{\chi}}}_2] \tag{5.29}$$

According to [27] the homogenized tangent moduli of the unit cell can be calculated with:

$$L^{\mathrm{H}}_{ijkl} = \frac{\overset{ij}{\underset{\sim}{\boldsymbol{\chi}}}^{\mathrm{T}} \underset{\approx}{\boldsymbol{K}}(\Lambda) \overset{kl}{\underset{\sim}{\boldsymbol{\chi}}}}{V} \tag{5.30}$$

with V being the volume of the unit cell. In [13] it was shown that the occurrence of a long wave instability corresponds to the loss of rank one convexity of the homogenized moduli.

$$(L^{\mathrm{H}}_{ijkl}(\Lambda) n_j n_l) g_k = 0 \quad \text{or} \quad \det |L^{\mathrm{H}}_{ijkl}(\Lambda) n_j n_l| = 0 \tag{5.31}$$

with

$$\underset{\sim}{\boldsymbol{n}} = \{\cos(\varphi), \sin(\varphi)\cos(\psi), \sin(\varphi)\sin(\psi)\}^{\mathrm{T}} \quad 0 \leq \varphi \leq \pi \quad 0 \leq \psi \leq 2\pi \tag{5.32}$$

for the 3D case and

$$\underset{\sim}{\boldsymbol{n}} = \{\cos(\varphi), \sin(\varphi))\}^{\mathrm{T}} \quad 0 \leq \varphi \leq \pi \tag{5.33}$$

for the 2D case.

One has to vary φ and ψ on a reasonably fine grid for each load parameter Λ. The unconstrained, incremental tangent stiffness matrix $\underset{\approx}{\boldsymbol{K}}$ of the unit cell is provided by ABAQUS. The critical load parameter for the macroscopic onset-of-failure Λ_{h} is the lowest Λ for which Equation (5.31) is fulfilled. The direction of the band of the corresponding buckling mode (see [23]) is determined by the corresponding $\underset{\sim}{\boldsymbol{n}}$.

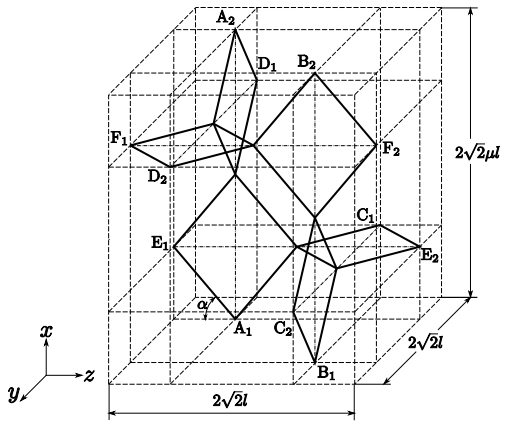

Figure 6.1: Kelvin Cell, elongated in rise direction (x-direction).

6 The Kelvin Cell

In [16] different models for the prediction of the nonlinear response of open cell foams under compressive loading were developed. In this work the foam was idealized as being perfectly periodic. The fundamental building block of the periodic micro structure was modeled as a regular, 14-sided polyhedron [26] with the ligaments being modeled as beams. This generic unit cell geometry will be referred to as Kelvin Cell (see Figure 6.1). In [16], the principal geometric properties of tested open cell foams were transferred to an idealized Kelvin Cell model. This model has the following features:

- straight ligaments with Plateau border cross-sections and nonuniform area distribution along the longitudinal axis,
- anisotropic cell geometry, cells elongated in rise direction,
- giving a reasonable representation of the material in the nodes,
- considering the effect of shear deformation in the beam model.

All foams tested in [16] and [14] were polyester urethane foams manufactured by the company FOAMEX. Average cell sizes were of 3, 10, 20, 45 and 100 ppi (pores per inch), respectively. The relative densities of the tested foams varied from 2.2% to 2.8%. The results of the measurements of the geometric properties and the material constants can be found in Table 1 in [16].

The Kelvin Cell used in this thesis is similar to those used in [14], [16] and [17]. In the latter one the Bloch Wave method was used for the search of the critical state of a foam under uniaxial and triaxial compressive loading. To verify the Bloch Wave program written during the present thesis the results obtained for the Kelvin Cell model are compared to those reported in [17].

6.1 Characteristic Cell

6.1.1 Cell Dimesions

As already mentioned the open cell foam is idealized as being perfectly periodic with the Kelvin Cell as its fundamental building block. The measurements in [16] showed, that the foam exhibits anisotropy. Thus the cell is elongated in x-direction (rise direction). The Kelvin Cell is a space filling 14-sided polyhedron consisting of 6 squares and 8 hexagons with the edges being of length l. In the case of an open cell foam all edges of the Kelvin Cell are treated as beams. For the isotropic cell one receives for the cell dimension $h = 2\sqrt{2}l$. To model the anisotropy reported in [16], [14] and [17] all ligaments with a non-vanishing projection in the x-direction are elongated to $l/\sqrt{2}\cos\alpha$ with the angle between the longitudinal beam axis and the y-z-plane being $\alpha \geq \pi/4$ (see Figure 6.1). The length of the ligaments in the directions normal to x (transverse direction) remains unchanged. The height of the elongated cell can be given as:

$$h_1 = 2\sqrt{2}l \tan\alpha \tag{6.1}$$

The width of the cell remains unchanged:

$$h_2 = 2\sqrt{2}l \tag{6.2}$$

For the parameter of anisotropy μ one receives:

$$\mu = \frac{h_1}{h_2} = \tan\alpha, \quad \alpha \geq \frac{\pi}{4} \tag{6.3}$$

To reproduce the results in [17] the anisotropy factor was set to $\mu = 1.3$.

6.1.2 Material Behavior

For modeling the material behavior the rate-dependence of the base material (polyester urethane) is neglected (see [16]). The material is assumed to be linearly elastic with the values of the material constants E, ν taken from Table 1 in [16]:

$$\begin{aligned} E &= 69 \text{ MPa} \quad \text{Young's Modulus} \\ \nu &= 0.49 \quad \text{Poissons Ratio} \end{aligned}$$

6.1.3 Ligament Geometry

In [16] measurements of the area and the length of the ligaments of the polyester urethane foams were performed. The ligaments have a three-cusp hypocycloid cross section known as Plateau borders (see Figure 6.2) and a nonuniform area distribution along their longitudinal axis. In [16] the measured data of the area distribution over the normalized length of the ligaments were fitted with the following symmetric function:

$$A(\xi) = A_0 f(\xi) = A_0(a\xi^4 + b\xi^2 + 1), \quad \xi = \frac{x}{l} \tag{6.4}$$

with $a = 86$ and $b = 1$. For the three-cusp hypocycloid cross section area one receives for the section properties (area A, moment of inertia about the y- and the z-axis I_y, I_z, respectively, and torsional rigidity J) (from [16]):

$$A = \left(\sqrt{3} - \frac{\pi}{2}\right) r^2, \quad I_y = I_z = \frac{1}{24}\left(20\sqrt{3} - 11\pi\right) r^4, \quad J = 0.0021 r^4 \tag{6.5}$$

with r as radius of the cross section for fixed ξ (see Figure 6.2). All results received in [16] are applied to the Kelvin Cell used in the present work.

6.1.4 Effect of Shear Deformation

The ligaments in the foams examined in [16] are not very slender. Thus, a Timoshenko type correction (ligaments treated as shear-deformable beams) was used to describe the deformation introduced by the shear stresses. The calculations made in [16] are energy

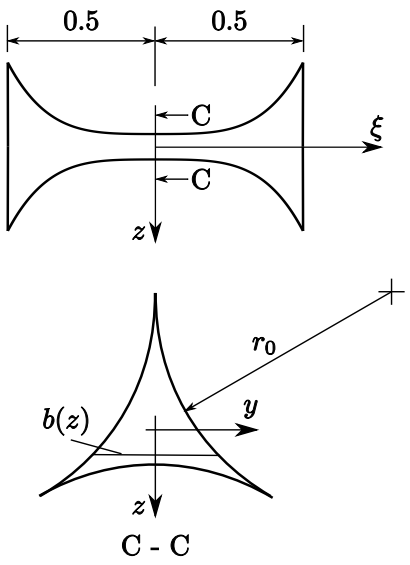

Figure 6.2: Geometry definition of foam ligaments.

based. The correction was introduced to the strain energy with V as shear force by:

$$U_{\mathrm{s}} = \int_{-l/2}^{l/2} \beta \frac{V^2(\xi)}{2GA} l \mathrm{d}\xi, \quad \text{with} \quad \beta = \frac{A}{I_y^2} \int_z \frac{Q^2(z)}{bz} \mathrm{d}z \tag{6.6}$$

$Q(z)$ is the first moment of area about the y-axis (see Figure 6.2) and $b(z)$ is the width of the cross section at a distance z from the y-axis. The integral to determine β is over the whole cross section of the ligament. For the Plateau border cross section shown in Figure 6.2, $\beta = 1.24$ (see [16])

6.1.5 Relative Density

In [16] a power law relationship fitted to the measured data for the relative density is found to have the following form:

$$\frac{\rho^*}{\rho} = k \left(\frac{r_0}{l} \right)^n \tag{6.7}$$

With r_0 as the radius at midspan and l as ligament length. The constants k and n depend on the anisotropy parameter. They are listed in Table 6.1 (from [16]).

Table 6.1: Parameters for the power law relationship of the corrected relative density. From [16].

μ	n	k
1	1.7392	0.1803
1.1	1.7426	0.1791
1.2	1.7433	0.1637
1.3	1.7449	0.1580
1.4	1.7474	0.1350
Uniform cross-section.	1.8968	0.1395

The Kelvin Cell used in the present work has a height of 7.42 mm. This value is taken from Table 1 in [16] for an anisotropy factor of $\mu = 1.3$. With Equation (6.1) and with the parameter of anisotropy $\mu = 1.3$ one receives for the ligament length $l = 2.018$ mm. The relative density was chosen similar to [17] as $\rho^*/\rho = 0.025$. With the corresponding constants from Table 6.1 one receives with Equation (6.7) for r_0: $r_0 = 0.7015$ mm.

6.1.6 F.E.M. Model

The characteristic cell (Kelvin Cell) is shown in Figure 6.1. Similar to [17] the ligaments are discretized using three-noded, quadratic beam elements (ABAQUS element type B32). For each ligament eight elements with individually uniform cross-sectional area are used. The area of each element can be evaluated from the symmetric function given in Equation (6.4). Thus one receives for the discretized cross-sectional area function $f(\xi)$ (see [16]):

$$f(\xi) = \begin{cases} 1.0, & 0.0 \leq |\xi| \leq 0.2 \\ 1.482, & 0.2 < |\xi| \leq 0.3 \\ 2.574, & 0.3 < |\xi| \leq 0.4 \\ 4.993, & 0.4 < |\xi| \leq 0.5 \end{cases} \tag{6.8}$$

For the definition of the cross-section properties the beam general section feature of ABAQUS is used. I_y ($I_z = I_y$) and J are calculated in a way that they correspond to the area of the element by using Equation (6.5).

To take the additional shear deformation into account the shear correction factor $\beta = 1.24$

(see Equation (6.6)) is included in the Finite element model.[2]

Appropriate periodic boundary conditions have to be applied to the unit cell. To generate the required coupling equations, which link the master and slave degrees of freedom, the CBC-program by Daxner and Pahr is used in the present work. For the manual input of these equations for the single unit cell one can build pairs of nodes located on opposite sides of the cell.

The Kelvin Cell has three pairs of opposite boundary faces (index $i = 1, 2, 3$). $\bullet_1$ and $\bullet_2$ stand for the master and slave side (not BW master and BW slave although they are the same for the Kelvin Cell). For the coupling equations of the displacement and rotational degrees of freedom between master and slave boundary faces one finds:

$$u_{i1} - u_{i2} = u_{i1}^{\text{ref}} - u_{i2}^{\text{ref}} \tag{6.9}$$

$$\theta_{i1} - \theta_{i2} = 0 \tag{6.10}$$

with $\bullet_{ij}^{\text{ref}}$ as displacements of corresponding points on opposite faces defined as reference displacements, with for example A_1 and A_2 as reference points (see Figure 6.1).

As mentioned in Section 6.1.2 the material is assumed to be linearly elastic with Young's Modulus $E = 69$ MPa and Poisson's Ratio $\nu = 0.49$.

The whole unit cell consists of 24 ligaments each discretized with 8 beam elements. Thus we receive for the model of the unit cell 192 elements, 378 nodes and a total number of 2268 degrees of freedom.

As already mentioned the CBC-program by Daxner and Pahr was used to generate the coupling equations. The program generates additional nodes (point masses) in the corners of the unit cell (see Figure 6.3).

According to the 3D unit cell model in Section 2.1, SWB, SEB, NWB and SWT are used as master nodes (not BW master nodes). Note, that the added point masses are only used for the boundary conditions and load application in the F.E.M model. They don't affect the Bloch Wave method, because these nodes are ignored by the implemented algorithm.

[2] *TRANSVERSE SHEAR STIFFNESS is used to define the shear stiffess of the beam elements in the ABAQUS input file. The shear stiffness of a beam element is estimated by multiplying the shear stiffness GA obtained for the cross section of the beam with $1/\beta$.

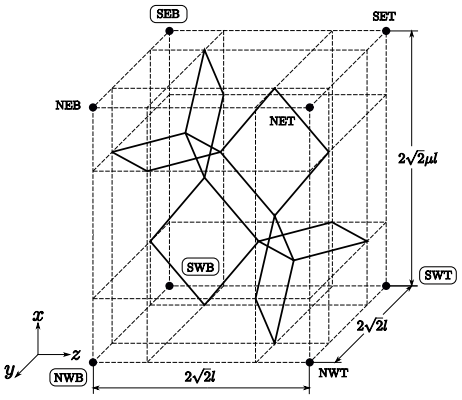

Figure 6.3: Point masses in the corners of the unit cell generated by the CBC-program.

To avoid rigid body movements some of the displacements of the master nodes,

$$\begin{aligned} \underset{\sim}{u}_{\mathrm{SWB}} &= \{0,0,0\}, \\ \underset{\sim}{u}_{\mathrm{SEB}} &= \{u_{\mathrm{SEB}},0,0\}, \\ \underset{\sim}{u}_{\mathrm{NWB}} &= \{u_{\mathrm{NWB}},v_{\mathrm{NWB}},0\}, \end{aligned} \tag{6.11}$$

and one internal node of the Kelvin Cell are constrained.

6.2 Prediction of the Elastic Moduli

For the prediction of the elastic moduli of the Kelvin Cell foam two different methods are used. The first method uses the equations given in Table 4, Panel B in [16]. This equations take the non-uniform area distribution and the deformation due to shear into account. Secondly, the Finite Element model is used to get a prediction of the elastic constants.

With the Equations from Table 4 and the constants given in Table 5 of [16] one receives for the relative elastic modulus in rise and transverse direction ($\bar{r} = \frac{r_0}{l}$):

$$\begin{aligned} \frac{E_1^*}{E} &= 0.001702 \\ \frac{E_2^*}{E} &= 0.000807 \end{aligned} \tag{6.12}$$

The initial elastic modulus in rise direction is about twice the initial elastic modulus in transverse direction ($\frac{E_2^*}{E_1^*} = 0.474$).

To get the initial elastic moduli from the Finite Element model the unit cell is loaded in rise/transverse direction with compressive loads applied to the master nodes. Loading the master nodes ensures that the unit cell reacts to these concentrated loads like the infinite structure would react to homogenized applied stresses ([24]). The loads are applied in a linear perturbation analysis. In rise direction, SEB is loaded in x-direction, and for the transverse direction NWB is loaded in y-direction. For the relative elastic moduli in rise and transverse direction, respectively one receives:

$$\begin{aligned} \frac{E_1^*}{E} &= 0.001731 \\ \frac{E_2^*}{E} &= 0.000821 \end{aligned} \tag{6.13}$$

The elastic moduli obtained with the Finite Element model are about 1.7% higher than those received with the equations given in [16]. For the normalization of stress results in the following, the elastic moduli calculated with the Finite Element model are used.

6.3 Uniaxial Compression in Rise Direction

To receive the nonlinear compressive response in rise direction (x-direction) a compressive load is applied to a single undeformed Kelvin Cell ($N_1 = 1$) at the SEB master node (see Figure 6.3). The standard Newton Raphson method with a constant step size of $\Delta\Lambda = 10^{-3}$ is used in the solution procedure. The reference load corresponding to $\Lambda = 1.0$ has a value of 405 N. For each increment along the loading path ABAQUS provides the stiffness matrices of the deformed Kelvin Cell. The element stiffness matrices are assembled to form the tangent stiffness matrix of the structure. The tangent stiffness matrix is processed using the Bloch Wave program (see Appendix A) and a check is made whether or not the critical state is established. For small increment sizes ABAQUS normally aborts the analysis due to convergence problems before this critical state is achieved. To reach the critical state or postcritical states the stabilization method provided by ABAQUS is used. It will be shown in Section 6.4 that the stabilization algorithm does not significantly influence the solution achieved with the Bloch Wave analysis for this particular unit cell.

The search for the strictly periodic mode is treated separately from the standard Bloch

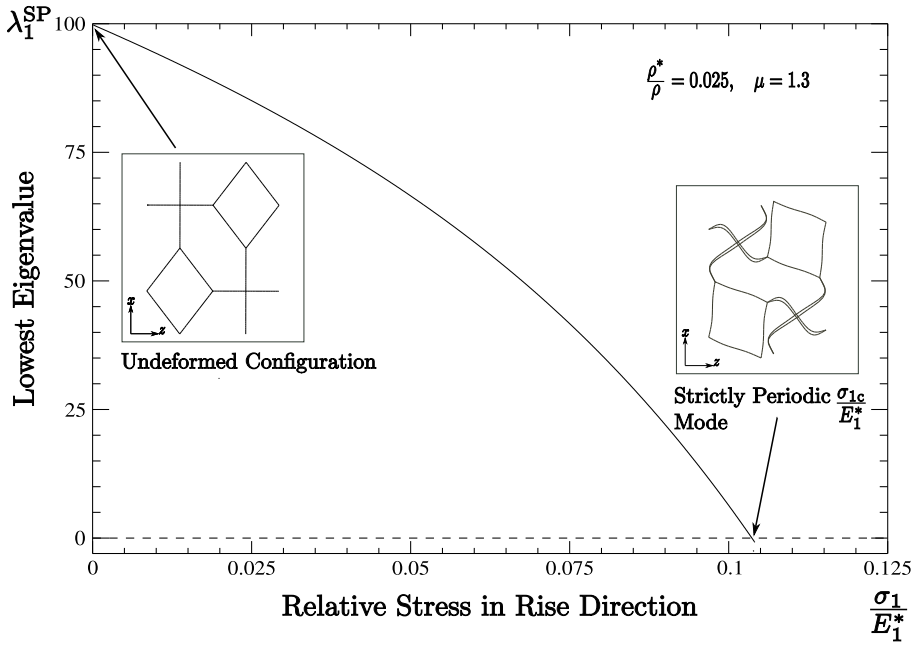

Figure 6.4: Lowest eigenvalue depending on the applied load for the search of the strictly periodic mode; rise direction.

Wave analysis. In this case the reduced stiffness matrix $\mathring{\underset{\approx}{\boldsymbol{K}}}$ has to be constrained against rigid body movements (see Appendix A.3). In Figure 6.4 the lowest eigenvalue λ_1^{SP} of the constrained matrix $\mathring{\underset{\approx}{\boldsymbol{K}}}$ is plotted against the stress in rise direction normalized by the elastic modulus in rise direction $\frac{\sigma_1^{\mathrm{SP}}}{E_1^*}$. If $\lambda_1^{\mathrm{SP}} = 0$ the critical state corresponding to a mode local to one unit cell, referred to as strictly periodic mode, is established. If the critical state if found to occur between two increments, linear interpolation is used to get closer to the critical state. For the Kelvin Cell loaded in rise direction one finds for the relative critical stress corresponding to the strictly periodic mode:

$$\frac{\sigma_{1c}^{\mathrm{SP}}}{E_1^*} = 0.10365 \tag{6.14}$$

The macroscopic onset of failure, for which the wavelength of the eigenmode is infinite in rise direction ($N_1 = \infty$), is found to occur for a relative critical stress of:

$$\frac{\sigma_{1c}^{\mathrm{H}}}{E_1^*} = 0.08985 \tag{6.15}$$

The critical stress corresponding to the macroscopic onset of failure is significantly lower

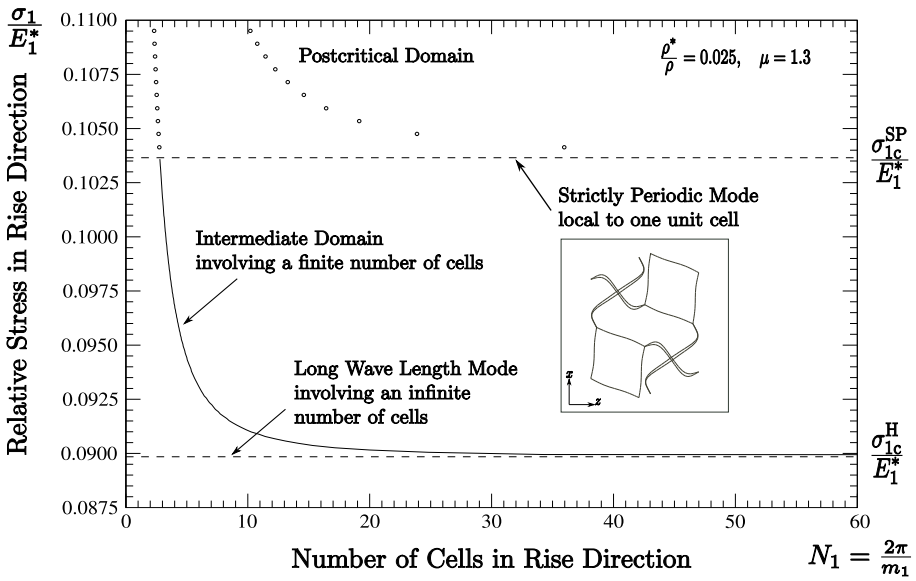

Figure 6.5: Results of the Bloch Wave Analysis in rise direction.

than the one corresponding to the strictly periodic mode. In Figure 6.5 the critical stresses corresponding to the macroscopic onset of failure and the strictly periodic mode are included as horizontal dashed lines. For finding the critical stresses for a finite number of cells forming a column in rise direction ($1 < N_1 < \infty$) the Bloch Wave method is used. The critical stress for the strictly periodic mode forms the upper limit with regard to the usefulness of results obtained by of the Bloch Wave Analysis (BWA). Although the BWA delivers results in the postcritical domain (see Figure 6.5), no buckling stresses higher than those corresponding to the strictly periodic mode are physically meaningful. Therefore, a column consisting of two unit cells ($N = 2$) exhibits the strictly periodic mode. For a higher number of cells the critical stress drops and the mode wavelength increases. The critical stress remains almost constant for columns consisting of more than 20 cells ($N_1 > 20$). For $N \to \infty$ the Bloch Wave results for the critical stress approach asymptotically the critical stress corresponding to the macroscopic onset of failure. Thus, the (theoretically) infinite periodic foam loaded in rise direction exhibits a long wave length mode. This results are in agreement with those reported in [17].

6.4 Uniaxial Compression in Transverse Direction

To receive the compressive response in transverse direction a single Kelvin Cell is loaded under compression, with the compressive load (reference load $F_2 = 380\,\mathrm{N}$) being applied

to the SWT master node. The standard Newton Raphson algorithm with a step size of $\Delta\Lambda = 10^{-3}$ is used for the incremental solution. To establish the critical state and to reach postcritical states during the ABAQUS analysis the automatic stabilization mechanism provided by ABAQUS is used.

Figure 6.6 shows the lowest eigenvalue of the strictly periodic mode plotted against the relative stress in transverse direction. The search for the strictly periodic mode and the macroscopic onset of failure show that the strictly periodic mode and the long wave length mode are separated by a small intermediate domain (see Figure 6.7). For the critical stresses corresponding to the strictly periodic mode $\frac{\sigma_{2c}^{SP}}{E_2^*}$ and the long wave length mode $\frac{\sigma_{2c}^{H}}{E_2^*}$ normalized by the elastic modulus in transverse direction E_2^* one finds:

$$\begin{aligned} \frac{\sigma_{2c}^{SP}}{E_2^*} &= 0.149706, \\ \frac{\sigma_{2c}^{H}}{E_2^*} &= 0.149484. \end{aligned} \tag{6.16}$$

The values received for σ_{2c}^{SP} and σ_{2c}^{H} are lower than the corresponding values σ_{1c}^{SP} and σ_{1c}^{H} for the rise direction and separated only by a small intermediate domain. To get more Bloch Wave points within the intermediate domain the step size of the Newton Raphson algorithm within this domain is further reduced. Figure 6.7 shows the results for the Bloch Wave Analysis (BWA) of the loading in transverse direction. The predicted critical modes are strictly periodic and independent of the number of cells in transverse direction for columns consisting of up to about 60 cells. For configurations with more than 60 cells in transverse direction the critical stress drops and the wavelength of the critical mode approaches asymptotically towards infinity.

For columns consisting of 40 and 125 cells an accompanying eigenvalue analysis using ABAQUS is performed. For the eigenvalue analysis the automatic stabilization mechanism is omitted. The calculated critical loads corresponding to these cell columns are lower than those calculated by the Bloch Wave Analysis (see Figure 6.7). The column consisting of 40 cells exhibits a strictly periodic mode whereas for the 125 cell column a long wave length mode is predicted (see Figure 6.7). Although the values for the critical loads of these two configurations are slightly lower than those of the BWA the results confirm the observations made by the BWA.

The eigenvalue analysis for both configurations is repeated using the stabilization mecha-

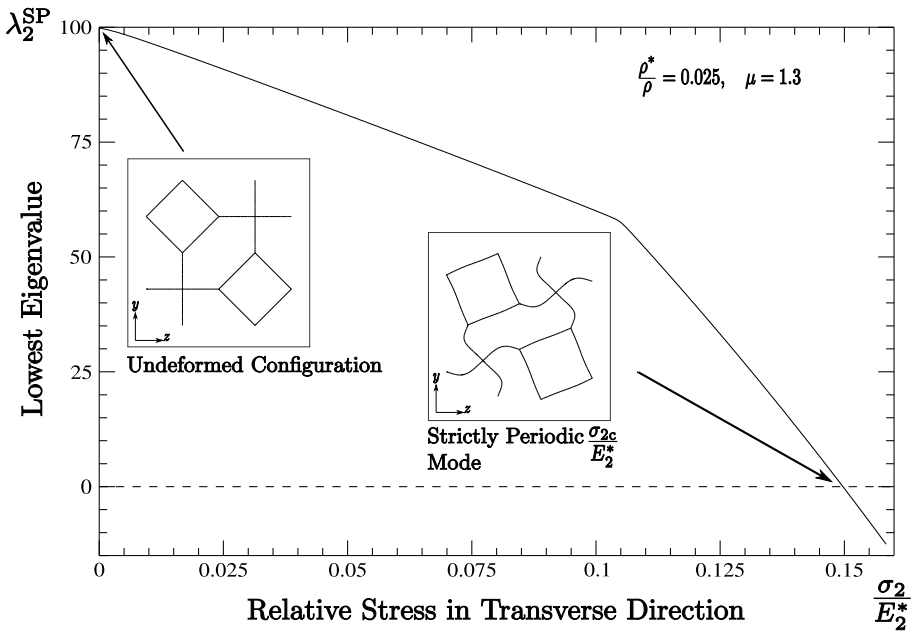

Figure 6.6: Lowest eigenvalue depending on the applied load for the search of the strictly periodic mode; transverse direction.

nism provided by ABAQUS. For this case the critical loads are closer to the BWA results than those found by the eigenvalue analysis without the stabilization mechanism being active (see Figure 6.7). The critical mode for the 40 cell cluster is still strictly periodic and the 125 cell column still exhibits long wave length buckling.

The used stabilization mechanism influences the entries of the element stiffness matrices, and the critical state is established at a higher load level. Thus the critical loads found by the BWA are slightly shifted to higher values, but the mode wave lengths are not influenced by the stabilization algorithm.

6.5 Triaxial Loading

To investigate the behavior of the anisotropic Kelvin foam ($\mu = 1.3$) under triaxial loading conditions the foam is loaded along a radial path in stress space defined by

$$\{\sigma_1, \sigma_2, \sigma_3\} = \Sigma\{1, \kappa, \kappa\} \tag{6.17}$$

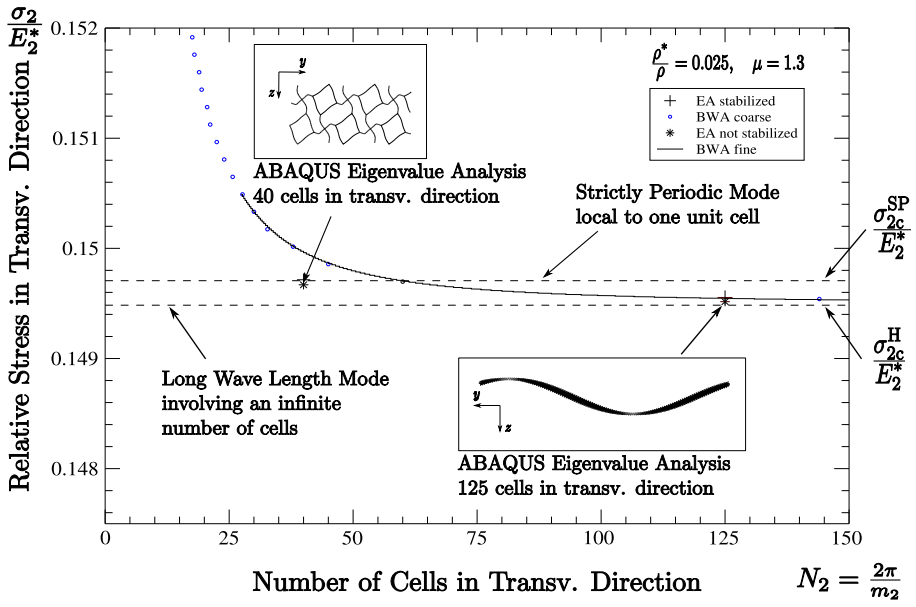

Figure 6.7: Results of the Bloch Wave analysis in transverse direction.

with

$$\begin{aligned} 0 &\leq \kappa \leq 1 \\ \Sigma &= \sigma_{1c}(\mu)\Lambda \quad \text{with} \quad 0 \leq \Lambda \leq 1 \end{aligned} \tag{6.18}$$

where $\sigma_{1c}(\mu)$ is the critical stress corresponding to the strictly periodic mode for uniaxial loading in rise direction and Λ is the load parameter. Therefore, $\kappa = 0$ represents uniaxial loading in rise direction and $\kappa = 1$ represents pure hydrostatic pressure. The material of the examined Kelvin Cell is assumed to be linearly elastic. Thus, the failure surfaces are independent of the load path followed. Therefore, the above described method is a practical way to construct the failure surface in the $\frac{\sqrt{3J_2}}{\sigma_c}$ versus $\frac{I_1}{3\sigma_c}$ plane. I_1 is the first invariant of the stress tensor, J_2 is the second invariant of the deviatoric stress tensor, and σ_c is the critical stress of an isotropic foam ($\mu = 1$) of infinite extent, having the same density as the anisotropic foam, loaded under uniaxial compression. For I_1 and $\sqrt{3J_2}$ one defines:

$$\begin{aligned} I_1 &= \sigma_{ii} \\ \sqrt{3J_2} &= \sigma_{\text{MISES}} \end{aligned} \tag{6.19}$$

To construct the failure surface κ is varied from 0 to 1. For each triaxial loading case the standard Newton Raphson algorithm with a step size of $\Delta\Lambda = 0.002$ is used. To reach the critical state for all triaxial loading cases during the ABAQUS analysis the stabilization algorithm provided by ABAQUS is used. It was shown in Section 6.4 that the stabilization method does not significantly influence the solution. To achieve the triaxial loading conditions the following master nodes of a single undeformed Kelvin Cell are assigned to compressive loads:

SEB	compressive load F_1 (corresponding to σ_1) in x direction
NWB	compressive load F_2 (corresponding to σ_2) in y direction
SWT	compressive load F_3 (corresponding to σ_3) in z direction

Like for the uniaxial compression in rise direction (see Section 6.3) F_1 is set to 405 N. According to Equation (6.17) one findes for σ_2 and σ_3:

$$\sigma_3 = \sigma_2 = \frac{F_1}{A_1}\kappa \tag{6.20}$$

with $A_1 = (2\sqrt{2}l)^2$ as the undeformed unit cell surface in the y-z plane (see Figure 6.1). For σ_2 and σ_3 one can write:

$$\sigma_2 = \frac{F_2}{A_2}, \qquad \sigma_3 = \frac{F_3}{A_2} \tag{6.21}$$

where $A_2 = \mu(2\sqrt{2}l)^2$ is the undeformed unit cell surface in the x-y and the x-z plane (see Figure 6.1). Using Equations (6.20) and (6.21) one finds for F_2 and F_3:

$$F_3 = F_2 = \mu\kappa F_1 \tag{6.22}$$

The usage of undeformed, initial surface areas implies that the stresses are given in terms of nominal and not of true stresses.

Figure 6.8 shows the deformation in rise direction u_1^{SEB} of the SEB master node plotted against the load parameter Λ in the case of pure hydrostatic pressure. Although the stabilization algorithm is used, the ABAQUS analysis is aborted before $\Lambda = 1$ is reached. At $\Lambda_{\mathrm{stop}} = 0.43$ the solution branches from the trivial loading path. No increments with $\Lambda > \Lambda_{\mathrm{stop}}$ can be treated with the Bloch Wave program, because the program does not deliver any physically meaningful results on the non-trivial loading path. A similar diagram can be drawn for all triaxial loading cases. Λ_{stop} depends on κ and can be evaluated for each triaxial loading case. All increments of the ABAQUS analysis with $\Lambda > \Lambda_{\mathrm{stop}}$ are ignored in the following analysis. This was no restriction to the analysis

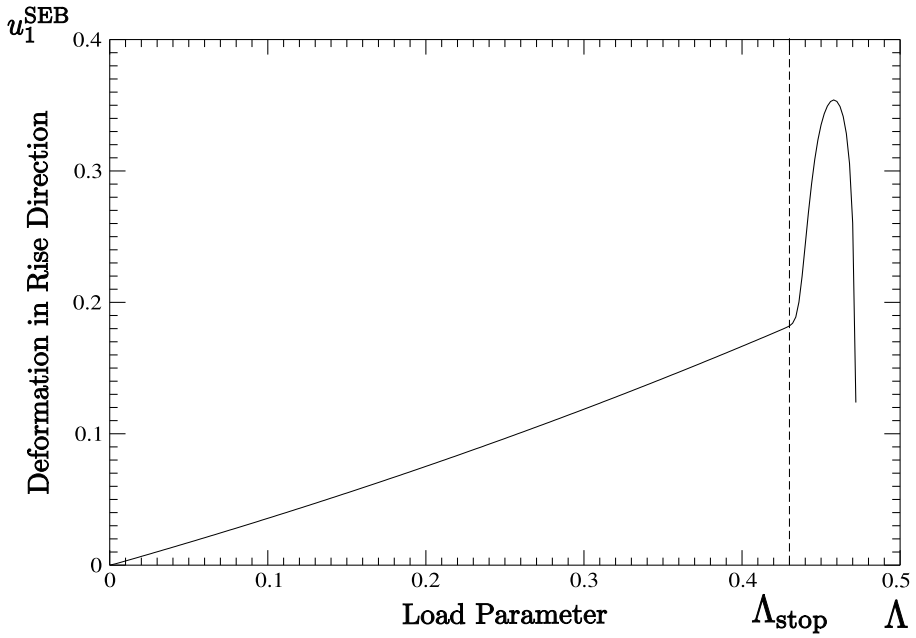

Figure 6.8: Deformation of the SEB master node plotted against the load parameter for hydrostatic loading.

made, because it turned out that the critical state for each triaxial loading case is found to occur before Λ_{stop} is reached.

To determine the critical stresses for all investigated values of κ and the nature of the corresponding mode all three parts of the Bloch Wave Program (see Appendix A) are applied to each triaxial loading case. The results are summarized in Figure 6.9. I_1 and $\sqrt{3J_2}$ are normalized by the critical stress σ_c under uniaxial compressive loading for an isotropic foam ($\mu = 1$) with infinite extent. The critical mode for uniaxial loading in rise direction ($\kappa = 0$) corresponds to a long wave length mode (see Section 6.3). The critical mode remains global in nature as long $\kappa \lessapprox 0.6$. For intermediate values of κ the corresponding mode involves only a few cells. For triaxial loading cases close to pure hydrostatic pressure ($\kappa \gtrapprox 0.675$) the critical mode becomes local to a single unit cell (strictly periodic mode). The failure envelope calculated in this section is in good agreement with the one reported in [17].

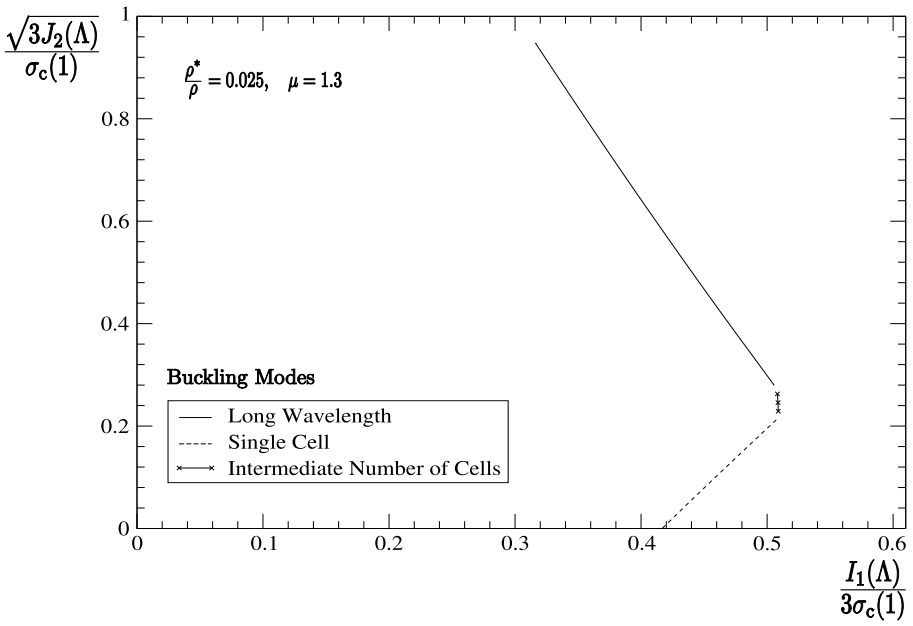

Figure 6.9: Anisotropic foam failure envelope in $\frac{\sqrt{3J_2}}{\sigma_c}$ versus $\frac{I_1}{3\sigma_c}$ plane.

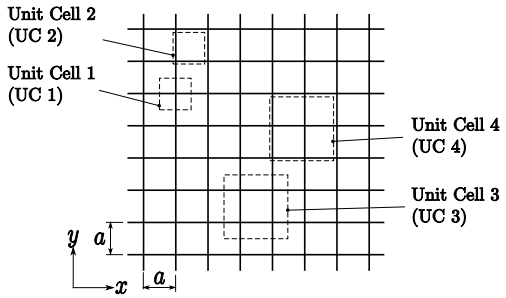

Figure 7.1: Periodic lattice with infinite extent in x- and y-direction.

7 Periodic 2D Lattices

For testing the Bloch Wave analysis Program for 2D unit cells a two dimensional square periodic lattice is assumed (see Figure 7.1). The lattice has infinite extent in x- and y-direction. In order to obtain a two dimensional problem, only deformations in the x-y plane are allowed.

7.1 Characteristic Cell

The smallest geometrically periodic unit of the lattice can be modeled in two different, but mechanically equivalent ways (see Figure 7.2). Both unit cells (Unit Cell 1 and Unit Cell 2) are not able to reproduce the buckling mode of the periodic lattice depicted in Figure 7.4. This buckling mode occurs for square lattices which are braced against lateral sway and are loaded under compression [5]. Unit Cell 3 and Unit Cell 4, depicted in Figure 7.3, are able to reproduce the buckling mode shown in Figure 7.4. Both UC3 and UC4 are also geometrically periodic units of the infinite square lattice. UC3 is mechanically equivalent to UC4. Because of the fact that UC1, UC2, UC3, and UC4 are different possibilities to represent the same infinite periodic lattice the Bloch Wave Analysis (BWA) program must deliver the same results for the critical stress corresponding to a buckling mode with infinite wavelength (macroscopic onset-of-failure) for all four unit cells. The Bloch Wave Analysis part of the BWA program should deliver the same results for UC1 and UC2 and for UC3 and UC4. The critical load corresponding to a buckling mode local to one unit cell (strictly periodic mode) should be the same for UC1 and UC2 and for UC3 and UC4.

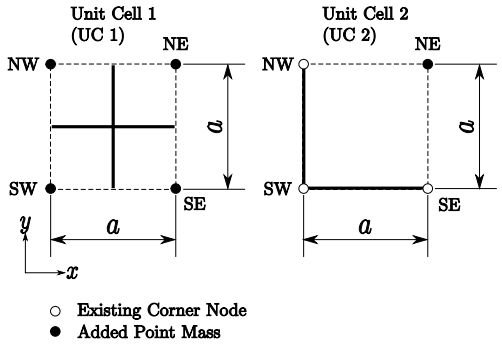

Figure 7.2: Smallest geometrically periodic units of an infinite square periodic lattice.

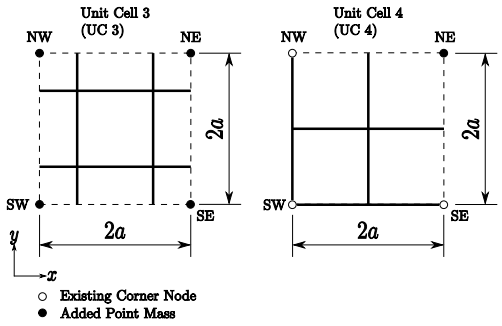

Figure 7.3: Unit cells of an infinite square periodic lattice; able to handle the buckling mode shown in Figure 7.4.

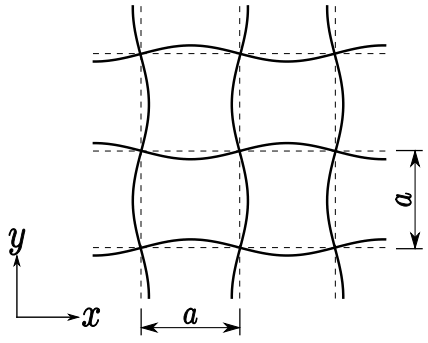

Figure 7.4: Buckling mode of a square lattice braced against lateral sway.

7.2 F.E.M. Model

The material of the periodic lattice is assumed to be linearly elastic with the following values for the elastic modulus E and the Poisson's ration ν:

$$\begin{aligned} E &= 70000\,\text{MPa} \\ \nu &= 0.3 \end{aligned}$$

All four unit cells (UC1, UC2, UC3, and UC4) are used to model the square periodic lattice with the lattice parameter a being 10 mm. The ligaments of all four unit cells are modeled using quadratic beam elements in space (B32 in ABAQUS) with an element length of 1 mm and square cross-sectional area. The beam section orientation for the vertical and horizontal beams is shown in Figure 7.5. The cross section has a width w of 1 mm and a height h of 0.5 mm. One receives a total number of 20 elements and 41 nodes with 123 active degrees of freedom (DOFs) for UC1 and UC2 and a total number of 80 elements and 160 nodes with 480 active DOFs for UC3 and UC4. The periodic boundary conditions are defined manually using Equations 2.1 and 2.3 given in Section 2.1. To use these equations, additional point masses are added where no Finite Element node exists in the corners of the unit cell (see Figures 7.2 and 7.3). To avoid rigid body movements some of the displacements of the SW and SE master nodes are constrained:

$$\begin{aligned} \underset{\sim}{\boldsymbol{u}}_{\text{SW}} &= \{0, 0\}, \\ \underset{\sim}{\boldsymbol{u}}_{\text{SE}} &= \{u_{\text{SE}}, 0\}. \end{aligned}$$

For UC1 and UC 3 the master nodes in the corners of the unit cell are not connected to the other nodes of the unit cell model by any elements (see Figures 7.2 and 7.3). Therefore, the displacements in x- and y- direction of an internal node have to be constrained additionally to avoid rigid body movements.

Note, that for a 2D problem the displacements in z- direction and the rotations about the x- and the y- axis have to be constrained for all nodes in the unit cell.

As already mentioned quadratic beam elements in space (B32) are used instead of quadratic beam elements for 2D problems (B22) to model the ligaments of the periodic lattice. This is done for testing the program against the usage of elements with the wrong dimensional-

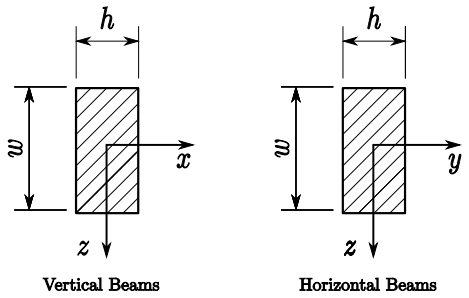

Figure 7.5: Beam section orientation of vertical and horizontal beams.

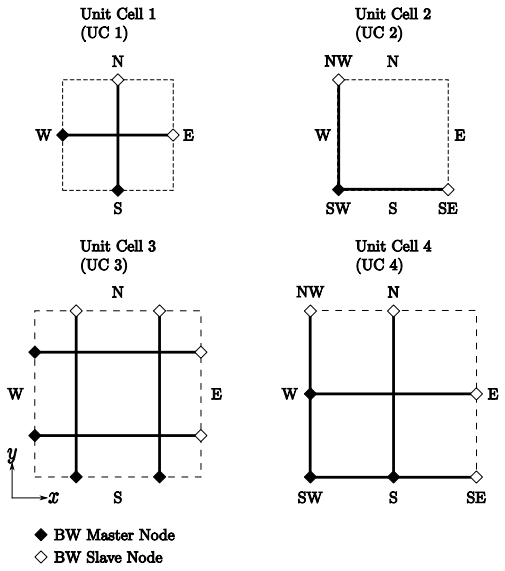

Figure 7.6: Bloch Wave master and Bloch Wave slave nodes for UC1 to UC4.

ity. To have a pure 2D problem the displacements in z- direction and the rotations about the x- and y- axis of all nodes in the unit cell UC1 to UC4 are constrained during the ABAQUS analysis. The Bloch Wave analysis program uses the unconstrained (!!) tangent stiffness matrix, therefore, the problem that acctually is a 2D problem is treated as 3D problem by the BWA program. This fact would lead to wrong results delivered by the BWA program. In Appendix B a workaround for this problem is presented.

The Bloch Wave (BW) master nodes and the Bloch Wave slave nodes are not necessarily equal to the master nodes and the slave nodes defined for the periodic boundary conditions. The BW master and slave nodes for all four unit cells are shown in Figure 7.6. For example SEB of UC4 is a master node for the definition of the periodic boundary conditions,

whereas it is a BW slave node. UC1 has two BW master nodes (one on the West side and one on the South side of the unit cell) and two BW slave nodes (one on the East side and one on the North side of the unit cell) whereas UC2 has only one BW master node in the South West corner of the unit cell and two BW slave nodes (one in the South East corner and one in the North West corner of the unit cell). UC3 has four BW master nodes (two on the West side and on the South side of the cell) and four BW slave nodes (two on the East side and two on the North side of the cell). For UC4 one finds one BW master node in the South West corner of the cell and one BW master node on the West and on the South side of the unit cell, respectively. UC4 has four BW slave nodes (one in the South East corner, one in the North West corner, one on the East side and one on the West side of the unit cell). The size of the matrices used in the BWA program depends strongly on the number of the master and slave nodes of the unit cells and has an influence on the computational time required for the analysis. Therefore, one can see that UC2 should give the shortest computational time needed followed by UC1. UC4 should need less computational time than UC3 but more than UC1.

7.3 Uniaxial Compression

To test the Bloch Wave analysis (BWA) program UC1 to UC4 are subjected to a compressive load in x-direction. For all unit cells the compressive load (reference load $F_1 = 290\,\mathrm{N}$ for UC1 and UC2 and F_1=145 N for UC3 and UC4) is applied to the SE master node (see Figures 7.2 and 7.3). The standard Newton Raphson method with a constant step size of the load parameter $\Delta\Lambda = 0.001$ is used for the ABAQUS analysis. The stabilization algorithm provided by ABAQUS is omitted during the analysis for all four unit cells.

For UC1 and UC2, Figure 7.7 depicts the lowest eigenvalue λ_1^{SP} of the constrained matrix $\underset{\approx}{\mathring{\boldsymbol{K}}}$ plotted against the stress in x-direction σ_1. If $\lambda_1^{\mathrm{SP}} = 0$ the critical state corresponding to the strictly periodic mode is established. If the critical state is found to occur between two increments linear interpolation is used to get closer to the critical state. The eigenvalues received for UC2 are much higher than those received for UC1 and the critical state for UC2 is established at a higher critical load than for UC1.

$$\sigma_{1\mathrm{c,UC1}}^{\mathrm{SP}} = 570.838\ \frac{\mathrm{N}}{\mathrm{mm}^2} \tag{7.1}$$

$$\sigma_{1\mathrm{c,UC2}}^{\mathrm{SP}} = 796.425\ \frac{\mathrm{N}}{\mathrm{mm}^2} \tag{7.2}$$

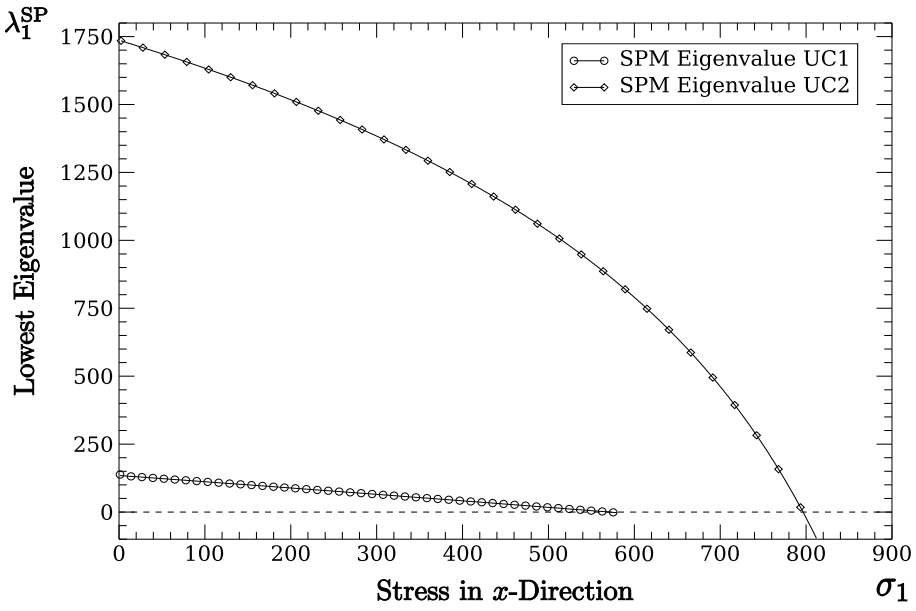

Figure 7.7: Lowest eigenvalue depending on the applied load for the search of the strictly periodic mode of Unit Cell 1 and Unit Cell 2; x-direction.

For the strictly periodic mode analysis $\overset{\circ}{\underset{\approx}{\boldsymbol{K}}}$ must be constrained against rigid body translations. For UC2 the master vector of all nodal DOFs can be written as:

$$\underset{\sim}{\boldsymbol{u}}_1 = \{u_{\mathrm{SW}}, v_{\mathrm{SW}}, \theta_{\mathrm{SW}}\}^{\mathrm{T}} \tag{7.3}$$

For the constrained master vector therefore, one finds:

$$\underset{\sim}{\boldsymbol{u}}_1 = \{0, 0, \theta_{\mathrm{SW}}\}^{\mathrm{T}} \tag{7.4}$$

The DOFs of the master vector influence the corresponding degrees of freedom of the slaved nodes and the internal nodes of the unit cell (see Equations 4.22 and 4.28). For UC2 only one rotational DOF of the master vector remains unconstrained. Thus, all other nodes have only the rotational degree of freedom remaining unconstrained. It is not possible to reproduce a strictly periodic mode with only the rotational degrees of freedom being active. Therefore, the results of the strictly periodic mode (SPM) analysis for UC2 are not physically meaningful and must be ignored. To receive meaningful results with the SPM analysis at least two BW master nodes are necessary.

The SPM analysis results for UC3 and UC4 are shown in Figure 7.8.The lowest eigenvalue λ_1^{SP} of the constrained matrix $\overset{\circ}{\underset{\approx}{\boldsymbol{K}}}$ is plotted against the stress in x-direction σ_1. At the

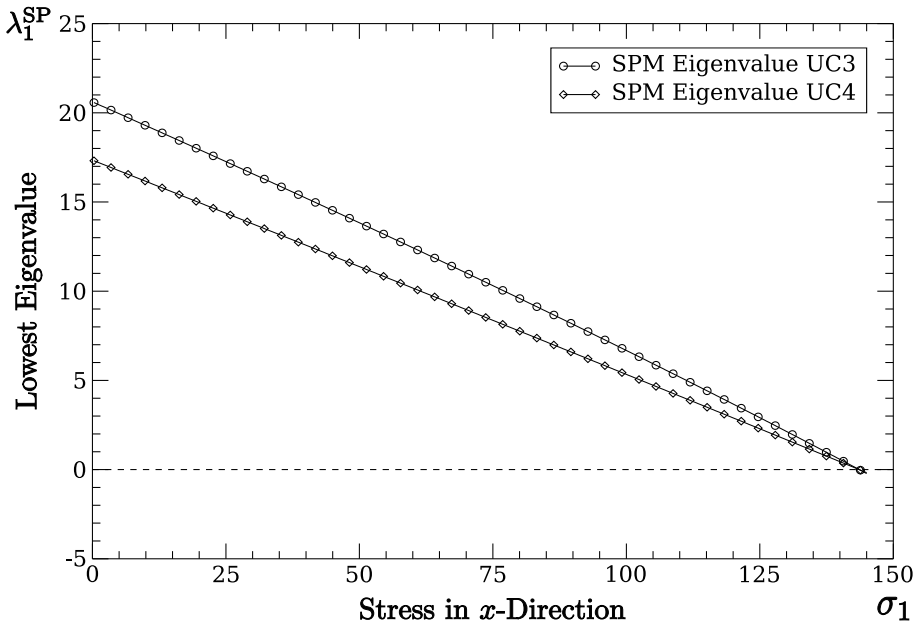

Figure 7.8: Lowest eigenvalue depending on the applied load for the search of the strictly periodic mode of Unit Cell 3 and Unit Cell 4; x-direction.

beginning of the Strictly Periodic Mode analysis the λ_1^{SP} corresponding to the constrained matrix $\underset{\approx}{\mathring{\boldsymbol{K}}}$ of Unit Cell 3 is higher than the eigenvalue received for Unit Cell 4. For Unit Cell 3 and Unit Cell 4 the critical state is established at the same stress in x-direction :

$$\sigma_{1\mathrm{c,UC3}}^{\mathrm{SP}} = \sigma_{1\mathrm{c,UC4}}^{\mathrm{SP}} = 143.620\,\mathrm{N/mm^2} \tag{7.5}$$

For the relative critical stress in x-direction $\sigma_{1\mathrm{c}}^{\mathrm{H}}$ corresponding to a buckling mode with infinite wavelength (macroscopic onset-of-failure (MOF), $N_1 = \infty$) one finds for UC1 to UC4:

$$\sigma_{1\mathrm{c,UC1}}^{\mathrm{H}} = \sigma_{1\mathrm{c,UC2}}^{\mathrm{H}} = \sigma_{1\mathrm{c,UC3}}^{\mathrm{H}} = \sigma_{1\mathrm{c,UC4}}^{\mathrm{H}} = 82.518\,\mathrm{N/mm^2} \tag{7.6}$$

The results of the SPM and the MOF analysis of UC1 to UC 4 are drawn into Figures 7.10 to 7.13 as dashed lines. The results delivered by the BWA program for UC1 to UC4 are depicted in Figures 7.10 to 7.13.

To verify the results achieved with the BWA program, accompanying eigenvalue analyses are performed for columns consisting of a variable number ($N_1 = 1, 2, 10, 26$) of unit cells

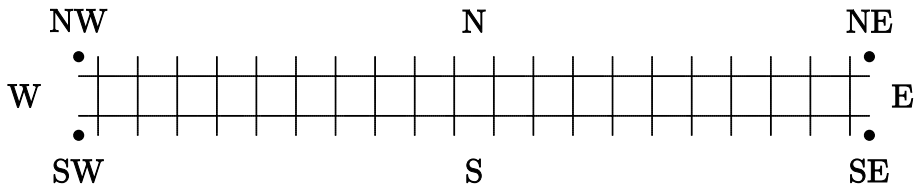

Figure 7.9: Added point mass in the corners of a column consisting of 10 unit cells.

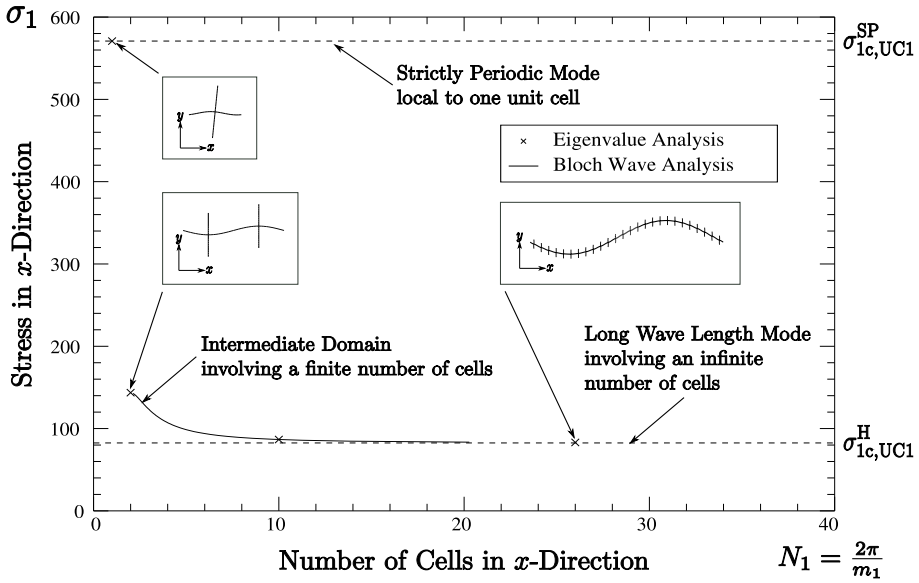

Figure 7.10: Results of the Bloch Wave analysis for Unit Cell 1.

stacked in x-direction using either UC1, UC2, UC3 or UC4. The columns are loaded under compression in x-direction. For all columns the periodic boundary conditions are generated manually. To use the equations given in Section 2.1 additional point masses are added in all column corners where no Finite Element node can be found. Figure 7.9 displays the added point masses in the corners of a column consisting of ten unit cells of type UC 3. The results evaluated for the accompanying eigenvalue analysis for UC1 to UC4 are added in Figure 7.10 to 7.13.

The results received with the BWA program for UC1 are displayed in Figure 7.10 where σ_1 is the stress in the horizontal ligaments. It is remarkable that the critical load for a column made of two unit cells stacked in x-direction is significantly lower than the critical load corresponding to the strictly periodic mode. Further increasing the number of unit cells decreases the critical load while the wave length of the corresponding buckling mode in-

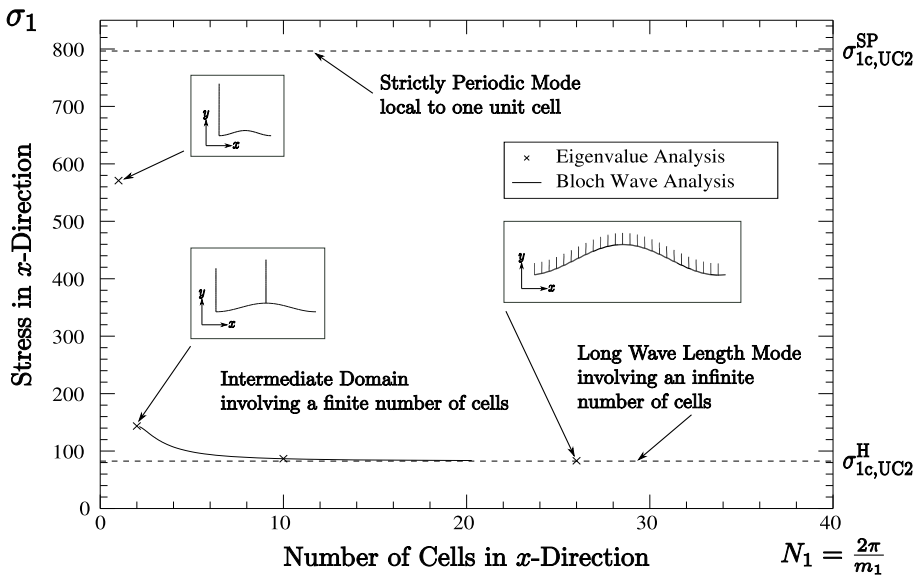

Figure 7.11: Results of the Bloch Wave analysis for Unit Cell 2.

creases. For an increasing number of unit cells the critical load approaches asymptotically to the critical load corresponding to a buckling mode involving an infinite number of unit cells. The results found by the accompanying eigenvalue analysis are in good agreement with the results received by the BWA program.

Figure 7.11 depicts the BWA results received for UC2. As already mentioned the results of the SPM analysis for UC2 are not physically meaningful. Therefore, the critical load received for the accompanying eigenvalue analysis of a single unit cell is different from the critical load received by the SPM analysis. All other results received with the BWA program are in good agreement with the results of the accompanying eigenvalue analysis and the results received for UC1.

The results received with the BWA program for UC3 and UC4 are displayed in Figure 7.12 (UC 3) and in Figure 7.13 (UC 4), respectively. The results found for UC 3 are equal to those found for UC 4. In both cases the strictly periodic mode is shown by a column consisting of a single unit cell. The critical load drops significantly for a column made of two unit cells stacked in x - direction. For an increasing number of unit cells the critical load approaches asymptotically to the critical load corresponding to a buckling mode involving an infinite number of unit cells.

Figure 7.14 depicts the comparison of the results received for UC1 and UC2 and Figure

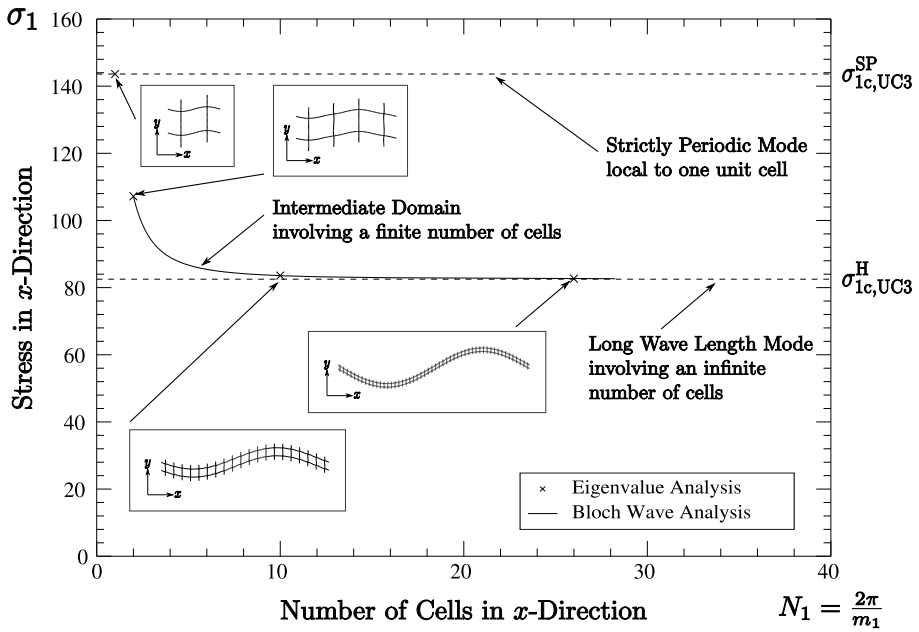

Figure 7.12: Results of the Bloch Wave analysis for Unit Cell 3.

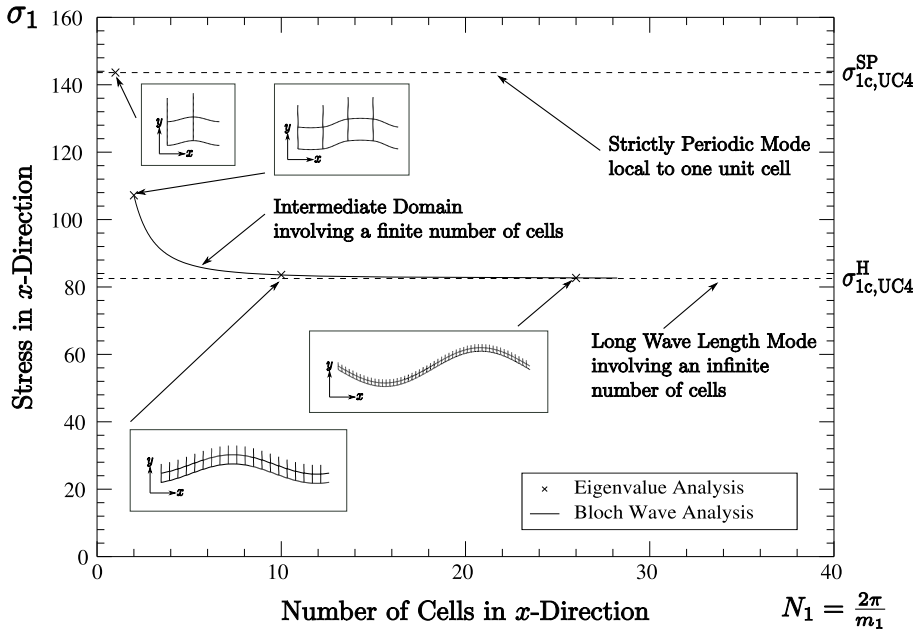

Figure 7.13: Results of the Bloch Wave analysis for Unit Cell 4.

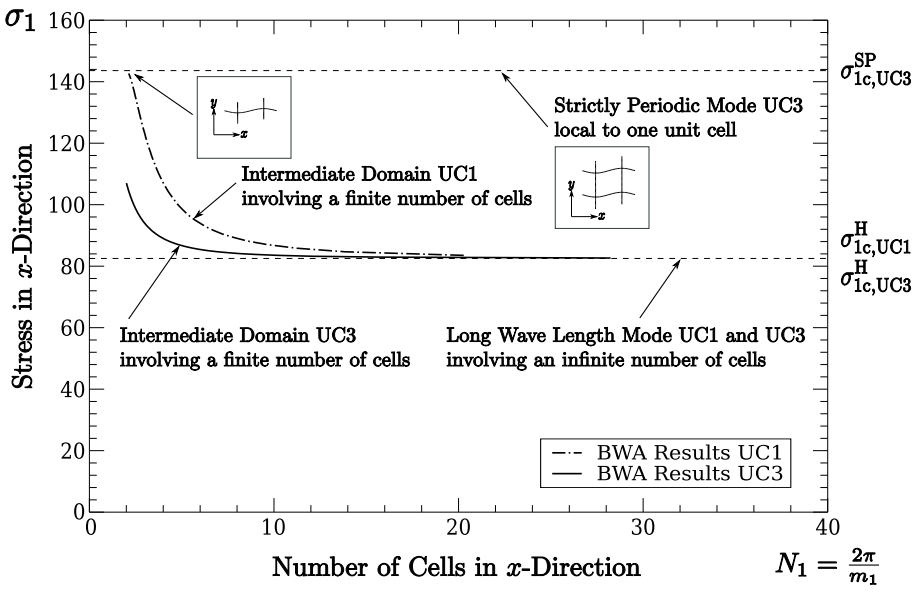

Figure 7.14: Comparison of the results of UC1 and UC3.

7.15 shows the comparison of the results received for UC2 and UC4. The critical stress in x-direction for a column consisting of two UC1 is equal to the critical stress for the strictly periodic mode received for UC3. This is reasonable because a column consisting of two UC1 is equal to a single unit cell of type UC2 (in x-direction). For an inreasing number of unit cells the differences between the critical loads received for UC1 and UC3 are negligible. The statements given for UC1 and UC3 are also true for UC2 and UC4 (see Figure 7.15).

7.4 Bi-axial Loading

The behavior of the periodic lattice is investigated under bi-axial loading conditions. Like for the uniaxial case UC1, UC2, UC3 and UC4 are used to model the periodic lattice. All unit cells are loaded under a radial loading path defined by:

$$\{\sigma_1, \sigma_2\} = \Sigma\{1, \kappa_1\} \tag{7.7}$$

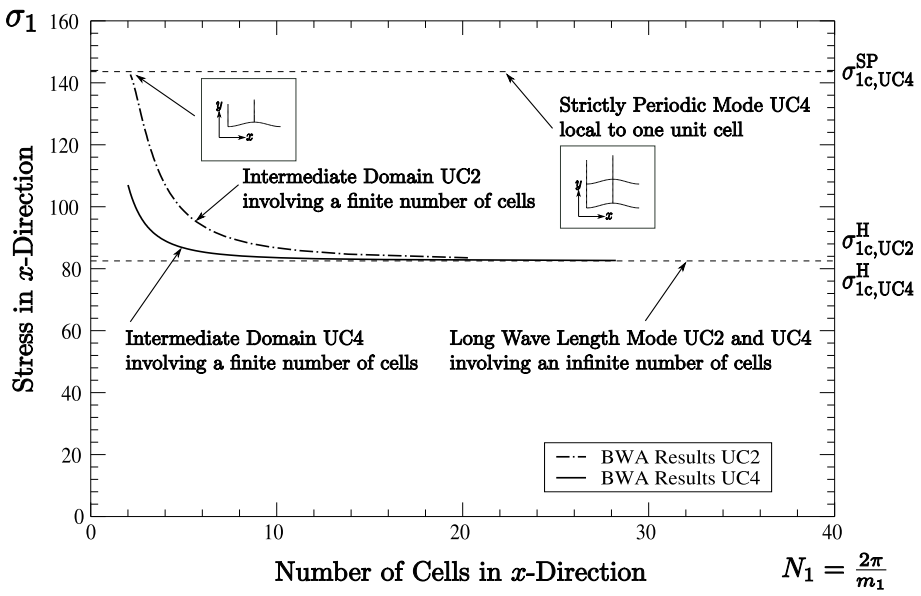

Figure 7.15: Comparison of the results of UC2 and UC4.

with

$$\begin{aligned} 0 &\leq \kappa_1 \leq 1 \\ \Sigma &= \sigma_{1c}\Lambda \quad \text{with} \quad 0 \leq \Lambda \leq 1 \end{aligned} \tag{7.8}$$

and

$$\{\sigma_1, \sigma_2\} = \Sigma\{\kappa_2, 1\} \tag{7.9}$$

with

$$\begin{aligned} 0 &\leq \kappa_2 \leq 1 \\ \Sigma &= \sigma_{1c}\Lambda \quad \text{with} \quad 0 \leq \Lambda \leq 1 \end{aligned} \tag{7.10}$$

with Λ as the load parameter and σ_{1c} as the critical stress in the horizontal ligaments corresponding to the strictly periodic mode of the lattice loaded in x-direction. $\kappa_1 = 0.0$ represents uniaxial loading in x-direction and $\kappa_2 = 0.0$ represents uniaxial loading in y-direction. $\kappa_1 = 1.0$ and $\kappa_2 = 1.0$ represent pure hydrostatic pressure. Because the

mechanical properties of all unit cells are equal in x- and y-direction, one can write:

$$\sigma_{1c} = \sigma_{2c} \tag{7.11}$$

where σ_{2c} is the critical stress in the vertical ligaments corresponding to the strictly periodic mode of the lattice loaded in y-direction.

For each value of κ_1 and κ_2 an ABAQUS analysis is performed using the Standard Newton Raphson algorithm with a step size of $\Delta\Lambda = 0.002$. To achieve the bi-axial loading conditions the following master nodes are assigned to compressive loads:

SE compressive load F_1 (corresponding to σ_1) in x-direction

NW compressive load F_2 (corresponding to σ_2) in y-direction

The reference loads of F_1 and F_2 are set to 290 N for UC1 and UC2 and to 145 N for UC3 and UC4. For σ_1 and σ_2 one finds:

$$\sigma_1 = \frac{F_1}{A_1}, \qquad \sigma_2 = \frac{F_2}{A_2} \tag{7.12}$$

with A_1 as the sum of the cross-sectional areas of all horizontal ligaments in the unit cell ($A_1 = wh$ for UC1 and UC2, $A_1 = 2wh$ for UC3 and UC4) and A_2 as the sum of the cross-sectional areas of all vertical ligaments in the unit cell ($A_2 = wh$ for UC1 and UC2, $A_2 = 2wh$ for UC3 and UC4). Because $A_2 = A_1$ one finds for F_2:

$$F_2 = \kappa_1 F_1 \tag{7.13}$$

F_1 can also be expressed in terms of F_2. With Equations (7.12), (7.9) and $A_2 = A_1$ one receives for F_1:

$$F_1 = \kappa_2 F_2 \tag{7.14}$$

For the evaluation of the wavelength of the critical buckling mode and the corresponding critical load for each value of κ_1 and κ_2 all three parts of the BWA program are executed for each bi-axial loading case. The BWA program delivers the same results for all four unit cells.

For UC1, UC2, UC3 and UC4 the critical mode of a periodic lattice with infinite extent assigned to a compressive load in x-direction corresponds to a long wave length mode (see also Figures 7.10 to 7.13). For all bi-axial loading cases the critical stresses found by the macroscopic onset-of-failure analysis are much lower then those found for the strictly periodic mode or the Bloch Wave analysis. Therefore, the critical buckling mode remains

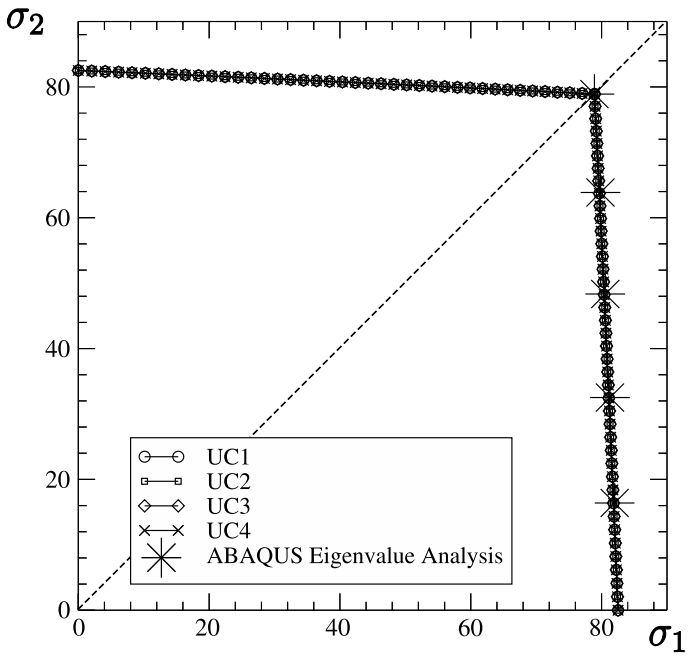

Figure 7.16: Results for all bi-axial loading cases; evaluated using UC1, UC2, UC3 and UC4.

global in nature for all bi-axial loading cases. In Figure 7.16, the critical normal stresses in the vertical ligaments σ_2 are plotted against the critical normal stresses in the horizontal ligaments σ_1. To verify the results delivered by the BWA program an accompanying eigenvalue analysis is performed. In Figures 7.10 to 7.13 one can see, that the critical load for a column consisting of 25 cells is close to the critical load corresponding to a buckling mode with infinite wavelength. Therefore, a periodic lattice consisting of 25×25 cells is used to verify the MOF results of the bi-axial loading cases. The periodic lattice is assigned to the radial loading conditions given in Equations (7.7). Periodic boundary conditions are applied to the periodic lattice consisting of 25×25 cells. The results received by the accompanying eigenvalue analysis are in perfect agreement with the results received with the BWA program (see Figure 7.16). Ohno et al. [20] analyzes 2D periodic lattices subjected to bi-axial in-plane loadings. Figure 3. in [20] displayes the critical buckling stresses corresponding to periodic lattices consisting of different numbers of base cells. For the long wavelength mode the results received in [20] are comparable to those received in the present work.

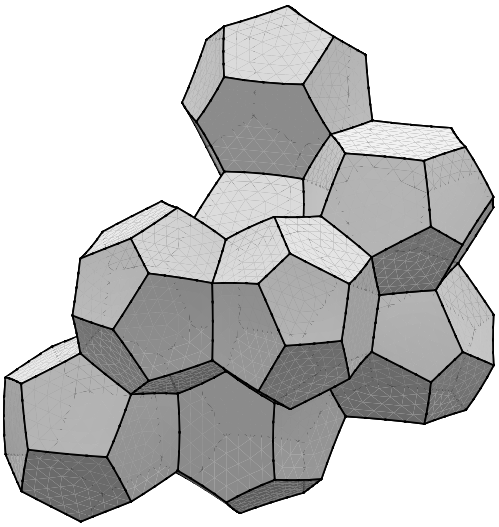

Figure 8.1: Space filling unit cell of the Weaire-Phelan foam. From [6]

8 The Weaire-Phelan Cell

The Kelvin problem was formulated in 1887 by Lord Kelvin (see [26]). The aim of the Kelvin problem is to find a periodic structure which fills a given fraction of space with equal sized cells and minimum surface area. The Weaire-Phelan foam found in 1994 by Denis Weaire und Robert Phelan (of Trinity College Dublin) is like the Kelvin cell (see Section 6) a solution of the Kelvin problem and beats the Kelvin cell by about 0.3% in surface area.

8.1 Characteristic Cell

Figure 8.1 shows the unit cell of a Weaire-Phelan foam which fills space when replicated in a cubic lattice. This unit cell consists of eight cells of two different types: two irregular pentagonal dodecahedron and six 14-hedra. To use the BWA program on the Weaire-Phelan foam a cubic unit cell is required (see Figure 8.2). The cell dimension of the Weaire-Phelan unit cell used in the present work is $2 \times 2 \times 2$ mm.

As already mentioned the Weaire-Phelan foam consists of two different cell types. The pressure in the different cell types is not the same, therefore, all faces shared by an dodecahedron and a 14-hedron cell are curved. In the present work this surface curvature is ignored for all Weaire-Phelan Cells used.

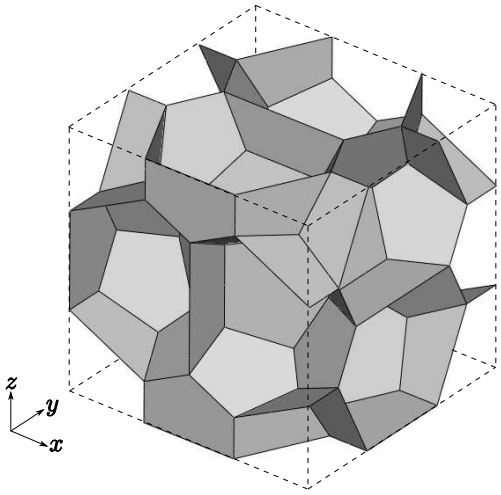

Figure 8.2: Cubic unit cell of the Weaire-Phelan foam. From [6].

8.2 F.E.M. Model

The geometry of the cubic unit cell shown in Figure 8.2 is provided by Dipl. Ing. Robert Bitsche. The faces of the unit cell are meshed using linear shell elements of ABAQUS type S4. The size of the tangent matrix of a structure is limited by Python's Numeric module to about 16000×16000. Thus, the number of elements to be used for meshing the Weaire-Phelan unit cell is limited. The F.E. model has a total number of 1632 elements, 1604 nodes and 9624 degrees of freedom. The meshed Weaire-Phelan Cell is depicted in Figure 8.4. It turned out that the Weaire-Phelan Cell is sensitive to small geometric imperfections. For a detailed description see Appendix C. To avoid the geometric imperfections only one eighth of the unit cell is meshed (see Figure 8.3). The node which lie on (or close to) a surface of the reduced unit cell are forced to have exactly the surface coordinates. The edges of the unit cell are added with dashed lines in Figure 8.3. The full unit cell can be constructed by mirroring the reduced cell about the mirror planes shown in Figure 8.3. The elements in the mirror planes and the elements on the opposite unit cell surfaces must not be reflected.

The shell thickness is calculated using (from [6]):

$$t = \rho_{\text{rel}} \frac{V_{\text{uc}}}{A_{\text{SE}}} \tag{8.1}$$

with V_{uc} as the total volume of the cubic unit cell, A_{SE} as the surface area of all faces in

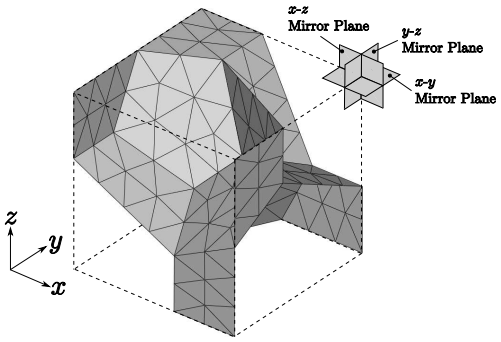

Figure 8.3: One eighth of the Weaire-Phelan Cell meshed with elements of ABAQUS type S3R. For the actual analysis quadliteral elements of ABAQUS type S4 are used.

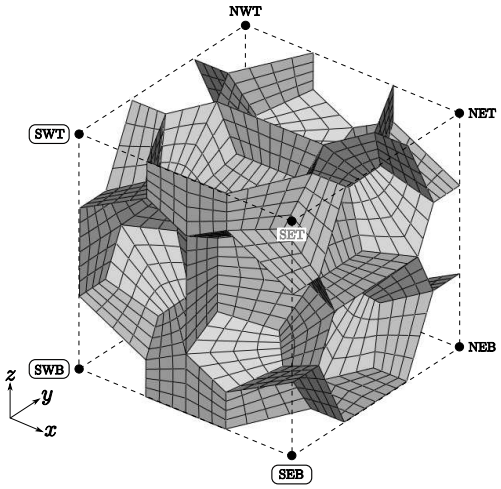

Figure 8.4: Meshed unit cell of the Weaire-Phelan foam.

a unit cell and ρ_{rel} as the relative density of the foam. For the relative density one finds

$$\rho_{\mathrm{rel}} = \frac{V_{\mathrm{s}}}{V_{\mathrm{us}}} \tag{8.2}$$

where V_{s} is the volume of the solid material of the unit cell. To ensure elastic buckling the shell thickness must be rather small. This results in a small relative density ρ_{rel}. Thus the relative density is assumed to be 1% ($\rho_{\mathrm{rel}} = 0.01$). With the appropriate values for V_{uc} and A_{SE} (from [6]):

$$V_{\mathrm{uc}} = 8\,\mathrm{mm}^3 \quad A_{\mathrm{SE}} = 21.1539\,\mathrm{mm}^2 \tag{8.3}$$

one receives for the shell tickness:

$$t = 0.0037818. \tag{8.4}$$

The bulk material is assumed to be isotropic and linear elastic with the following values for the elastic modulus E_{s} and Poissons ratio ν_{s}:

$$\begin{aligned} E_{\mathrm{s}} &= 70000\,\mathrm{MPa} \\ \nu_{\mathrm{s}} &= 0.3 \end{aligned} \tag{8.5}$$

The periodic boundary conditions are specified using the CBC-program. The CBC-program generates additional point masses in the corners of the cubic unit cell (Figure 8.4). This point masses do not influence the solution of the F.E.M. analysis or the results of the BWA program. To avoid rigid body movements some of the displacement degrees of freedom of the master nodes in the corners of the cell must be constrained:

$$\begin{aligned} \underset{\sim}{\boldsymbol{u}}_{\mathrm{SWB}} &= \{0, 0, 0\} \\ \underset{\sim}{\boldsymbol{u}}_{\mathrm{SEB}} &= \{u_{\mathrm{SEB}}, 0, 0\} \\ \underset{\sim}{\boldsymbol{u}}_{\mathrm{NWB}} &= \{u_{\mathrm{NWB}}, v_{\mathrm{NWB}}, 0\} \end{aligned} \tag{8.6}$$

The master nodes in the corners of the unit cell are not linked by any elements to the other nodes of the unit cell model therefore, all displacement and rotational degrees of freedom of an internal node must additionally be constrained.

8.3 Determination of the Elastic Modulus

For the determination of the elastic modulus the Weaire-Phelan unit cell is subjected to a compressive load in x-direction. The load is applied in a linear pertubation analysis to the SEB master node (see Figure 8.4). The deformation of the loaded unit cell is read from the ABAQUS results file. For the relativ elastic modulus $\frac{E^*}{E_s}$, normalized by the elastic modulus of the bulk material one finds:

$$\frac{E^*}{E_s} = 0.003458 \tag{8.7}$$

8.4 Uniaxial Compression

The compressive load in x-direction is applied to the SEB master node of a single cubic unit cell of the Weaire-Phelan foam and has a reference value of 0.5 N. The standard Newton Raphson method with a constant step size $\Delta\Lambda = 0.01$ of the load parameter Λ. In comparison to the step sizes used for the Kelvin cell ($\Delta\Lambda = 0.001$) and the periodic lattices ($\Delta\Lambda = 0.002$) the step size used for the Weaire-Phelan Cell is rather large. Because of the larger number of elements used in the Weaire-Phelan model the computational time for a single analysis step of the BWA program is much higher than the computational time needed for the Kelvin cell or the periodic lattices. To keep the required computational time within equitable bounds, it is reasonable to increase the step size of the F.E.M. Analysis. The results are verified using the accompanying eigenvalue analysis on columns consisting of different numbers of unit cells ($N_1 = 1, 40, 80$).

Figure 8.5 displays the result received by the SPM analysis and the accompanying eigenvalue analysis (ALEA) applied to a single unit cell of the uniaxial case. The critical state corresponding to the strictly periodic mode is established for a critical stress in rise direction of:

$$\sigma_{1c} = 0.09913\,\mathrm{N/mm^2} \tag{8.8}$$

The macroscopic onset of failure analysis delivers no result for the Weaire-Phelan Cell loaded in x-direction and the standard Bloch Wave analysis does not deliver any results for all m_1 for $N_1 > 1$. For loads higher than the critical load found by the SPM analysis all lowest eigenvalues of the reduced stiffness matrix $\overset{\circ}{\underset{\approx}{\boldsymbol{K}}}$ are negative independent of the wave number m_1. For $N_1 = 40$ and $N_1 = 80$ the accompanying eigenvalue analysis is time consuming, therefore, these structrues are pre-loaded close to the critical state

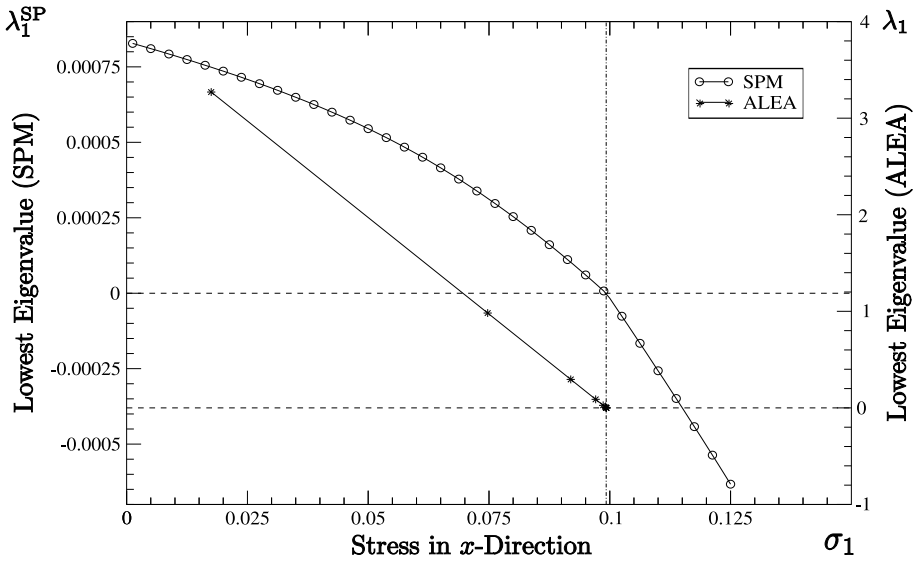

Figure 8.5: Comparison between the results of the SPM analysis and the accomanying linear eigenvalue analysis of a single unit cell for the uniaxial loading case.

found by the SPM analysis, and then the eigenvalue buckling prediction of ABAQUS is used to determine the eigenvalue and the corresponding buckling mode of the structure. For $N_1 = 40$ and $N_1 = 80$ no critical buckling modes involving multiple cells or an infinite number of cells are found to occur. The critical stress found by the accompanying eigenvalue analysis is equal to the critical stress found by the SPM analysis, and the corresponding buckling mode is local to a single unit cell.

8.5 Pure Hydrostatic Pressure

The Weaire-Phelan Cell is also subjectd to compressive loading defined by:

$$\{\sigma_1, \sigma_2, \sigma_3\} = \Sigma\{1, 1, 1\} \tag{8.9}$$

with

$$\Sigma = \sigma_{1c}\Lambda \quad \text{with} \quad 0 \leq \Lambda \leq 1 \tag{8.10}$$

with Λ being the load parameter and σ_{1c} being the critical stress corresponding to the strictly periodic mode for uniaxial loading in x-direction. For the triaxial loading the following master nodes of a single Weaire-Phelan Cell are assigned with compressive loads:

SEB	compressive load F_1 (corresponding to σ_1) in x direction
NWB	compressive load F_2 (corresponding to σ_2) in y direction
SWT	compressive load F_3 (corresponding to σ_3) in z direction

The reference loads F_1, F_2 and F_3 are set to 0.4 N. The standard Newton Raphson method with a constant step size of the load parameter of $\Delta\Lambda = 0.01$ is used. All parts of the BWA program are used for identifying the critical loads and the wave length of the corresponding buckling modes.

Only the SPM analysis part of the program delivers any meaningful results. Figure 8.6 displays the lowest eigenvalue of the reduced stiffness matrix plotted against the mean stress $\sigma_m = \frac{\sigma_{ii}}{3}$. The critical state corresponding to the strictly periodic mode is established at:

$$\sigma_{\mathrm{mc}} = 0.04524\,\mathrm{N/mm^2} \tag{8.11}$$

After the critical state is established all lowest eigenvalues of the reduced stiffness matrix $\overset{\approx}{\boldsymbol{K}}^{\circ}$ are negative independent of the wave numbers m_i. To verify the results of the BWA program the eigenvalue buckling prediction of ABAQUS is used on arrays consisting of $2 \times 2 \times 2$, and $4 \times 4 \times 4$ cells [3]. The microsections are pre-loaded close to the critical state found by the SPM analysis and then the eigenvalue buckling prediction of ABAQUS is used to determine the eigenvalue and the corresponding buckling mode of the models. For the tested models the critical stress corresponds to the critical stress found by the SPM analysis. Figure 8.6 depicts the critical buckling mode for a array consisting of $4 \times 4 \times 4$ cells.

[3] The buckling eigenvalue prediction for $6 \times 6 \times 6$ cells was not possible due to the huge numerical requirements.

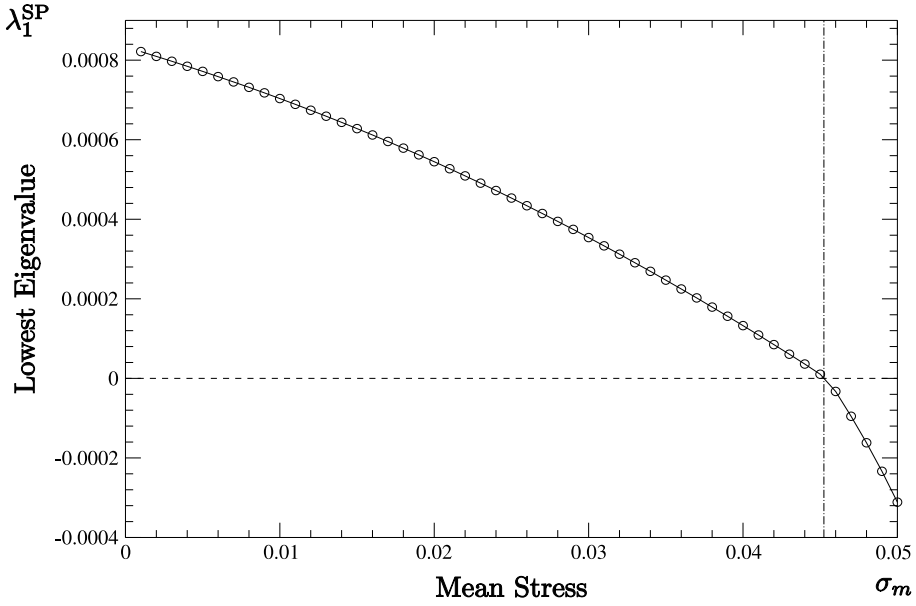

Figure 8.6: Results of the SPM analysis for the case of pure hydrostatic pressure.

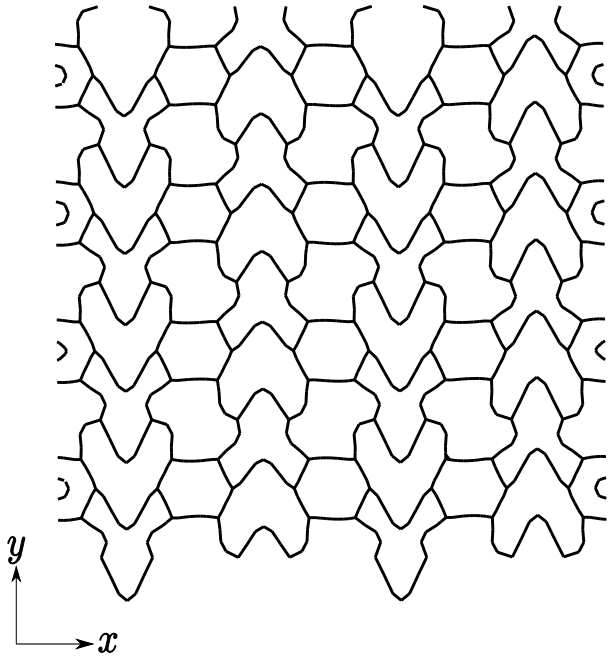

Figure 8.7: Predicted buckling mode of a microsection consisting of 4x4x4 unit cells. Structure cut at $z = 0.1\,\text{mm}$.

9 Conclusions

In the present thesis the microscopic and macroscopic onset-of-failure concepts were used to detect the onset of buckling in periodic structures loaded under compression. The Finite Element representation of the macroscopic onset-of-failure concept, presented in [17], was extended to arbitrary unit cells, and both, the microscopic and macroscopic onset-of-failure concepts were applied to different periodic structures.

One of these periodic structures was an open cell foam, represented by space-filling Kelvin Cells. A Kelvin unit cell model was subjected to uniaxial and a set of triaxial loads. The results obtained with the microscopic and macroscopic onset-of-failure concept were in good agreement with the results reported in the literature. It turned out that the detection of the critical stresses and the corresponding buckling modes strongly depend on the step size of the load parameter $\Delta\Lambda$ used in the ABAQUS analysis. For the Kelvin Cell loaded in transverse direction the critical stress corresponding to a buckling mode with infinite wavelength and the critical stress corresponding to the strictly periodic mode are only separated by a small interval. This small interval can only be detected if $\Delta\Lambda$ is small enough. Reducing $\Delta\Lambda$, however, increases the required numerical effort significantly.

In the analysis of the 2D periodic lattice it was shown that the results for the critical stress and the corresponding buckling mode are independent of the cell count of the periodic unit used for the analysis. The 2D periodic lattice was modeled using four different unit cells the smallest of which corresponds to the smallest periodic building block of the structure. All four cells were subjected to uniaxial and bi-axial compressive loads. The results for all unit cells were in perfect agreement. Nevertheless, the minimum size of the unit cell is restricted to at least two active Bloch Wave master nodes, because otherwise the results for the strictly periodic mode are not physically meaningful. This is due to the fact that for the strictly periodic mode analysis the displacement degrees of freedom of a Bloch Wave master node must be subjected to additional constraints.

The investigated Weaire-Phelan Cell had a large number of active degrees of freedom and, therefore, was close to the limitations of the Numeric module of the programming language "Python". The cell was subjected to pure hydrostatic pressure and a uniaxial compressive load. For both load case the critical buckling mode is local to a single unit cell and, like the corresponding critical stress, independent of the number of basis cells that form the periodic structure. The verification of the results obtained for the Weaire-Phelan Cell by an accompanying linear eigenvalue analysis of fully resolved multi-cells failed even for arrays consisting of a low number of unit cells due to excessive numerical requirements.

In the present work it was shown that both, the microscopic and macroscopic onset-of-failure concept are powerful tools for the search of the critical stress and the corresponding buckling mode of periodic structures loaded under compression.

A Bloch Wave Program

A.1 Introduction

The Bloch Wave analysis (BWA) program facilitates the search for the critical state of periodic structures loaded under compression. All analysis steps are performed on one fundamental building block of the microstructure, the so-called unit cell, instead of dealing with the whole, potentially infinite structure. The program only works for rate-independent materials.

For the implementation of the program, the PYTHON language was chosen. PYTHON runs on all major operating systems and is an easy to learn and stable programming language. One negative aspect of this language is, that the size of the matrices that can be handled with the Numeric module of Python is limited. Therefore, the number of nodes (or degrees of freedom) in a unit cell is currently restricted.

This chapter gives an short overview over the input files required for running an analysis and the output files written by the BWA program. The three main parts of the BWA program will be described briefly.

A.2 Flow Diagram

Figure A.1 gives an overview of all steps needed to perform a Bloch Wave analysis. The Bloch Wave Program itself consists of three different parts, which can be executed independently and which process four different types of input files.

All information about the unit cell is given in the ABAQUS input file containing nodal, element, material and section definitions. The equations defining the periodic boundary conditions can either be put in manually, or, alternatively, the CBC-program (Cube-periodic Boundary Conditions) by Daxner and Pahr can be used for their automatic generation.

The ABAQUS/Standard analysis (load controlled Newton-Raphson) delivers two different files: the .dat file from which the increment time information is read and the .mtx file containing the element stiffness matrices of all elements in the unit cell for each increment.

The fourth input file for the BWA program is the command file. It is an user written .txt

file defining all program settings.

Each part of the program writes a number of output files by default. For the BWA part an optional output file can be generated containing the displacement fields of the critical modes found in the analysis.

In the next subsections all input and output files will be described in greater detail.

A.3 Main Parts of the Program

The Bloch Wave analysis Program consists of three parts which can be executed independently.

In the neighborhood of $\underset{\sim}{\boldsymbol{m}} = 0$ two different modes coexist. For $\forall m_i = 0$ the critical mode is strictly periodic to the unit cell, whereas for one $m_i \to 0$ the buckling mode is global in nature.

The case of $\forall m_i = 0$ should be treated by the Strictly Periodic Mode Part of the program. In this part of the program, Equation (4.34) must be restricted against rigid body translation, so the displacement degrees of freedom of one master node (BW master, see Chapter 3) of the unit cell are constrained. The reduced stiffness matrix $\overset{\circ}{\underset{\approx}{\boldsymbol{K}}}$ can be partitioned in the following way:

$$\bar{\underset{\sim}{\boldsymbol{u}}}_1^{\mathrm{T}} \overset{\circ}{\underset{\approx}{\boldsymbol{K}}} \underset{\sim}{\boldsymbol{u}}_1 = \left(\begin{array}{c} \bar{\underset{\sim}{\boldsymbol{u}}}_{1\mathrm{U}}^{\mathrm{T}}, \underset{\sim}{\boldsymbol{0}}^{\mathrm{T}} \end{array} \right) \left[\begin{array}{cc} \overset{\circ}{\underset{\approx}{\boldsymbol{K}}}_{\mathrm{UU}} & \overset{\circ}{\underset{\approx}{\boldsymbol{K}}}_{\mathrm{UB}} \\ \overset{\circ}{\underset{\approx}{\boldsymbol{K}}}_{\mathrm{BU}} & \overset{\circ}{\underset{\approx}{\boldsymbol{K}}}_{\mathrm{BB}} \end{array} \right] \left(\begin{array}{c} \underset{\sim}{\boldsymbol{u}}_{1\mathrm{U}} \\ \underset{\sim}{\boldsymbol{0}} \end{array} \right) \tag{A.1}$$

with

$$\dim(\underset{\sim}{\boldsymbol{0}}) = (3 \times 1) \tag{A.2}$$

$$\dim(\overset{\circ}{\underset{\approx}{\boldsymbol{K}}}_{\mathrm{UU}}) = (\mathrm{len}(\underset{\sim}{\boldsymbol{u}}_1) \times \mathrm{len}(\underset{\sim}{\boldsymbol{u}}_1)) \tag{A.3}$$

The vector $\underset{\sim}{\boldsymbol{0}}$ represents the zero-valued displacements of the constrained master node and $\underset{\sim}{\boldsymbol{u}}_{1\mathrm{U}}$ represents the unknown displacements and rotations of the unconstrained master nodes as well as the rotations of the constrained master node, with $\bar{\underset{\sim}{\boldsymbol{u}}}_{1\mathrm{U}}$ being its conjugate complex. The reduced stiffness matrix $\overset{\circ}{\underset{\approx}{\boldsymbol{K}}}$ has to be sorted and split accordingly. For the calculation of the lowest eigenvalue of the reduced stiffness matrix only $\underset{\approx}{\boldsymbol{K}}_{\mathrm{UU}}$ is used.

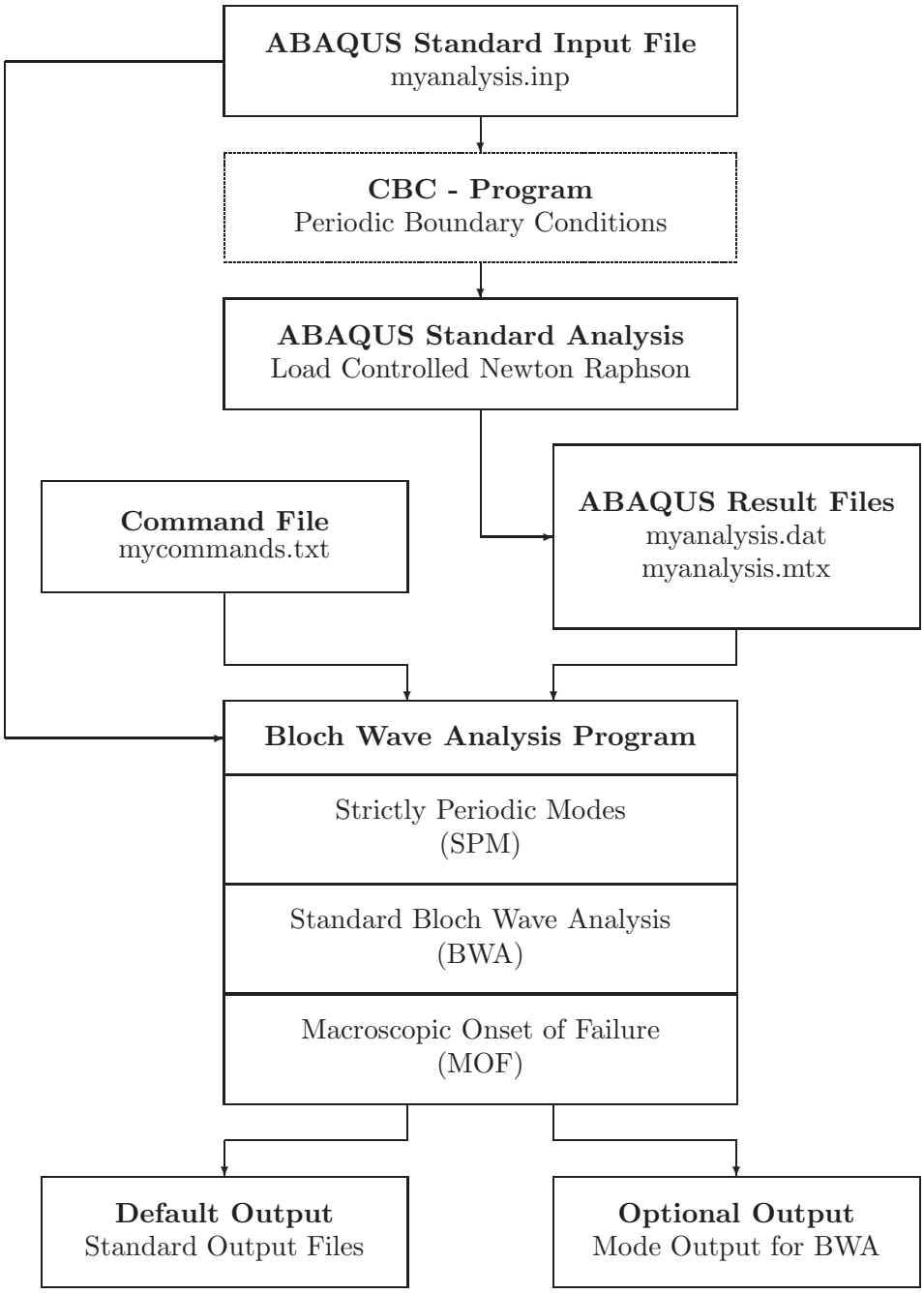

Figure A.1: Flow diagram of a Bloch Wave analysis for periodic structures.

For $m_i \to 0$ one should use the macroscopic onset-of-failure part of the program. In all other cases ($0 < m_i < 2\pi$) the search for the critical state can be performed by using the Standard Bloch Wave analysis part. This part is the computationally most expensive one, because all possible combinations of the wave numbers m_1, m_2, m_3 have to be investigated on a reasonably fine grid.

A.4 Input Files

The user has no influence on the data read from the .dat file and the .mtx file, therefore, only the command file and the ABAQUS input file will be described in detail.

A.4.1 The Command File

The command file is a standard .txt file allowing the user to define all necessary parameters for executing the Bloch Wave analysis Program. In the following the available commands will be explained briefly.

***INPUT**

First line:	name of the input file without file extension .inp
Last line:	**

With *INPUT the ABAQUS input files are defined. Repeat the first line as often as necessary. The command has to finish with ** in the last line. If more than one input file is given, the program loops over all given input files. The corresponding .dat and .mtx files must be given in the same order as the input files.

***RESULT**

First line:	name of the .dat files of the ABAQUS analysis including file extension .dat
Last line:	**

*RESULT gives a list of all .dat files received from ABAQUS standard analysis. Repeat the first line as often as necessary to read all .dat files. The order of the .dat files has to be the same as the order of the ABAQUS input files. The command has to finish with ** in the last line.

***MATRIX**

First line:	name of the .mtx file of the ABAQUS analysis including file extension .mtx
Last line:	**

*MATRIX gives a list of all .mtx files received from the ABAQUS standard analysis. Repeat the first line as often as necessary to define all .mtx files. The order of the .mtx files has to be the same as the order of the ABAQUS input files. the command has to finish with ** in the last line.

***INDIR**

First and only line:	Path of the directory where all input files for the Bloch Wave Program can be found.

For the current implementation of the program only one input and one output directory can be defined.

***OUTDIR**

First and only line:	Path of the directory where all output files should be written to.

***STRICTLY_PERIODIC_MODE**

First and only line:	Number of the first and last increment of the SPM analysis, separated by commas

If the keyword *STRICTLY_PERIODIC_MODE is set then the program part for the search of a strictly periodic mode (SPM) will be executed. For the SPM analysis the output file myinput_SPMallincrements.dat is written. For example:

*STRICTLY_PERIODIC_MODE
42, 52
In this case the SPM-analysis is performed for increments from number 42 to number 52.

***BLOCH_WAVE_ANALYSIS**

First line:	Number of the first and last increment of the Standard Bloch Wave analysis (BWA)
Second line:	$m_{1\text{start}}$, $m_{1\text{end}}$, $m_{1\text{step}}$
Third line:	$m_{2\text{start}}$, $m_{2\text{end}}$, $m_{2\text{step}}$
Fourth line:	$m_{3\text{start}}$, $m_{3\text{end}}$, $m_{3\text{step}}$

If *BLOCH_WAVE_ANALYSIS is set, the BWA-part of the Bloch Wave analysis program is executed. To exclude strictly periodic modes ($\forall m_i = 0$) at least one $m_{i\text{start}}$ must be greater than zero. Only if one wave number is not of interest (in the 2D case, for example, this would be m_3) the corresponding values are set to $m_{i\text{start}} = m_{i\text{end}} = 0$. The parameter $m_{i\text{step}}$ can be given any value greater than zero. All values must be separated by commas. As an example, an input for the 2D-case is given:

*BLOCH_WAVE_ANALYSIS
34, 69
10, 1, 360
10, 1, 360
0.0, 0.0, 1

$m_{i\text{start}}$, $m_{i\text{end}}$ and $m_{i\text{step}}$ are given in fractions of π:

$$\begin{aligned} 10 &\Rightarrow \frac{\pi}{10} \\ 1 &\Rightarrow \pi \\ 0.5 &\Rightarrow 2\pi \end{aligned}$$

***MACROSCOPIC_ONSET_OF_FAILURE**

First line:	Number of the first and last increment for the Macroscopic Onset-of-Failure analysis
Second line:	φ_{start}, φ_{end}, φ_{step}
Third line:	θ_{start}, θ_{end}, θ_{step}

If the command *MACROSCOPIC_ONSET_OF_FAILURE is set, the macroscopic onset-of-failure part of the Bloch Wave analysis program is executed. φ_{start} and θ_{start} can be given any value lower than π or 2π, respectively. ϕ_{step} and θ_{step} must be set to a value greater than zero. Like in the Bloch Wave analysis input φ_{start}, φ_{end}, φ_{step} and θ_{start}, θ_{end}, θ_{step} are given in fractions of π

***CRITICAL_MODE_OUTPUT**

First and only line: inc_start, inc_end, No.X, No.Y, No.Z

If the *CRITICAL_MODE_OUTPUT keyword is given, the nodal displacements describing the critical mode found in a standard Bloch Wave analysis will be written to an output

file for all increments from inc_start to inc_end. No.X, No.Y and No.Z are the unit cell counts in x-, y- and z-direction, respectively, for displaying the critical mode. If no mode output should be written then this command has to be omitted.

***DOF_PER_NODE**

First and only line: Number of the nodal degrees of freedom depending on the element type used in the model

Set this value equal to the nodal degrees of freedom of the elements used.

***2D_CASE**

If the *2D_CASE keyword is set then the modeled structure (all elements must be in the x-y plane) is treated as a 2D problem. Therefore, the displacement in z-direction and the rotations about the x- and y-axis are constrained. For example, all elements used to model a structure are in the x-y plane and the used elements have more nodal degrees of freedom than actually being active in a 2D problem. If the *2D_CASE keyword is set then the problem is treated as a 2D problem, else the problem is treated as a 3D problem.

***LOAD**

First and only line: F1, F2, F3

F1	Concentrated reference load on the master node in x-direction
F2	Concentrated reference load on the master node in y-direction
F3	Concentrated reference load on the master node in z-direction

Set the values for the force components equal to the values definded under *CLOAD in the ABAQUS input file.

A.4.2 ABAQUS Input File

The Bloch Wave analysis Program reads the nodal and element information from the ABAQUS input file. The nodal data is required to determine the size of the unit cell and to find all master nodes and their corresponding slave nodes. For the assembly of the tangent stiffness matrix of the unit cell one needs the coincidence table of each element. Therefore, the element information is also read from the input file. Nodal and element data of the unit cell are also used for generating a number of cells in each direction to display the critical mode if the *CRITICAL_MODE_OTUPUT key word is set in the command

file. To simplify the reading procedure some restrictions are made for the ABAQUS input file:

- All nodes must be defined within one *NODE command. Otherwise, the nodal data is not read correctly.
- 2D unit cells must be defined in the x-y-plane.
- All unit cells must be rectangular (2D) or cuboid-shaped (3D).
- The edges of the unit cell must be parallel to the axes of the global coordinate system.

A.5 Output

A.5.1 Search for the Strictly Periodic Mode

The output for the search for the strictly periodic mode is written to a file named " myinput_SSPMallincrements.dat". This file has five columns with the increment number i being written to column one. In column two one can find the eigenvalue of the reduced matrix for increment i. In columns three to five the corresponding load values for F1 to F3 are displayed.

The eigenvalue, displayed in column two, changes its sign as soon as the critical state is achieved.

A.5.2 Standard Bloch Wave Analysis

For each increment of the standard Bloch Wave analysis a separate output file is written by default. myanalysis_*inc*BWA.dat (with *inc* as increment number) has four columns with the first one displaying the eigenvalue of the reduced stiffness matrix of the unit cell (see Section 4.2). If the eigenvalue becomes zero then the critical state along the loading path is reached. The values of the dimensionless wave numbers m_1 to m_3 are written to columns two to four.

If the critical state is established in one increment i then the lowest eigenvalue and the corresponding wave numbers of the eigenmode for this state are written to a separate file

myanalysis_BWAallincrements.dat. The columns from left to right are: increment number i, m_1, m_2, m_3, eigenvalue increment i, eigenvalue increment $i-1$, F1, F2, F3.

If the CRITICAL_MODE_OTUPUT keyword is set in the command file an additional output file myanalysis_BWAmodeoutput.inp is written for the given increments. This file is structured like an ABAQUS input file. The critical mode is applied as a displacement field perturbing the undeformed structure. To display the critical mode one has to run a ABAQUS standard analysis using this file as the input file. The BWA program does not read any section properties of the elements from the old ABAQUS input file myanalysis.inp (see Figure A.1). Therefore, these properties have to be definded manually by the user in the new input file myanalysis_BWAmodeoutput.inp.

A.5.3 Macroscopic Onset-of-Failure

As mentioned in Chapter 5 the macroscopic onset-of-failure is indicated by the loss of rank one convexity of the homgenized tangent moduli. If this critical state is established, the critical load and the direction of the band of the corresponding buckling mode is written to a file myanalysis_MOF.dat.

B Special Treatment of 2D and 1D Problems

As already mentioned in Section 7 two dimensional and one dimensional unit cells can be modeled with elements that have more nodal degrees of freedom than actually being active in a 2D F.E.M. analysis. For this case the *2D_CASE keyword is introduced in the BWA program input file (see Section A). The Bloch Wave analysis (BWA) program normally uses the complete element stiffness matrices to assemble the tangent stiffness matrix of the unit cell. The size of the coupling matrix used for the Bloch Wave analysis also depends on the nodal degrees of freedom of the element. For that reasons the BWA program delivers wrong results for these specific 2D (1D) problems.

To avoid this problem the following workarounds are included in the BWA program. The workarounds are valid both for 2D and 1D problems, although only the 2D case is mentioned.

B.1 Tangent Stiffness Matrix

To keep the reading procedure of the element stiffness matrices as simple as possible the whole element stiffness matrices are read. The size of the tangent stiffness matrix $\underset{\approx}{\boldsymbol{K}}$ can be evaluated as

$$\dim(\underset{\approx}{\boldsymbol{K}}) = (n_{\mathrm{N}} * n_{\mathrm{dof}}) \times (n_{\mathrm{N}} * n_{\mathrm{dof}}) \tag{B.1}$$

with n_{N} being the total number of nodes in the unit cell model and n_{dof} being the number of nodal degrees of freedom. For the size of the 2D stiffness matrix $\underset{\approx}{\boldsymbol{K}}_{\mathrm{2D}}$ on receives

$$\dim(\underset{\approx}{\boldsymbol{K}}_{\mathrm{2D}}) = (n_{\mathrm{N}} * n_{\mathrm{act}}) \times (n_{\mathrm{N}} * n_{\mathrm{act}}) \tag{B.2}$$

with n_{act} being the number of active nodal degrees of freedom. For the assembly of the 2D tangent stiffness matrix only the entries in the element stiffness matrix corresponding to active degrees of freedom are taken into account. Therefore, the coincidence tables used to assemble the tangent stiffness matrix have to be modified. The following example will describe the procedure used for adapting the coincidence tables.

Figure B.1 shows an example of a coincidence table for a shear deformable linear beam element in space with six nodal degrees of freedom. The first row contains the local degrees of freedom and the second row shows the corresponding global degrees of freedom of all

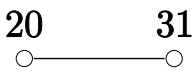

Local	1	2	3	4	5	6	7	8	9	10	11	12
Global	114	115	116	117	118	119	180	181	182	183	184	185

Figure B.1: Coincidence table of a shear deformable beam element with six nodal degrees of freedom.

entries in the element stiffness matrix. The node numbers of the beam element can also be found in Figure B.1. The nodal displacement vector $\underset{\sim}{\boldsymbol{u}}_n$ of node n of the beam element can be written as:

$$\underset{\sim}{\boldsymbol{u}}_n = \{u, v, w, \theta_\mathrm{x}, \theta_\mathrm{y}, \theta_\mathrm{z}\}^\mathrm{T} \tag{B.3}$$

with u, v and w being the nodal displacements in x-, y-, and z-direction and θ_x, θ_y, and θ_z being the rotations about the x-, y-, and z-axis.

In the 2D case the displacement in x-direction and the rotations about the x- and y-axis are not active and therefore, the nodal displacement vector of node n of the beam element is reduced to:

$$\underset{\sim}{\boldsymbol{u}}_n = \{u, v, \theta_\mathrm{z}\}^\mathrm{T} \tag{B.4}$$

The corresponding coincidence table of the same element as above is shown in Figure B.2. The coincidence table has the same length as the table of the general case. For the unused degrees of freedom (DOF) of the element nodes the global DOF entries are set to 999999. Because the size of the tangent stiffness matrix is limited to approximately 16000×16000 by the Python module Numeric, 999999 is never used for an active DOF. For the calculation of the global DOF numbers only the active degrees of freedom are taken into account. The assembly of the tangent stiffness matrix proceeds the normal way, except for the fact that the entries of the element stiffness matrix, which have a 99999 entry for their global DOF, are ignored.

B.2 Strictly Periodic Mode Analysis

The strictly periodic mode analysis is treated separately by the BWA program. The reduced tangent stiffness matrix $\underset{\approx}{\mathring{\boldsymbol{K}}}$ must be constrained against rigid body movements

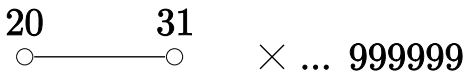

Local	1	2	3	4	5	6	7	8	9	10	11	12
Global	57	58	×	×	×	59	90	91	×	×	×	92

Figure B.2: Reduced coincidence table of a shear deformable beam element with three active nodal degrees of freedom.

(see Section A.3). For the 2D and the 1D case Equation (A.1) is still valid if Equation (A.2) is changed to the following equation:

$$\dim(\underset{\sim}{\mathbf{0}}) = (2 \times 1) \tag{B.5}$$

This change is reasonable because the translation in z-direction was already constrained in the assembly of the tangent stiffness matrix of the 2D problem. Therefore, $\overset{\circ}{\underset{\approx}{\boldsymbol{K}}}$ must only be constrained against the translations in x- and y- direction.

B.3 All Other Procedures

For all other procedures of the BWA program the number of nodal DOF is simply set to the number of active DOF. Thus, e.g., for the coupling matrix $\underset{\approx}{\boldsymbol{\nu}}$ used during a Bloch Wave analysis procedure and for the special functions $\overset{ij}{\underset{\sim}{\boldsymbol{\chi}}}$ and the elongation matrix $\underset{\approx}{\boldsymbol{\omega}}$ used in the macroscopic onset-of-failure procedure only the active degrees of freedom are taken into account.

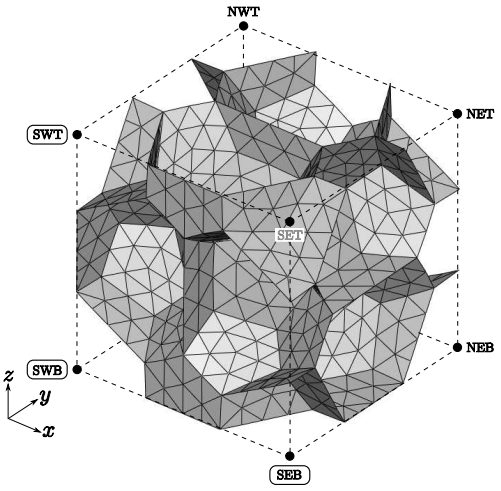

Figure C.1: Meshed Weaire-Phelan Cell using linea tria elements.

C Weaire-Phelan Cell - Effect of Geometric Imperfections

C.1 F.E.M. Model

To reduce the computational time required by the Bloch Wave Analysis program a coarser mesh than in Section 8 is used.

The cubic unit cell is meshed using linear shell elements of ABAQUS type S3R. The meshed structure is depicted in Figure C.1. The meshed unit cell has a total number of 1140 elements and 588 nodes with 3528 degrees of freedom.

The shell thickness and the bulk material properties are the same as in Section 8:

$$\begin{aligned} t &= 0.0037818\,\text{mm} \\ E_\text{s} &= 70000\,\text{MPa} \\ \nu_\text{s} &= 0.3 \end{aligned} \tag{C.1}$$

The periodic boundary conditions are specified using the CBC-program. To avoid rigid body movements all degrees of freedom of an internal node of the unit cell and some of

the displacement degrees of freedom of the master nodes (see Figure C.1) are constrained:

$$\begin{aligned} \underset{\sim}{\boldsymbol{u}}_{\mathrm{SWB}} &= \{0,0,0\} \\ \underset{\sim}{\boldsymbol{u}}_{\mathrm{SEB}} &= \{u_{\mathrm{SEB}},0,0\} \\ \underset{\sim}{\boldsymbol{u}}_{\mathrm{NWB}} &= \{u_{\mathrm{NWB}},v_{\mathrm{NWB}},0\} \end{aligned} \tag{C.2}$$

C.2 Results of the Strictly Periodic Mode Analysis

The standard Newton Raphson method is used as the solution procedure. The loading path is evaluated using two different step sizes $\Delta\Lambda$ for the load parameter Λ: case 1 (C1) has a constant step size of $\Delta\Lambda = 0.01$ and case 2 (C2) has a constant step size of $\Delta\Lambda = 0.0025$. For both cases the compressive reference load applied to the SEB master node has a value of 2.5 N for $\Lambda = 1.0$.

The results of the Strictly Periodic Mode analysis for the cases C1 and C2 are depicted in Figure C.2. The lowest eigenvalues found by the SPM analysis are plotted against the stress in x-direction σ_1 of the unit cell. For C1 the lowest eigenvalue becomes negative at $\sigma_1 \approx 0.475\,\mathrm{N/mm^2}$ whereas the lowest eigenvalue of C2 remains positive. For higher values of σ_1 the eigenvalues for C1 become positive again. For $\sigma_1 = 0.5\,\mathrm{N/mm^2}$ the lowest eigenvalue of C1 becomes negative and the analysis for C2 terminates.

C.3 Results of the Accompanying Eigenvalue Analysis

Additionally to the strictly periodic mode analysis a accompanying linear eigenvalue analysis (ALEA) is performed. The results of the ALEA are depicted in Figure C.2. The lowest eigenvalue of the ALEA is plotted against σ_1. The critical load is not established during the ALEA because while, the lowest eigenvalue approaches zero, it has a minimum at $\sigma_1 \approx 0.475\,\mathrm{N/mm^2}$ and then increases again. This minimum matches the occurrence of the first negative eigenvalue in the SPM analysis for C1. The analysis terminates at $\sigma_1 \approx 0.5\,\mathrm{N/mm^2}$ because ABAQUS encounters an error during the analysis. The deformation plot of the Weaire-Phelan unit cell shows the occurrence of local cell wall buckling (see Figure C.2). For a geometrically perfect structure the buckling of the affected cell faces should not be possible during a static analysis. The reason for this behavior can be found in small geometric imperfections of the nodes on the affected faces. Results for a

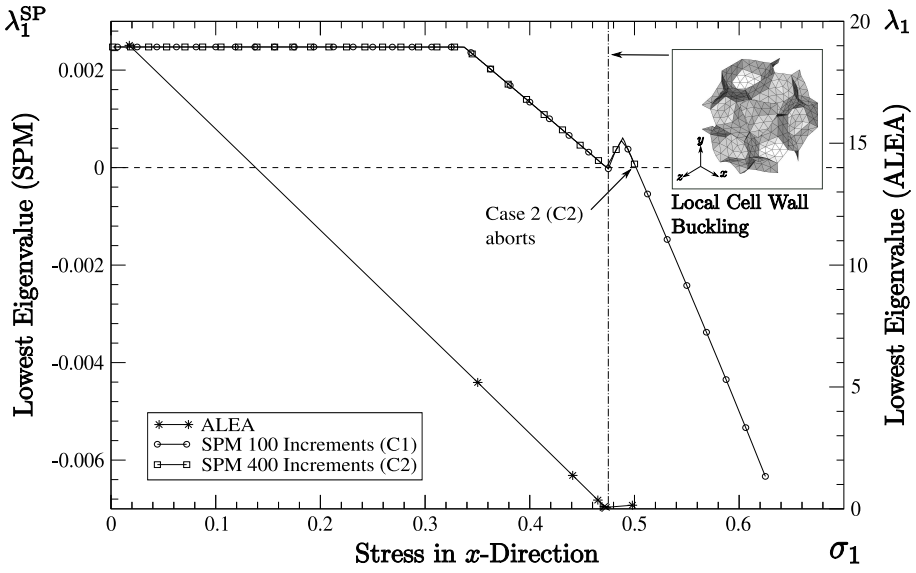

Figure C.2: Results of the SPM analysis for the Weaire-Phelan Cell.

cell with perfect geometry can be found in Section 8.

References

[1] ABAQUS, Inc. *ABAQUS/Standard Theory Manual, Version 6.8*. Dassault Systèmes Simulia Corp., Providence, RI, USA, 2008.

[2] ABAQUS, Inc. *ABAQUS/Standard User's Manual, Version 6.8*. Dassault Systèmes Simulia Corp., Providence, RI, USA, 2008.

[3] M. F. Ashby, A. G. Evans, J. W. Hutchinson, and N. A. Fleck. Metal foams: a design guide. Technical report, Engineering Department, University of Cambridge, Cambridge, UK, August 1998. Version 4.

[4] Klaus-Jürgen Bathe. *Finite Elemente Methoden, 2. Auflage*. Springer Verlag, Berlin Heidelberg, 2002.

[5] Z.P. Bažant and L. Cedolin. *Stability of Structures*. Oxford University Press, New York, 1991.

[6] R. Bitsche. Space-filling polyhedra as mechanical models for solified dry foams. Diploma thesis, Vienna University of Technology, Vienna, 2005.

[7] F. Bloch. Über die quantenmechanik der elektronen in kristallgittern. *J. Appl. Mech. ASME*, 52(7–8):555–600, 1929.

[8] H. J. Böhm. *Lecture Notes Composite Engineering, Part II*. 2006.

[9] S. C. Cowin. Properties of the anisotropic elasticity tensor. *J. Mech. appl. Math.*, 42/2:249–266, 1989.

[10] T. Daxner. *Multi-Scale Modeling and Simulation of Metallic Foams*. Fortschritt-Berichte VDI, Reihe 18, No. 285. VDI Verlag, Düsseldorf, 2003.

[11] T. Daxner and F. G. Rammerstorfer. *Vorlesungsbehelf zur Vorlesung Nichtlineare Finite Elemente Methoden*. 2005/06.

[12] V. S. Deshpande and N. A. Fleck. Isotropic constitutive models for metallic foams. *J. Mech. Phys. Solids*, 48:1253–1283, 2000.

[13] Müller S. Triantafyllidis N. Geymonat, G. Homogenization of nonlinearly elastic materials, microscopic bifurcation and macroscopic loss of rank-one convexity. *Arch. Ration. Mech. Anal.*, 122:231–290, 1993.

[14] L. Gong and S. Kyriakides. Compressive response of open cell foams. Part II: Initiation and evolution of crushing. *Int. J. Sol. Struct.*, 42(5–6):1381–1399, 2005.

[15] L. Gong and S. Kyriakides. A general theory of uniqueness and stability in elastic-plastic solids. *J. Appl. Mech. ASME*, 73:807–814, Sept. 2006.

[16] L. Gong, S. Kyriakides, and W.-Y. Jang. Compressive response of open cell foams. Part I: Morphology and elastic properties. *Int. J. Sol. Struct.*, 42(5–6):1355–1379, 2005.

[17] L. Gong, S. Kyriakides, and N. Triantafyllidis. On the stability of Kelvin cell foams under compressive loads. *J. Mech. Phys. Solids*, 53:771–794, 2005.

[18] R. Hill. On the Crushing Stress of open cell foams. *J. Mech. Phys. Solids*, 6:236–249, 1958.

[19] Alex Martelli. *Python in a Nutshell, Second Edition*. O'Reilly Media, Inc., Sebastopol, CA, 2006.

[20] N. Ohno, D. Okumura, and T. Niikawa. Long-wave buckling of elastic square honeycombs subject to in-plane biaxial compression. *Int. J. Mech. Sci.*, 46:1697–1713, 2004.

[21] N. Ohno, D. Okumura, and H. Noguchi. Microscopic symmetric bifurcation condition of cellular sollid based on a homogenization theory of finite deformation. *J. Mech. Phys. Solids*, 50:1125–1153, 2002.

[22] D. Okumura, N. Ohno, and H. Noguchi. Elastoplastic microscopic bifurcation and post-bifurcation behavior of periodic cellular solids. *J. Mech. Phys. Solids*, 52:641–666, 2004.

[23] J. R. Rice. The localization of plastic deformation. In W.T. Koiter, editor, *Proceedings of the ICTAM 1976*, pages 207–220, Amsterdam, 1976. North Holland Publishing Co.

[24] R. J. M. Smit, W.A.M. Brekelmans, and H.E.H. Meijer. Prediction of the mechanical behavior of non-linear heterogeneous systems by multi-level finite element modeling. *Comput. Methods Appl. Mech. Eng.*, 155:181–192, 1998.

[25] A. Srikantha Phani, J. Woodhouse, and N. A. Fleck. Wave propagation in two-dimensional periodic lattices. *J. Acoust. Soc. Am.*, 119:1995–2000, 2006.

[26] W. (Lord Kelvin) Thompson. On the division of space with minimal partitional area.

[27] N. Triantafyllidis, M. D. Nestorović, and M. W. Schraad. Failure surfaces for finitely strained two-phase periodic solids under general in-plane loading. *J. Appl. Mech. ASME*, 73:505–515, May 2006.

[28] M. Šilhavý. On isotropic rank 1 convex functions. *Proceedings of the Royal Society of Edinburgh*, 129A:1081–1105, 1999.

[29] D. Weaire, editor. *The Kelvin Problem.* Taylor & Francis, London, 1996.

[30] D. Weaire and S. Hutzler. *The Physics of Foams.* Clarendon Press, Oxford, 1999.